Forschungszentrum Karlsruhe
Technik und Umwelt

Wissenschaftliche Berichte
FZKA 5580

Thermohydraulics Design and Thermomechanics Analysis of Two European Breeder Blanket Concepts for DEMO

Part 1: BOT Helium Cooled Solid Breeding Blanket
Part 2: Dual Coolant Self-cooled Liquid Metal Blanket

P. Norajitra

Institut für Materialforschung
Projekt Kernfusion

Juni 1995

Forschungszentrum Karlsruhe
Technik und Umwelt
Wissenschaftliche Berichte
FZKA 5580

Thermohydraulics Design and Thermomechanics Analysis of Two European Breeder Blanket Concepts for DEMO

Part 1: BOT Helium Cooled Solid Breeding Blanket
Part 2: Dual Coolant Self-cooled Liquid Metal Blanket

P. Norajitra

Institut für Materialforschung

Projekt Kernfusion

Forschungszentrum Karlsruhe GmbH, Karlsruhe
1995

Forschungszentrum Karlsruhe GmbH
Postfach 3640, 76021 Karlsruhe

ISSN 0947-8620

Abstract

Two different breeding blanket concepts are being elaborated at Forschungszentrum Karlsruhe within the framework of the DEMO breeding blanket development, the concept of a helium cooled solid breeding blanket and the concept of a self-cooled liquid metal blanket. The breeder material used in the first concept is Li_4SiO_4 as a pebble bed arranged separate from the beryllium pebble bed, which serves as multiplier. The breeder material zone is cooled by several toroidally-radially configurated helium cooling plates which, at the same time, act as reinforcements of the blanket structures. In the liquid metal blanket concept lead-lithium is used both as the breeder material and the coolant. It flows at low velocity in poloidal direction downwards and back in the blanket front zone. In both concepts the First Wall is cooled by helium gas.

This report deals with the thermohydraulics design and thermomechanics analysis of the two blanket concepts. The performance data derived from the Monte-Carlo computations serve as a basis for the design calculations. The coolant inlet and outlet temperatures are chosen with the design criteria and the economics aspects taken into account. Uniform temperature distribution in the blanket structures can be achieved by suitable branching and routing of the coolant flows which contributes to reducing decisively the thermal stress. The computations were made using the ABAQUS computer code. The results obtained of the stresses have been evaluated using the ASME code. It can be demonstrated that all maximum values of temperature and stress are below the admissible limit.

Zusammenfassung

Thermohydraulische Auslegung und thermomechanische Analyse von zwei europäischen Brutblanketkonzepten für DEMO

Im Rahmen der DEMO-Brutblanketentwicklung werden im Forschungszentrum Karlsruhe zwei unterschiedliche Brut-Blanketkonzepte ausgearbeitet, nämlich das Konzept eines heliumgekühlten Feststoffbrutblankets und das Konzept eines selbstgekühlten Flüssigmetallblankets. Als Brutstoff wird beim ersteren Li_4SiO_4 in Form von Kugelschüttung verwendet, die von der als Multiplier dienenden Beryllium-Kugelschüttung getrennt angeordnet ist. Die Kühlung der Brutstoffzone erfolgt durch zahlreiche toroidal-radial angeordnete Heliumkühlplatten, die gleichzeitig als Versteifung für die Blanketstruktur dienen. Beim Flüssigmetallblanketkonzept wird Bleilithium als Brutstoff und als Kühlmittel zugleich verwendet. Es strömt mit geringer Geschwindigkeit in poloidaler Richtung nach unten und im vorderen Blanketbereich wieder zurück. Die Erste Wand wird in beiden Konzepten vom Heliumgas gekühlt.

Der vorliegende Bericht befaßt sich mit der thermohydraulischen Auslegung und der thermomechanischen Analyse von beiden Blanketkonzepten. Als Basis für die Auslegungsrechnungen dienen die Leistungsdaten aus den Monte-Carlo-Rechnungen. Unter Berücksichtigung der Auslegungskriterien und der wirtschaftlichen Gesichtspunkte werden die Kühlmittelein- und -austrittstemperaturen gewählt. Durch geeignete Aufteilung und Anordnung der Kühlmittelströme kann eine gleichmäßige Temperaturverteilung in den Blanketstrukturen erreicht werden, die zur entscheidenden Reduktion der Wärmespannung beiträgt. Die Berechnungen wurden mit dem Rechenprogramm ABAQUS durchgeführt. Die Bewertung der Spannungsergebnisse erfolgte nach dem ASME-Code. Es konnte gezeigt werden, daß alle Maximalwerte der Temperatur und der Spannung unterhalb der zulässigen Grenze liegen.

PART 1

BOT Helium Cooled Solid Breeding Blanket

Contents

Part 1

1 Introduction

The concept of a helium cooled solid breeding blanket has been elaborated at FZK for a couple of years within the framework of breeding blanket development for DEMO. The breeder material used have been lithium orthosilicate (Li_4SiO_4) pebbles (0.1 ÷ 0.5 mm dia.) while beryllium pebbles (2 mm dia.) have been used as neutron multiplier. The whole blanket is cooled by helium gas. Cold helium gas is first passed through the First Wall and the preheated helium is subsequently routed through the breeder material zone.

In the latter named reference concept [1] the breeder material zone is cooled by cooling coils of tube. The breeder material zone accommodates a mixture of a pebble bed of Li_4SiO_4 and beryllium pebbles differing in size. This lowers the relatively high power density of pure Li_4SiO_4 pebble beds, especially in the radial front zone, and the thermal conductivity of the bed is increased by beryllium with its better thermal conductivity. However, this advantage is counteracted by problems of material compatibility, especially at elevated temperature and under irradiation. Moreover, the optimization of cooling proves to be difficult with tube coils on account of the limited number of turns, the pipe length, and the radii of pipe elbows. As a result, it can e. g. not be avoided that temperature peaks occur in the gussets between the pipe elbows. Moreover, the arrangement of tube coils must be adapted to the tapered blanket cross section in poloidal direction.

Another solution [2] in which the cooling tube coils are replaced by cooling plates offers itself as an alternative to this concept. The Li_4SiO_4 and the beryllium pebble beds are divided by cooling plates into separate chambers. This solution offers the following advantages:

- Reduction of the number of material contacts.
- More degrees of freedom in cooling channel design and optimization of cooling, any shape of cooling channels feasible (e. g. by milling).
- Cooling plates serve at the same time as reinforcing elements of the blanket structure.
- By parallel arrangement of the cooling plates the locations of the heat source and sinks and, consequently, of the temperature maximum are well defined.

The subject of this report is a thermohydraulics design for the new reference concept including a solution based on cooling plates.

2 General Layout of the Blanket

The design layout of the blanket geometry is achieved by CAD.

Figure 1 is a representation of the inboard and outboard solid blankets. The principal dimensions of an outboard blanket can be seen in Fig. 2.

The outboard segment is welded in poloidal direction from eight aprons of 950 mm height each and a straight extension piece. The relatively dense occupation by cooling and stiffening plates, respectively, can be easily recognized in Fig. 2. Compared with the old reference concept, the manifold system at the bottom part of the blanket has been greatly simplified.

Figure 3 shows the design layout of an outboard blanket segment in an isometric representation. The whole blanket structure is made from 1.4914 martensitic steel (EU designation MANET). The U-shaped First Wall, total thickness 25 mm, together with the supporting and shielding structures, makes up a stiff segment box. Within the First Wall parallel cooling channels (□ 14 x 18 mm) are arranged with 24 mm channel spacing. They are passed in alternating directions by cooling gas at 80 bar, supplied from two cooling systems. The alternating directions of flow in the cooling channels of the First Wall contribute to achieving a uniform temperature within the external structure and thus to minimizing thermal stresses. Moreover, emergency cooling in case of failure of a cooling system is guaranteed by the separate supply systems 1 and 2.

Inside the segment box 8 mm thick cooling plates are rigidly welded radially with the external structure at poloidal spacings of 19 and 53 mm, respectively. The Li_4SiO_4 pebble beds, 11 mm layer thickness, and the beryllium pebble beds, respectively, 45 mm layer thickness, are provided between the cooling plates (Figs. 4 to 6). The helium cooling channels, 4 mm depth of cooling channel, are housed within the cooling plates.

In the inboard blanket segment (Fig. 1) the helium gas is instantaneously fed into the parallel cooling channels of the First Wall while flowing downward from the blanket top without reversing at the bottom end. The helium cooling gas at 250 °C enters the outboard blanket segment from top (Fig. 2), first flows downward through the main supply channels on the rear side while getting warmed up but negligibly. Having been reversed on the bottom end of the blanket, the helium gas from the two systems is gradually carried into the parallel cooling channels of the First Wall. Then it is passed through the cooling channel integrated in the plates by means of a header/manifold system (Fig. 5). The cooling plates are connected to the header/manifold system in such a manner that they are passed in alternating

directions. This gives a homogeneous temperature distribution in the breeding zone.

3 Method of Design

3.1 Blanket Power

The computations are based on the blanket powers determined by the Monte Carlo method [3].

Figures 7 to 9 show the radial power density distributions in steel, Li_4SiO_4 and beryllium for the central zone of the outboard blanket. The maximum power density is about 26 W/cm^3 for steel, about 37 W/cm^3 for Li_4SiO_4, and about 15 W/cm^3 for beryllium.

The heat flux density on the surface of the First Wall, input by the plasma, is assumed to be 40 W/cm^2 on the average and 50 W/cm^2 at the maximum, respectively.

3.2 Design Criteria and Coolant Flows

The total helium flow required in a blanket segment is determined from the total power to be removed from the segment and from the helium enthalpy rise. The total power of the segment is calculated from the volumetric and surface power of the First Wall (for a mean surface power density of 40 W/cm2) and from the volumetric power of the total breeding zone and the rest of steel structures. The maximum value of the power density on the surface of 50 W/cm^2 is taken into account in the determination of the helium flow required for the central blanket zone.

The inlet temperature of the helium cooling gas is assumed to be 250 °C, taking into account the DBTT (ductile brittle transition temperature) of MANET steel. The assumed mean outlet temperature of helium is 450 °C, taking into account the flow conditions. This corresponds to a total enthalpy rise of the helium cooling gas of 200 K. The mean cooling gas pressure is assumed to be 80 bar.

Regarding the First Wall exposed to the highest thermal load, the additional criterion applies that the First Wall temperature must not exceed about 550 °C at the maximum, taking into account the creep rupture strength of MANET.

4 Design Calculation for the Outboard Blanket Segment

4.1 Thermal Power to be Removed

Surface power:	40×10^4 W/m^2 · 10.583 m^2	=	4.233 MW
Volumetric power (according to [3]):		=	32.79 MW
Total		=	37.023 MW

4.2 Required Helium Mass Flow

The helium flow for a blanket segment with two cooling systems is:

$$\dot{m}_{He,1\ segment} = \frac{Q}{c_p \cdot \Delta T_{He}} = \frac{37.023x10^6\ W}{5.2x10^3\ \frac{J}{kgK} \cdot (450\text{-}250)\ K} = 35.6\ \frac{kg}{s}$$

This is equivalent to a flow per helium cooling system of

$\dot{m}_{He,\ 1\ system} = 17.8$ kg/s.

4.3 Distribution of Helium Flow in the Center of the Blanket

4.3.1 Thermal Power to Be Removed from a 72 mm Thick Poloidal Layer

Surface power:	39,026 W
at max. 50 W/cm^2	
Volumetric power:	
First Wall/Side Walls	38,033 W
Volumetric power:	
breeding zone	
ceramic (11 mm)	123,583 W
beryllium (45 mm)	110,609 W
two cooling plates (16 mm)	41,042 W
Total	352,293 W

4.3.2 Helium Flow Ratio for First Wall/Cooling Plates

For a pebble bed unit of 72 mm layer thickness in poloidal direction (Fig. 6) a helium supply ratio is obtained of two cooling plates each to three First Wall channels which gives

$$\dot{m}_{1\,PL} = 1.5 \cdot \dot{m}_{1\,FWK} \qquad (1)$$

Taking into account poloidal warming of helium in the main pipes, the inlet and outlet temperatures of helium in the central zone of the blanket are assumed to be 251 °C and 449 °C, respectively. Thus, the total enthalpy rise from entrance of the First Wall up to leaving the cooling plate is 198 K:

$$\Delta T_{1\,FWK} + \Delta T_{1\,PL} = 198 \qquad (2)$$

$$\frac{Q_{FW/SW}}{c_{pHe} \cdot 3 \cdot \dot{m}_{1\,FWK}} + \frac{Q_{BER/CER}}{c_{pHe} \cdot 2 \cdot \dot{m}_{1\,Pl}} = 198 \qquad (3)$$

with $Q_{FW/SW} = 39{,}026 + 38{,}033 = 77{,}059\ W$

$Q_{BER/CER} = 123{,}583 + 110{,}609 + 41{,}042 = 275{,}234\ W$

Equation (1) in (3) yields:

$$\dot{m}_{1\,FWK} = \frac{1}{5.2x10^3 \frac{J}{kgK} \cdot 198\,K} \cdot \left(\frac{77059 + 275234}{3} \right) W$$

$= 0.11405$ kg/s

$\dot{m}_{1\,PL} = 1.5 \cdot \dot{m}_{1\,FWK} = 0.17108$ kg/s

$$\Delta T_{1\,FWK} = \frac{77059\ W}{5.2x10^3 \frac{J}{kgK} \cdot 3 \cdot 0.11405 \frac{kg}{s}} = 43.3\,K$$

$\Delta T_{1\,PL} = 198\text{-}43.3 = 154.7$ K

This leads to the distribution of helium flows and temperatures represented in the following table:

Outboard	First Wall - Channel	Cooling Plate
$\dot{m}_{He}$ (kg/s)	0.11405	0.17108
$T_{He,\ inlet/outlet}$(°C)	251.0/294.3	294.3/449.0
$T_{m,\ He}$ (°C)	272.65	371.65
ΔT_{He} (K)	43.3	154.7

In this heat power balance the heat exchange between the breeding zone and the First Wall is neglected.

4.3.3 Design of the Cooling Channels Integrated in the Plates

The cross section of the breeding zone as a whole is divided into six cooling zones (Fig. 5). The thermal power to be removed from the respective cooling zone is calculated from the power data in [3]. Accordingly, assuming the same enthalpy rise for all cooling zones, the following distribution of flows is obtained:

	Cooling Zone					
	1	2	3	4	5	6
Q_{ab} (W)	28,546	23,756	23,274	20,638	22,773	18,630
$\dot{m}/\dot{m}_{1\ PL}$	0.2074	0.1726	0.1691	0.1500	0.1655	0.1354
$\dot{m}_{theor.}$ (kg/s)	0.0355	0.0295	0.0289	0.0257	0.0283	0.0232
$\dot{m}_{design}$ (kg/s)	0.0340	0.0300	0.0294	0.0262	0.0283	0.0232

The cooling channel cross sections are designed in such a manner that the helium velocity is maximum in the front zone and decreases radially towards the rear side in conformity with the distribution of the heat source densities. The helium velocity is chosen to adopt such a value that reasonable heat transfer conditions are achieved similar to those in the tube coil version and that no inadmissibly high pressure drops are produced (see next section).

Accordingly, the following channel geometry is obtained for the various cooling zone, both for the toroidal channel sections (front part) and for the radial channel segments (lateral part):

Outboard	Cooling Zone					
	1	2	3	4	5	6
Cooling channel number	3	3	4	5	8	8
Channel width (mm) (depth = 4 mm)						
- front part	6.4	6.9	5.5	5.5	5.5	5.5
- lateral part	6.8	6.9	5.5	6.0	6.0	6.0
Max. He velocity (m/s)	75	64	55	43	27	21
Total pressure drop (bar)	1.6	1.4	1.3	0.5	0.2	0.3

Figure 10 shows the cooling channels designed in this way. Additional dummy channels have been introduced in the lateral parts in order to reduce the excessive steel portion.

4.4 Helium Pressure Losses

The total pressure loss due to pipe friction and resistance is determined using the following equation:

$$\Delta p_{\lambda+\zeta} = \left(\lambda_R \cdot \frac{l}{d_h} + \Sigma\zeta \right) \cdot \frac{\rho}{2} \cdot c^2 \qquad (4)$$

with

$$c[m/s] = \frac{\dot{m}}{\rho \cdot A} \qquad (5)$$

$$Re = \frac{c \cdot d_h}{\upsilon} = \frac{c \cdot d_h}{\eta/\rho} \qquad (6)$$

and the constitutive equations for helium [5]:

$$\rho\,[kg/m^3] = 48.091 \cdot \frac{p\,[bar]}{T\,[K]} \tag{7}$$

$$\eta = 0.4646 \cdot T^{0.66}{}_{He}\,[K]\; x\; 10\text{-}6\,[kg/ms] \tag{8}$$

4.4.1 Pressure Loss in the Helium Main Pipes

Position (Fig. 2)	d_h (mm)	l (mm)	k (mm)	d_h/k (-)	c (m/s)	T_{He} (°C)	Re (-)	λ_R (-)	Resistance Numbers ζ [6]	Σζ	$\Delta p_{\lambda+\zeta}$ (bar)
1-2	199	18,334	0.02	9950	77	250	3.9×10^6	0.0125	2 bends 1), 90°: 0.137 1 bend, 30°: 0.022 blanket curvature, 90°: 0.066 reduction of area: 0.010 1reversal, 180°: 0.138	0.373	0.342
2-3 2) cold	169.3	10,395	0.02	8500	66 *	250	2.7×10^6 *	0.128	blanket curvature 0.07	0.10	0.077
hot	181.5	10,395	0.02	9075	80 *	450	2.2×10^6 *	0.013	bend 0.03		0.080
3-4	248	7272	0.02	12.400	68	450	2.5×10^6	0.0125	extension in area: 0.31 2 bends, 30°: 0.05 2 bends, 135 °: 0.21	0.57	0.118

Total: 0.617

* Mean over the total manifold length approx.

1) $\zeta_{bend} = \left[0.131 + 0.159 \cdot \left(\frac{dh}{R} \right)^{3.5} \right] \cdot \frac{\delta}{180}$ · *with R*:radius of curvature, *δ*:bending angle.

2) *The pressure loss in the Helium distributors can be determined by the equation:*

$$\Delta p_\lambda = \frac{0.043466 \cdot \eta_{He}^{0.2}}{\rho_{He}} \cdot \frac{\dot{m}^{1.8}}{d_h^{4.8}} \cdot \frac{l}{2}$$

4.4.2 Pressure Loss in the First Wall Cooling Channels

	d_h (mm)	l (mm)	k 1) (mm)	d_h/k (-)	c (m/s)	T_{He} (°C)	Re (-)	λ_R (-)	Resistance Numbers [6]	$\Sigma\zeta$	$\Delta p_{\lambda+\zeta}$ (bar)
FW/SW	15.75	2611	0.008	1969	64	273	2.4×10^5	0.0186	inflow SW: 0,10 2 bending radii: 0.137 outflow: 0.59 SW/header	0.827	0.569

1) mean surface roughness during fine milling and two milling operations

4.4.3 Pressure Loss during Inflow to First Wall/Cooling Plate and Reflow from Cooling Plate/Main Pipe

	d_h (mm)	l (mm)	k 1) (mm)	d_h/k (-)	c (m/s)	T_{He} (°C)	Re (-)	λ_R (-)	Resistance Numbers [6]	$\Sigma\zeta$	$\Delta p_{\lambda+\zeta}$ (bar)
Inflow FW/plate	24	213	0.02	850	56	294	3×10^5	0.020	inflow: 0.10 1bend: 90°: 0.07 outflow: 0.49	0.66	0.08
Reflow Plate/ main pipe	24	225	0.02	850	71	450	2.5×10^5	0.021	inflow: 0.10 outflow: 0.49	0.59	0.10

Total: 0.18

4.4.4 Pressure Loss in the Plates with Cooling Channels Integrated

Cooling Zone	$\dot{m}_{He}$ 1) (kg/s)	d_h 2) (mm)	l_{tot} (mm)	k 3) (mm)	d_h/k (-)	c_{He} (m/s)	T_{He} (°C)	Re (-)	λ_R (-)	Resistance Numbers ζ [6]	$\Sigma\zeta$	$\Delta p_{\lambda+\zeta}$ (bar)
1	0.0340	4.92/5.04	1935	0.005	994	75/63	375	6.5×10^4	0.023	inflow: 0.25		1.62
2	0.0300	4.34/4.63	1832	0.016	280	66/57	371	5×10^4	0.030	2x reversals:		1.55
3	0.0294	4.63/4.63	1700	0.025	185	56/56	371	4.5×10^4	0.034	0.30	1.46	1.31
4	0.0262	4.63/4.80	1528	0.025	185	40/37	370	3.3×10^4	0.034	outflow: 0.91		0.54
5	0,0283	4.63/4.80	1325	0.025	185	27/26	372	2.2×10^4	0.035			0.23
6	0.0232	4.63/4.80	2013	0.025	185	22/20	372	$1.8 \cdot 10^4$	0.036	inflow: 0.25 6x reversals: 0.90 outflow: 0.91	2.06	0.25

1) to be adjusted by suitable throttling

2) front part/lateral part

3) by coarse and fine milling with different milling operation

4.4.5 Compilation of the Blanket Pressure Losses for the Outboard

Helium main pipe :	0.617 bar
First wall cooling channels::	0.569 bar
Coolant channels integrated in plates:	1.620 bar
Inflow and reflow connections for cooling plates:	0.180 bar
Total	2.986 bar

The total determined pressure loss of 2.986 bar corresponds to 3.7% of the nominal pressure and is well below the limit of 4.9% according to which the maximum admissible compression pressure ratio of 1.05 must not be exceeded.

5 Design Calculation for the Inboard Blanket Segment

5.1 Thermal Power to be Removed

a) Blanket main part:

Surface power: 40×10^4 W/m^2 · 6.9375 m^2	= 2.775 MW
Volumetric power (breeding zone and steel structure):	= 16.31 MW
Total	= 19.085 MW

b) Shielding:

Volumetric power:	0.30 MW

c) Upper divertor:

Volumetric power (breeding zone)	1.78 MW

d) Lower divertor:

Volumetric power (breeding zone)	1.71 MW
Total	22.875 MW

5.2 Required Helium Mass Flow

The helium mass flow can be determined by the equation:

$$\dot{m}_{He} = \frac{Q}{c_p \cdot \Delta T_{He}} = \frac{Q\,[W]}{5.2x10^3 \frac{J}{kgK} \cdot (450\text{-}250)\,K}$$

with a temperature rise of helium ΔT_{He} of 200 K assumed for all systems.

This leads to the following helium mass flows:

Inboard	total mass flow for two cooling systems [kg/s]	mass flow of each cooling system [kg/s]
a) Blanket main part	18.351	9.175
b) Shielding	0.288	0.144
c) Upper divertor (breeding zone)	1.712	0.856
d) Lower divertor (breeding zone)	1.644	0.822
total	21.995	10.997

5.3 Distribution of Helium Flow in the Center of the Blanket

5.3.1 Thermal Power to Be Removed from a 72 mm Thick Poloidal Layer

Surface power:	30,672 W
at max. 50 W/cm^2	
Volumetric power:	
First Wall/Side Walls	33,960 W
Volumetric power:	
breeding zone	
ceramic (11 mm)	70,153 W
beryllium (45 mm)	62,018 W
two cooling plates (16 mm)	23,612 W
Total	220,415 W

5.3.2 Helium Flow Ratio for First Wall/Cooling Plates

The helium mass flow in a first wall channel and in a cooling plate of an inboard blanket segment can be determined from the eq. (1) through (3) (section 4.3.2),

with $Q_{FW/SW} = 30{,}672 + 33{,}960 = 64{,}632$ W

$Q_{BER/CER} = 70{,}153 + 62{,}018 + 23{,}612 = 155{,}783$ W

This leads to the distribution of helium flows and temperatures represented in the following table:

Inboard	First Wall - Channel	Cooling Plate
$\dot{m}_{He}$ (kg/s)	0.07136	0.10704
$T_{He,\ inlet/outlet}$(°C)	251.0/309.1	309.1/449.0
$T_{m,\ He}$ (°C)	280.1	379.1
ΔT_{He} (K)	58.1	139.9

In this heat power balance the heat exchange between the breeding zone and the First Wall is neglected.

5.4 Helium Pressure Losses

5.4.1 Pressure Loss in the Helium Main Pipes

Position (Fig. 1)	d_h (mm)	l (mm)	k (mm)	d_h/k (-)	c (m/s)	T_{He} (°C)	Re (-)	λ_R (-)	Resistance Numbers ζ [6]	Σζ	$\Delta p_{\lambda+\zeta}$ (bar)
1-2	112	4.000	0.02	5600	140	250	4.0×10^6	0.0125	3bends 1), 90°: 0.206, 2bends, 30°: 0.049 reduction of area: 0.010	0.260	0.514
2-3 2) cold	106	11.000	0.02	5300	96 *	250	2.6×10^6 *	0.128	bend 135 °: 0.105		0.214
3-3 hot	106	11.000	0.02	5300	134 *	450	2.1×10^6 *	0.013		0.105	0.303
3-4	112	4000	0.02	5.600	194	450	2.5×10^6	0.0125	3bends 1), 90°: 0.206 2bends, 30°: 0.044 reduction of area: 0.010	0.260	0.711

Total: 1.742

* Mean over the total manifold length approx.

1) $$\zeta_{bend} = \left[0{,}131 + 0{,}159 \cdot \left(\frac{dh}{R} \right)^{3.5} \right] \cdot \frac{\delta}{180} \cdot$$ *with R:*radius of curvature, *δ:*bending angle.

2) *The pressure loss in the Helium distributors can be determined by the equation:*

$$\Delta p_\lambda = \frac{0.043466 \cdot \eta_{He}^{0.2}}{\rho_{He}} \cdot \frac{\dot{m}^{1.8}}{d_h^{4.8}} \cdot \frac{l}{2}$$

5.4.2 Pressure Loss in the First Wall Cooling Channels

	d_h (mm)	l (mm)	k [1] (mm)	d_h/k (-)	c (m/s)	T_{He} (°C)	Re (-)	λ_R (-)	Resistance Numbers [6]	$\Sigma\zeta$	$\Delta p_{\lambda+\zeta}$ (bar)
FW/SW	15.75	1970	0.008	1969	41	280	1.5×10^5	0.019	inflow SW: 0,10 2 bending radii: 0.140 outflow: 0.59 SW/header	0.83	0.185

1) mean surface roughness during fine milling and two milling operations

Another pressure losses in the cooling plates including the inflow and reflow pressure losses are estimated from the values of the outboard by the law $\Delta p \sim \dot{m}^2$.

5.4.3 Compilation of the Blanket Pressure Losses for the Inboard

Helium main pipe including all distributors:	1.742 bar
First wall cooling channels:	0.185 bar
Coolant channels integrated in plates including all inflow and reflow connections:	0.633 bar
Total	2.560 bar

6 Power Requirements of the Helium Blower

The adiabatic power of a helium blower can be determined with the following equation:

$$P_{ad} = \dot{m} \cdot \frac{\chi}{\chi\text{-}1} \cdot R \cdot T \cdot \left[\left(\frac{p_2}{p_1} \right)^{\frac{\chi\text{-}1}{\chi}} - 1 \right]$$

with the helium gas constants R = 2078.75 J/kgK and $\chi = 5/3$.

The pressure losses in an outboard segment and an inboard segment, as determined in the preceeding chapters, amount to round 3 bar and 2.6 bar, respectively.

Assuming additional pressure losses in the heat exchanger and other components of about 1.0 bar, the total pressure losses in the whole helium loop will be round 4.0 bar in an outboard segment and 3.6 bar in an inboard segment, respectively. With an average system pressure of 80 bar we obtain for the outboard $p_1 = 78.0$ bar, $p_2 = 82.0$ bar and for the inboard $p_1 = 78.2$ bar, $p_2 = 81.8$ bar. For a given helium mass flow of 35.6 kg/s in an outboard segment and 22 kg/s in an inboard segment at T = 513 K the adiabatic blower power amounts to 1.9177 MW in an outboard segment and to 1.0652 MW in an inboard segment. Thus, the total blower power required for the whole reactor will be: (48x1.9177/0.8 + 32x1.0652/0.8) MW = (115.06 + 42.61) MW = 157.67 MW, if a blower efficiency of 0.8 is assumed.

7 2D Computation of the Temperature Distribution for the Outboard

7.1 Finite Element (FE) Network Generation

The computation is made for two dimensions with the help of the finite element computer code ABAQUS [7]. FE network generation [8] is performed with the GRAFEM software [9, 10] of our CAD system. The different loads and boundary conditions can be directly specified for ABAQUS. The data generated in this way are transmitted in ASCII format to the large processor via FZK-LAN.

In Fig. 11 a 2D network model is represented for a sector in the radial-poloidal plane (cf. Fig. 5). The model contains a total of six FW channels and four cooling plates in order to take fully into consideration the countercurrent helium flows in the First Wall and in the cooling plates. It is assumed for the countercurrent helium flows that in the one direction the maximum helium outlet temperature and in the other direction the minimum helium inlet temperature of the respective front section of the cooling channel prevail. The cooling channels passed in this way by "hot" and "cold" helium gas are marked (H) and (C), respectively, in the figure.

7.2 Material Data

7.2.1 Thermal Conductivity

The thermal conductivity for the Li_4Si0_4 pebble bed (0.1 ÷ 0.6 mm dia.) can be determined as a function of the temperature from the following equation [4]:

$$\lambda_{CER}\,[W/mK] = 0.708 + 4.51 \cdot 10^{-4}\ x\ T + 5.66\ x\ 10^{-7}\ x\ T^2 \qquad (9)$$

with T = local pebble bed temperature in [°C].

According to [4] and taking into account the difference in thermal expansion between the pebble bed and the surrounding steel structure, the following relation holds for the beryllium pebble bed with mixed pebble sizes (2 mm dia. + 0.08 ÷ 0.018 mm dia.):

$$\lambda_{BER}\,[W/mK] = 6.235 \cdot \{1 + 353 \cdot [\alpha_{BER} \cdot (T_{m,BER} - 20) - \alpha_{MA} \cdot (T_{m,MA} - 20)]\} \qquad (10)$$

with $T_{m,BER}$ [°C]: mean temperature of the beryllium pebble bed

$T_{m,MA}$ [°C]: mean tempeature of the MANET steel structure

α_{BER} [1/K]: thermal expansion coefficient for beryllium pebble bed (Eq. 11)

α_{MA} [1/K]: thermal expansion coefficient for MANET steel (Eq. 12)

$$\alpha_{BER}\,[1/K] = 8.43\cdot[1+1.36\text{x}10^{-3}\cdot(T_{m,BER}+273) - 3.53\text{x}10^{-7}\cdot(T_{m,BER}+273)^2]\text{x}10^{-6} \qquad (11)$$

$$\alpha_{MA}\,[1/K] = 9.7382\text{x}10^{-6} - 2.2234\text{x}10^{-9}\,(T_{m,MA}+273) + 1.4929\text{x}10^{-11}\,(T_{m,MA}+273)^2 - 1.0185\text{x}10^{-14}\cdot(T_{m,MA}+273)^3 \qquad (12)$$

The values corresponding to Eqs. (9) through (11) have been entered in Tables 2 through 4. A mean containment temperature of 310 °C as in the previous tube coil version has been assumed in determination of the thermal conductivity of the beryllium pebble bed.

The thermal conductivity and the thermal expansion coefficient (according to Eq. 12) as well as further strength characteristics of MANET steel have been compiled in Table 5.

7.2.2 Heat Transfer between Pebble Bed and Steel Wall

The heat transfer coefficient between the Li_4Si0_4 pebble bed and steel wall is assumed to be $0.6\text{x}10^4$ W/m^{2}K [4].

As in the preceding Section 5.2.1, the influence exerted by the differential thermal linear expansion between the pebble bed and the clamping steel structure on the heat transfer coefficient is taken into account with respect to the beryllium pebble bed. Accordingly, a relation [4] can be composed which reads:

$$\alpha_{BER/W}[W/m^2K] = 3308\cdot\{1+383.1\cdot[\alpha_{BER}\cdot(T_{m,BER}-20) - \alpha_{MA}\cdot(T_{m,MA}-20) + \left(\left(1+\frac{\Delta V}{V}\right)^{1/3}-1\right)]\}\cdot[1+9.239\cdot10^{-4}\,T_W] \qquad (13)$$

with $\Delta V/V$ = volume swelling of beryllium under neutron irradiation

T_W[°C] = local wall temperature

For the present calculations the Beginning Of Life (BOL) situation has been considered where the highest pebble bed temperatures are expected, thus $\Delta V/V = 0$. Furthermore the term in T_W for the calculation of the wall heat transfer coefficient α has been neglected to simplify the calculations. This term has not a large effect on α and in any case it is pessimistic to neglect it.

In Table 6 the values are entered which apply to $\alpha_{BER/W}$.

To ease the computational procedure, this heat transfer coefficient will be replaced below by an equivalent reduced thermal conductivity:

$$\frac{s}{\lambda_{red}} = \frac{1}{\alpha_{Kugelsch./St.}} + \frac{s}{\lambda_{St}} \qquad (14)$$

7.2.3 Heat Transfer Coefficient

The general formulation for convective heat transfer reads:

$$q = \alpha \cdot \Delta T \quad [W/m^2] \qquad (15)$$

with α [W/m²K] the heat transfer coefficient, and ΔT [K] the temperature difference between the wall and the coolant.

The determination of α is made using the relation

$$\alpha = \frac{Nu \cdot \lambda}{d_h} \; [W/m^2K] \qquad (16)$$

where Nu [-] means the Nusselt number, λ [W/mK] is the thermal conductivity of helium, and d_h [m] is the hydraulic diameter.

According to [5] the following Nusselt relation holds in our case:

$$Nu = 0.018744 \cdot Re^{0.8} \left(\frac{T_W}{T_E} \right)^{-0.18} \qquad (17)$$

where Re [-] is the Reynolds number, T_W [K] is the wall temperature, and T_E [K] is the inlet temperature.

The Reynolds number can be determined from

$$Re = \frac{c \cdot d_h}{v} = \frac{\dot{m}}{\rho \cdot A} \cdot \frac{d_h}{v} = \frac{\dot{m}}{A} \cdot \frac{d_h}{\eta} \qquad (18)$$

where c [m/s] is the velocity of helium, v [m^2/s] is the kinematic viscosity, ρ [kg/m^3] is the density, A [m^2] is the channel cross section, $\dot{m}$ [kg/s] is the mass flow, and η [kg/m·s] is the dynamic viscosity.

In [5] the temperature dependent relation for λ and η (Eq. 8) of helium is written as

$$\lambda_{He} = 3.623 \times 10^{-3} \cdot T_{He}^{0.66} \ [W/mK] \qquad (19)$$

$$\eta_{He} = 0.4646 \times 10^{-6} \cdot T_{He}^{0.66} \ [kg/m \cdot s] \qquad (20)$$

with T_{He} as the helium temperature in [K].

The data determined in this way have been entered in Table 7.

7.3 Radial Power Distribution

In Figs. 7 to 9 the radial power distributions are represented for steel, ceramic and beryllium. The development of the plots can be described with good accuracy by the following exponential law:

$$q\,[W/cm^3] = a \cdot e^{b \cdot r} \qquad (21)$$

where r is the running radius in [mm]. The factors a and b for the radial segments can be taken from the figures.

7.4 Result of Temperature Calculation

As the thermal conductivity of the beryllium pebble bed and the coefficient of heat transfer between the bed and the steel wall are a function of the mean bed temperature (see Eqs. 10 and 13), they can be determined solely by iterative computations. The beryllium pebble bed is divided radially into four sections. The first section includes the cooling zones 1 through 3 (Fig. 11) and the second section the cooling zones 4 and 5. The two remaining sections are housed in the cooling zone 6. By iterative computation
the following values are obtained for the mean temperature of the beryllium pebble bed:

Section 1 (zones 1 - 3):	553.1 ^{0}C
Section 2 (zones 4 - 5):	516.6 ^{0}C
Section 3 (zone 6, 1st half):	419.4 ^{0}C
Section 4 (zone 6, 2nd half):	406.7 ^{0}C
Whole bed:	468.9 ^{0}C

In this way, the respective material data can be determined from Eqs. 10 to 13. Moreover, the conditions of symmetry are used by setting equal the temperatures of the ceramic bed of the boundary planes of the A - A and D - D sections (Fig. 11a) to that of the C - C mid-plane. On account of the differences in flow routing in the First Wall and in the cooling plates, no "perfect" symmetry actually exists in the First Wall. This can be remedied by making a second computation with exchanged helium flow direction in the First Wall channels

(sequence: H - C - H - C - H - C - H instead of
C - H - C - H - C - H - C).

The temperatures of the C - C mid-plane determined in this way can then be completely transferred to the A - A and D - D boundary planes.

Figure 12 shows the temperature distribution iterated in this way in the front zone undergoing maximum thermal loading. The temperatures are represented as isotherms. The influence exerted by the counter-current helium flows in the cooling plates and in the First Wall can be well recognized by the slightly asymmetric position of the isotherms. The maximum temperature in the ceramic pebble bed is

907 °C, and in the beryllium pebble bed it is 637 °C. The maximum temperature of 515 °C for the First Wall is clearly below the tolerable design value of 550 °C.
In Fig. 13 the radial temperature development is represented for the beryllium pebble bed along the B - B cutting plane (Fig. 11a).
On account of the good thermal conductivity of beryllium and a relatively great thickness of the bed, heat removal through the First Wall down to a radial depth of about 40 mm can be well recognized here. Subsequently, the heat flow gets distributed into the colder rear region.

At the beginning of the cooling zone 6 stronger cooling down due to the still little preheated helium gas can be well recognized. Figure 14 shows the respective transverse temperature plot normal to the cooling plates running along the Y - Y route (Fig. 11a) and crossing the point of the temperature maximum. The temperature difference between the pebble bed and the wall is 29 K at the colder cooling plate and 24 K at the hotter cooling plate.

In Figs. 15 and 16 the corresponding temperature plots are represented for the ceramic pebble bed (C - C route and transverse to it X - X route, Fig. 11a). Here radial extension of the heat exchange with the First Wall is only about 17 mm due to poorer thermal conductivity and lesser thickness of the bed. Then the temperature level is rather constant up to the end of cooling zone 3.

The visible temperature peaks are caused by the uncooled dummy channels. The rear-most cooling channels of cooling zone 6 provide sufficient cooling of the closure plate (5 mm thickness) and the adjacent pebble bed. There is a maximum temperature difference of 24 K between the ceramic pebble bed and the steel wall.

Summarizing, the following results can be indicated:

Maximum temperature

First Wall:	515 ^{0}C
cooling plate:	512 ^{0}C
ceramic:	907 ^{0}C
beryllium:	637 ^{0}C

Maximum temperature difference:

First Wall:	107 K
cooling plate:	25 K

Maximum transition temperature difference:

ceramic pebble bed/steel wall: 24 K

beryllium pebble bed/steel wall: 29 K

Minimum ceramic temperature at the edge of the rear part of the breeding zone (approx. 0.2 % of the total ceramic volume):

between 300 ° and 350 °C, otherwise ≥ 350 °C.

8 Computation of Stress for the Outboard

8.1 Finite Element Model

A Continuum-Generalized-Plane-Strain-Element is used in the two-dimensional stress computation with the ABAQUS code. This element allows the stresses caused in the toroidal direction through differential thermal expansion to be additionally recorded as quasi-three-dimensional stresses. This is done by the integrated boundary condition that the levels of computation and control running parallel to each other remain plane. This so-called boundary condition for inhibition of bending is used in the computation for the cutting planes too. Besides the temperature distributions determined, a maximum loading by the internal pressure of 80 bar is assumed in the computations.

In the computation of stresses the FEM model (Fig. 11) used to compute the temperatures is further employed after elimination of the pebble bed elements. In this way, the distribution of temperatures calculated can be directly transferred to the secondary load case. Figure 17 shows the model of computation used for the steel structures. The points of connection of the cooling plates are assumed to be beam supports with a rigid clamping at about 5 mm spacing from the First Wall. For the left and right cutting planes symmetry and bending obstruction boundary conditions, respectively, are used.

8.2 Material Data and Admissible Limit of Loading

The structural material envisaged for the DEMO reactor is ferretic-martensitic steel 1.4914 (MANET). It excels by a higher strength, a higher thermal shock resistance, and a better swelling behavior compared with austenitic steel (316L). Drawbacks include the more complicated manufacture and the abrupt change in crack toughness below a certain temperature value which means that a minimum service temperature of the structural components is fixed at 250 °C.

The strength values and the thermal expansion coefficient of MANET steel are entered in Table 5 as a function of the temperature. The relatively low thermal expansion coefficient and the relatively high thermal conductivity exert a favorable effect on the thermal stress behavior, which is described by the thermal stress factor σ_T [MPa·m/W]$=\alpha \cdot E/\lambda(1-\nu)$, where α [1/K] is the thermal expansion coefficient, E [MPa] is the Young's modulus, λ [W/mK] is the thermal conductivity, and ν is the Poisson's ratio.

In the evaluation of the stresses reference is made to the rules contained in the ASME Code [12, 13]:

σ_{adm}	=	$1 \cdot S_{m,t}$	for primary membrane stresses ($\sigma_{p,m}$), average taken over the cross section
σ_{adm}	=	$1.5 \cdot S_{m,t}$	for primary membrane plus bending stresses ($\sigma_{p,m+b}$)
σ_{adm}	=	$3 \cdot S_m$	for primary and secondary stresses ($\sigma_{p,m+b} + \sigma_s$)

with $S_m = \min(\frac{2}{3} \cdot \sigma_{0.2}, \frac{1}{3} \cdot \sigma_u)$ und $S_{m,t} = \min(S_m, \frac{2}{3} \cdot \sigma_{R,t}, 1 \cdot \sigma_{1,t})$.

The symbols have the follwing meanings: $\sigma_{0.2}$ is the offset yield strength, σ_u is the ultimate tensile strength, $\sigma_{R,t}$ is the creep rupture strength, $\sigma_{1,t}$ is the 1% creep strain limit, and t is the time to failure, with $t = 2 \times 10^4$ h for steady-state operation of DEMO. The equivalent stress intensity used in the comparison with the admissible stress (σ_{adm}) is the von Mises stress derived according to the yielding criterion:

$$\sigma_v = \sqrt{\frac{(\sigma_1-\sigma_2)^2 + (\sigma_2-\sigma_3)^2 + (\sigma_3-\sigma_1)^2}{2}} \qquad (22)$$

where σ_1, σ_2, σ_3 are the principal stresses. The primary and secondary stresses are superposed at the stress component level.

The dependence of the strength characteristic S_m on the temperature and creep rupture strength is evident from Table 5. For a DEMO-specific lifetime of $2x10^4$ h the S_m value noticeably decreases above 500 °C. For instance, at 550 °C it is 98 MPa and at 600 °C it is still only 41 MPa.

8.3 Result of Stress Computation

It is assumed in stress computation that the differential thermal expansions of cooling plates with respect to each other is accommodated by the softer rear closure plate.

For the First Wall proper only the loads exerted by the internal pressure and the temperature distribution within the wall, as represented in Fig. 18, will apply.

A distinction is made between the following cases:

(a) Normal operation with 80 bar loading by internal pressure in the cooling channels and 1 bar in the interior of the blanket.

b) Accident due to 80 bar loading by internal pressure in the entire blanket.

Figures 19 and 20 show for case (a) the reference stress values for the internal pressure load case (primary stress) and for the internal pressure plus temperature load case (primary plus secondary stresses). The maximum primary membrane plus bending stresses of 56 MPa are still well below the 300 MPa limit corresponding to the temperature. In the case of superimposed loads, also the maximum stress of 311 MPa is far below the tolerable limit of 494 MPa.

Figures 21 and 22 make visible similar results of computation for case (b). In Fig. 21 a clearly higher maximum primary stress compared to case (a) can be recognized. However, the maximum value of 131 MPa is still far below the tolerable limit. In case of superimposed loads, the maximum stress is 361 MPa. Also in this case the safety margin with respect to the tolerable limit is still adequate.

9 3D Temperature und Stress Calculation for the Outboard Blanket Box

9.1 Generation of the 3D Finite Element Model

In the following computations the ABAQUS Finite Element computer code [7] will be used. To generate the three-dimensional (3D) network [8], the CAD system BRAVO3 [9, 10] will be referred to. For this, the GRAFEM program package will be used which, being a part of the graphics editor, is available in the BRAVO3 system.

First, the editor generates the wire models of the components to be computed which models are needed as initial geometries for generating the three-dimensional network using GRAFEM. At the same time, the geometrical model is converted into a mathematical model by dividing the object into a multitude of nodes and elements which have to be interconnected.

Several mapping techniques of the GRAFEM software can be used for network generation, which will be done by the following steps.

- Generation of boundary lines by having coincide individual circuits of algebraic curves of the wire model.
- Generation of surfaces/planes, which are defined by an external and, maybe, several internal boundary lines.
- Generation of volumes/bodies defined by 12 boundary lines.
- Generation of nodes with variable densities on the boundary lines.
- Generation of the network of solid elements, starting from a plane or a volume.

Thus, the geometric features of the Finite Element models are described if the nodes and elements have been designated and their mutual assignments interconnected; their locations are determined by the x/y/z coordinates. Each element is provided in addition with information, e. g. address, type, material, etc.

In the next step the various loadings and their boundary conditions are specified which have to be assigned to individual groups of nodes and elements. GRAFEM supports data formats of several Finite Element codes, e. g. ABAQUS in the case considered here.

Figure 23 shows the CAD generated Finite Element model. For reasons of symmetry, only half of the radial toroidal blanket cross section is used. In poloidal direction the model is given a total height of 36 mm corresponding to 1.5 x the channel pitch. In radial direction the model reaches up to the the rear wall of the helium main pipework system. The rear solid steel shielding, with autonomous cooling, is neglected for the sake of simplicity. It is supposed that the mean temperature of the steel shielding is kept at approximately the same level as that of the rear blanket part by a type of cooling still to be defined so that no additional relative thermal stress wil be generated.

For reasons lying in the procedure of computation, the thickness of the coolant plate with coolant channels integrated must be smeared from 8 mm to the 5.1 mm thickness of a solid steel plate. In this way, the same loading cross-section of the globally mainly tensile loaded coolant plates is maintained. The connecting pipes at the inlet and outlet of the coolant plate are also simplified by equivalent square profiles.

9.2 Computation of Temperature Distribution in the Steel Structure

The determination of thermal stresses in the blanket box calls for knowledge of the temperature differences among the individual structural components. In a coarse estimate of stresses an assumption made on the mean temperature of the First Wall, of the side walls and of the rear blanket segment would already be sufficient. Instead, a detailed temperature distribution in the steel structure will be assessed below in order to record also the local influence exerted by the maximum temperature in the front First Wall. In this procedure the radial power density distribution in steel (Fig. 7) is assumed.

For reasons lying in the computational procedure the pebble beds cannot be taken into account in addition in this model of computation. The contact temperature on the rear side of the First Wall with the pebble beds must therefore be estimated from the results obtained in the preceeding chapters. According to this estimation, it is on the average about 400 °C for the front radial zone of 200 mm length and about 325 °C, respectively, for the rest. Also, a mean temperature of 400 °C, in accordance with the results of the chapter 7, is assumed for the whole coolant plate.

On account of heat exchange with the pebble bed the helium enthalpy rise in the channels of the First Wall, determined before, must be corrected as well to a higher value in order to obtain the proper results. As an exact power balance cannot yet be made - it would call for much more comprehensive computations - the 49 K enthalpy rise known from the earlier tube coil version (see appendix) will be referred to below. Compared with this result, this value is higher by 5.7 K. Thus, in a first approximation, the following helium temperatures of the First Wall and side wall channel sections with the corresponding heat transfer coefficients α are obtained:

Outboard	Mean He-Temperature [°C]	α [W/m2K]
First Wall		
- top channel (hot)	286	5314
- bottom channel (cold)	266	5314
Side wall		
- top channel (hot)	297	5314
- bottom channel (cold)	254	5314
He main pipes		
- inlet channel	251	5266
- outlet channel	449	4866

9.3 Results

Figures 24 through 27 show the temperature distributions calculated for the central and side zones of the First Wall and for the rear zones accommodating the helium gas header and the helium main pipes. The maximum FW temperature is 519 °C (Fig. 7). Taking into account the helium enthalpy rises as corrected here, it agrees rather well with the 2D result in [7.4]. In the zone of the gas header the temperature is 300 °C. The maximum temperature at the He main outlet pipe is 493 °C (Fig. 27).

Figures 28 through 30 show the von Mises primary stresses calculated for the corresponding First Wall zones and for the He header zone. The deformation of the components resulting from 80 bar internal pressure loading of the blanket is represented with a multiplication factor of 50. Accordingly, the maximum primary

membrane stress in the First Wall is found to be 95 MPa at a mean temperature of 454 °C. This is well below the admissible value of 178 MPa. The maximum primary membrane plus bending stresses attain 80 MPa on the plasma facing wall having a maximum temperature of 520 °C and is thus well below the admissible limit of 180 MPa. A higher stress peak of 127 MPa in the FW coolant channel is also well below the 300 MPa limit on account of the low wall temperature.

The absolute maximum value of the primary stresses determined in the Helium header zone is 189 MPa for the primary membrane stress and 258 MPa for the primary membrane plus bending stresses. Also these stresses are still far below the admissible values of 227 MPa and 341 MPa, respectively. In the zone of the He main pipes only little stresses, 75 MPa at the maximum, are measured which are far below the limit value.

The corresponding primary plus secondary stresses have been represented in Figs. 31 through 34. In the front First Wall zone the maximum stress attains 332 MPa (Fig. 32) which is far below the admissible limit of 452 MPa corresponding to the respective temperature. The rest of maximum stresses occurring in the rear box zone, e. g. in the He header zone, 487 MPa (Fig. 33) and in the zone of the He main pipes, 382 MPa (Fig. 34) are also noticeably below the admissible limit.

The results of computation have been compiled in Table 8. The minimum safety factor $f_\sigma = \sigma_{adm}/\sigma_{max}$ is found to be 1.20 in the He header zone. Accordingly, the maximum admissible internal pressure for the blanket box results from linear extrapolation to be 96 bar.

10 Summary of Main Design Data

A) **Thermohydraulics**	outboard segment	inboard segment
First wall heat flux [MW/m^2]		
- maximum	0.5	0.5
- average	0.4	0.4
Max. power density [MW/m^3]		
- MANET	25	22
- ceramic	37	33
- beryllium	15	12
Helium cooling:		
- total Power to be extracted (nuclear-power + surface heat flux) [MW]	36	23
- pressure [MPa]	8	8
- temperature inlet/outlet [°C]	250/450	250/450
- mass flow rate [kg/s]	35.6	22
- max. velocity in cooling channels [m/s]	75	50
- pressure drop in segment [MPa]	0.3	0.26
- total pressure drop in the whole helium loop, approx. [MPa]	0.4	0.36
- max. temperature [°C]		
. First Wall	520	510*
. ceramic	910	890 *
. beryllium	640	600 *
. interface ceramic/steel	550	545*
. interface beryllium/steel	500	495*
- minimum temperature in ceramic pebble bed [°C]	300	300*
- blower performance, adiabatic ** [MW] (total for one reactor: 158 MW)	2.40	1.33

*) estimated.
**) blower efficiency of 80 % is assumed.

B) **Mechanical stresses in outboard segment, calculated for maximum surface heat load**	
Boundary conditions:	
- internal pressure [MPa]	8
- FW surface heat load [MW/m^2], average/maximum	0.4/0.5
Max. FW temperature [°C], at external plasma side of FW	520
von Mises stresses [MPa]:	
- primary membrane (helium header)	189
limit given by ASME	227
- primary membrane + bending (helium header)	258
limit given by ASME	341
- primary + secondary (external plasma side of FW)	332
limit given by ASME	452
max. allowable internal pressure in the segment box during operation (extrapolated) [MPa]	9.6

11 References

[1] M. Dalle Donne et al.
Conceptual Design of a Helium Cooled Solid Breeder Blanket Based on the Use of a Mixed Bed of Beryllium and Li_4Si0_4 Pebbles
Proc. 17th SOFT, Roma, 14.-18. Sept. 1992, Vol. 2, 1326.

[2] M. Dalle Donne, U. Fischer, P. Norajitra, G. Reimann, H. Reiser
European DEMO BOT Solid Breeder Blanket: The Concept Based on the Use of Cooling Plates and Beds of Beryllium and Li_4Si0_4 Pebbles
18th SOFT, Karlsruhe, 22.-26. August 1994.

[3] U. Fischer
Die neutronenphysikalische Behandlung eines (d,t)-Fusionsreaktors nach dem Tokamakprinzip (NET)
KfK 4790, Oktober 1990.

[4] M. Dalle Donne, et al.
Heat Transfer and Technological Investigations on Mixed Beds of Beryllium and Li_4Si0_4 Pebbles
Proc. ICFRM 6, Stresa, Italy, 27. Sept.-1. October 1993.

[5] M. Dalle Donne, S. Dorner, S. Taczanowski
Conceptual Design of Two Helium Cooled Fusion Blankets (Ceramic and Liquid Breeder) for INTOR
KfK 3584, August 1983.

[6] W. Kalide
Einführung in die technische Strömungslehre
Carl Hanser Verlag, München, 1971.

[7] Hibbitt, Karlsson Sorensen
ABAQUS User's Manual Version 4.9, Providence, R.I., USA.

[8] P. Norajitra, K. Müller
Internal KfK report, October 1994, unpublished.

[9] BRAVO3 GRAFEM User's Guide
Document No. A-22240-003
Applicon/Schlumberger, May 1984.

[10] BRAVO3 GRAFEM Command Reference Guide
Document No. 23718-006, Revision A, October 1989
Schlumberger CAD/CAM, Michigan, USA.

[11] K. Ehrlich
Internal KfK report, May 1986, unpublished.

[12] ASME Code III, edition 1986.

[13] E. Zolti, et al.
Interim Structural Design Criteria for Predesign of the NET Plasma Facing Components
NET/IN/86-14, March 1986.

12 Nomenclature

A [m^2]	flow cross section
A_o [m^2]	surface
α [W/m^2K]	heat transfer coefficient
α_{EXP} [1/K]	thermal linear expansion coefficient
b [mm]	cooling channel width
c [m/s]	velocity
c_p [J/kgK]	specific heat capacity
Δ_p [bar]	pressure drop
ΔT [K]	enthalpy rise
d_h [m]	hydraulic diameter
k [-]	pipe roughness
l [m]	length
λ [W/mK]	thermal conductivity
λ_R [-]	pipe friction coefficient
$\dot{m}$ [kg/s]	mass flow
Nu [-]	Nusselt number
η [kg/ms]	dynamic viscosity
p [bar]	pressure
Re [-]	Reynolds number
q [W/m^3]	heat source density
$q_{surface}$ [W/m2]	surface heat flow density
Q [W]	heat flow
T [K]	temperature
ρ [kg/m^3]	density
[°C]	temperature
v [m^2/s]	kinematic viscosity

Subscripts:

BER	beryllium
CER	ceramic
FW	First Wall
He	helium
λ	pipe friction
MA	MANET
max	maximum
SW	side wall
tot	total
ζ	flow resistance

Table 2:
Thermal conductivity of the Li_4Si0_4 pebble bed according to Eq (9).

T [°C]	λ [W/mK]
300	0.89
350	0.94
400	0.98
450	1.03
500	1.07
550	1.13
600	1.18
650	1.24
700	1.30
750	1.36
800	1.43
850	1.50
900	1.57
950	1.65
1000	1.72

Table 3:
Thermal conductivity of the beryllium pebble bed according to Eq (10).

$T_{m,BER}$ [°C]	λ [W/mK] at $T_{m,MA}$ =	
	310 °C	350 °C
350	9.4	8.2
400	11.3	10.1
450	13.2	12.1
500	15.3	14.1
550	17.4	16.2
600	19.5	18.4
650	21.7	20.6
700	24.0	22.8

Table 4: Thermal linear expansion coefficient of beryllium pebble bed and steel according to Eqs. (11) and (12)

T [°C]	α/20 °C x10-6 [1/K]	
	Be Bed	MANET
300	14.02	11.45
350	14.42	11.68
400	14.80	11.90
450	15.16	12.09
500	15.51	12.24
550	15.85	12.34
600	16.17	12.40
650	16.48	12.40
700	16.77	12.33
750	17.04	12.18

Table 5: Material data for 1.4914 steel (MANET) [11]

T [°C]	λ [W/mK]	E x10³ [MPA]	ν [-]	α_{EXP}/20 °C x10⁻⁶ [1/K]	$\sigma_{0.2}$ 1) [MPa]	σ_u 2) [MPa]	Sm [MPa]	$S_{m,2x10^4h}$ [MPa]
20	24.2	217	0.27	10.11	614	773	258	258
50	24.4	215	0.27	10.23	619	773	258	258
100	24.7	213	0.28	10.46	623	767	256	256
150	24.9	209	0.28	10.70	621	755	252	252
200	25.2	206	0.28	10.95	612	737	246	246
250	25.4	202	0.28	11.20	597	712	237	237
300	25.6	199	0.28	11.45	575	681	227	227
350	25.7	195	0.29	11.68	548	644	215	215
400	25.9	190	0.29	11.90	513	600	200	200
450	26.0	186	0.30	12.09	473	550	183	183
500	26.2	181	0.30	12.24	426	494	165	135
550	26.3	176	0.30	12.34	373	431	144	98
600	26.5	171	0.31	12.40	313	362	121	41

1) corresponds to designation $R_{p0,2}$ according to DIN 50145

2) corresponds to designation R_m according to DIN 50145

Table 6: Coefficient of heat transfer between beryllium pebble bed and steel wall according to Eq. (13)

$T_{m,BER}$ [°C]	$\alpha_{Be/W}$ x10⁴ [W/m²K] at $T_{m,MA}$ =	
	310 °C	350 °C
350	0.51	0.45
400	0.62	0.55
450	0.73	0.67
500	0.85	0.79
550	0.97	0.91
600	1.10	1.03
650	1.22	1.16
700	1.35	1.29

Table 7: Thermohydraulics data for the First Wall and coolant channels integrated in the plate in the middle zone of the outboard blanket.

Zone [1]		T_{He} [°C] Inlet	T_{He} [°C] Outlet	$T_{m,He}$ [°C]	$T_{m,W}$ [°C]	$\dot{m}$ [kg/s]	d_h x10^{-3} [m]	A x10^{-6} [m^2]	ρ_{He} [kg/m^3]	η_{He} x10^{-5} [kg/ms]	γ_{He} x10^{-6} [m^2/s]	c_{He} [m/s]	Re x10^{-5} [-]	Nu [-]	α [W/m^{2}K]
FW/SW	l	251.0	254.1	252.5	278	0.11405	15.75	252	7.32	2.902	3.964	61.8	2.456	381.3	5479
	m	254.1	291.2	272.6	398	0.11405	15.75	252	7.05	2.975	4.219	64.2	2.396	360.8	5314
	r	291.2	294.3	292.7	318	0.11405	15.75	252	6.80	3.047	4.480	66.6	2.340	362.1	5463
Cooling zone 1	l	294.3	319.4	306.9	332	0.0340	5.04	81.6	6.64	3.097	4.667	62.8	0.678	135.8	6509
	m	319.4	430.7	375.0	500	0.0340	4.92	76.8	5.94	3.332	5.613	74.6	0.654	126.2	6664
	r	430.7	455.8	443.2	468	0.0340	5.04	81.6	5.37	3.560	6.627	77.6	0.590	117.1	6452
2	l	294.3	318.5	306.4	331	0.0300	5.06	82.8	6.64	3.095	4.661	54.6	0.593	122.0	5814
	m	318.5	422.4	370.5	495	0.0300	5.06	82.8	5.98	3.317	5.547	60.6	0.553	110.5	5646
	r	422.4	446.6	434.5	460	0.0300	5.06	82.8	5.44	3.531	6.493	66.6	0.520	106.0	5766
3	l	294.3	314.0	304.2	329	0.0294	4.63	88.0	6.67	3.087	4.631	50.1	0.501	106.7	5548
	m	314.0	426.9	370.4	495	0.0294	4.63	88.0	5.98	3.317	5.547	55.9	0.467	96.4	5386
	r	426.9	446.7	436.7	462	0.0294	4.63	88.0	5.42	3.538	6.527	61.6	0.437	92.3	5501
4	l	294.3	310.7	302.5	327	0.0262	4.80	120.0	6.69	3.081	4.609	32.7	0.340	78.3	3920
	m	310.7	429.5	370.1	495	0.0262	4.63	110.0	5.98	3.315	5.541	39.8	0.333	73.6	4109
	r	429.5	445.8	437.6	463	0.0262	4.80	120.0	5.41	3.541	6.541	40.3	0.296	67.5	3886
5	l	294.3	302.0	298.1	323	0.0283	4.80	192.0	6.74	3.066	4.551	21.9	0.231	57.5	2864
	m	302.0	441.4	371.7	497	0.0283	4.63	176.0	5.97	3.321	5.565	26.9	0.224	53.7	3001
	r	441.4	449.1	445.2	470	0.0283	4.80	192.0	5.36	3.566	6.658	27.5	0.198	49.0	2837
6	l	294.3	348.2	321.2	346	0.0232	4.80	192.0	6.47	3.147	4.861	18.7	0.184	47.7	2439
	m	348.2	394.8	371.5	496	0.0232	4.63	176.0	5.97	3.320	5.562	22.1	0.184	45.8	2560
	r	394.8	448.7	421.7	447	0.0232	4.80	192.0	5.54	3.489	6.300	21.8	0.166	42.7	2423

1) l = left hand lateral part; m = front central part; r = right hand lateral part

Table 8: Computed von Mises Stresses in the outboard blanket box

Zone	max. Temp. [°C]	Max. Primary Stresses [MPa]						Max. Primary plus Secondary Stresses [MPa]		
		Membrane Stress			Membrane plus Bending Stresses					
		σ_{max}	σ_{adm}	f_σ[1)]	σ_{max}	σ_{adm}	f_σ	σ_{max}	σ_{adm}	f_σ
First Wall	519	95	178	1.87	127	300	2.36	332	452	1.36
He header	310	189	227	1.20	258	341	1.32	487	681	1.40
He main pipes	493	67	173	2.58	75	260	3.47	382	516	1.35

1) $f_\sigma = \sigma_{adm}/\sigma_{max}$

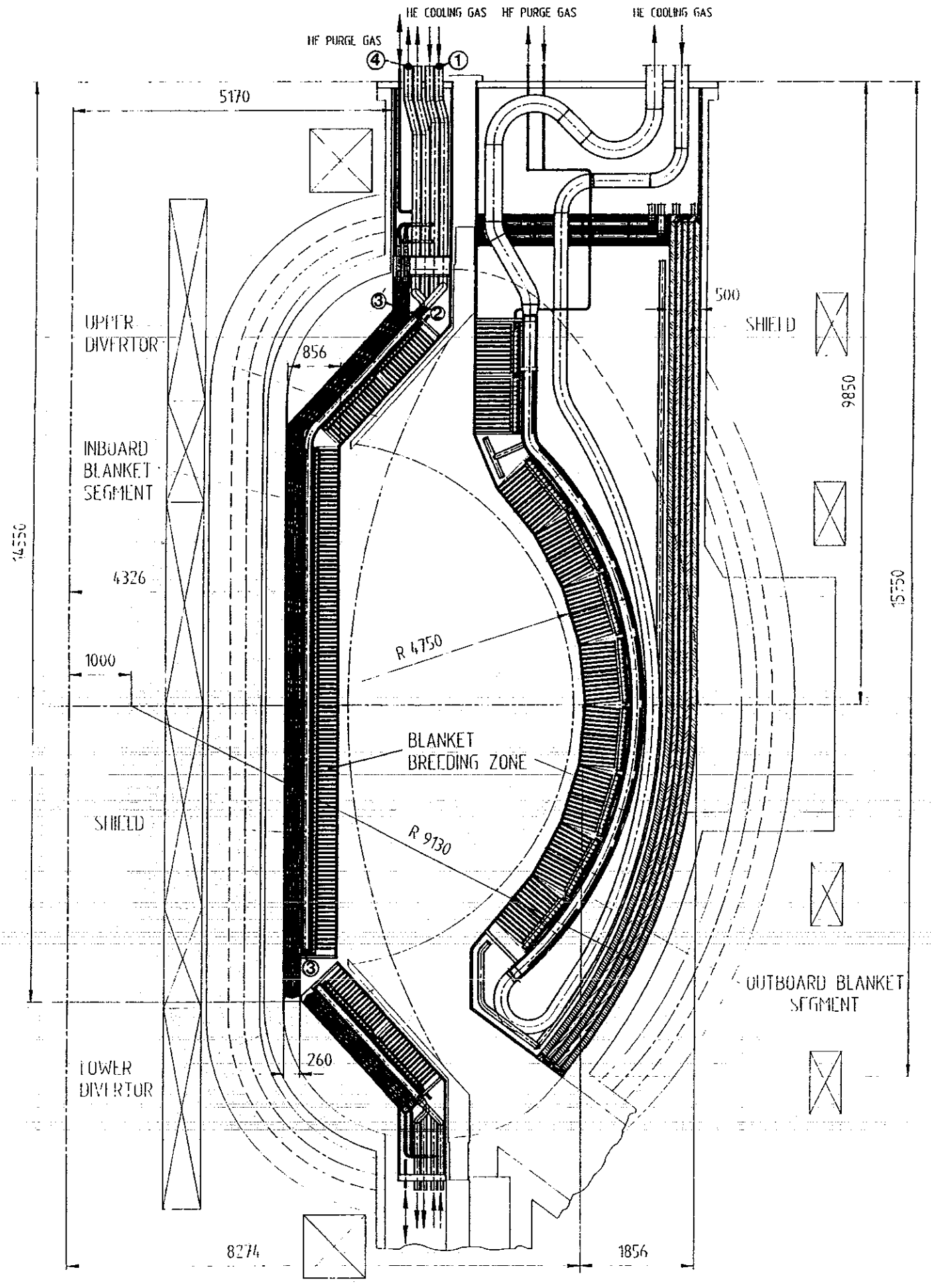

Fig. 1 : Radial-poloidal section through the torus.

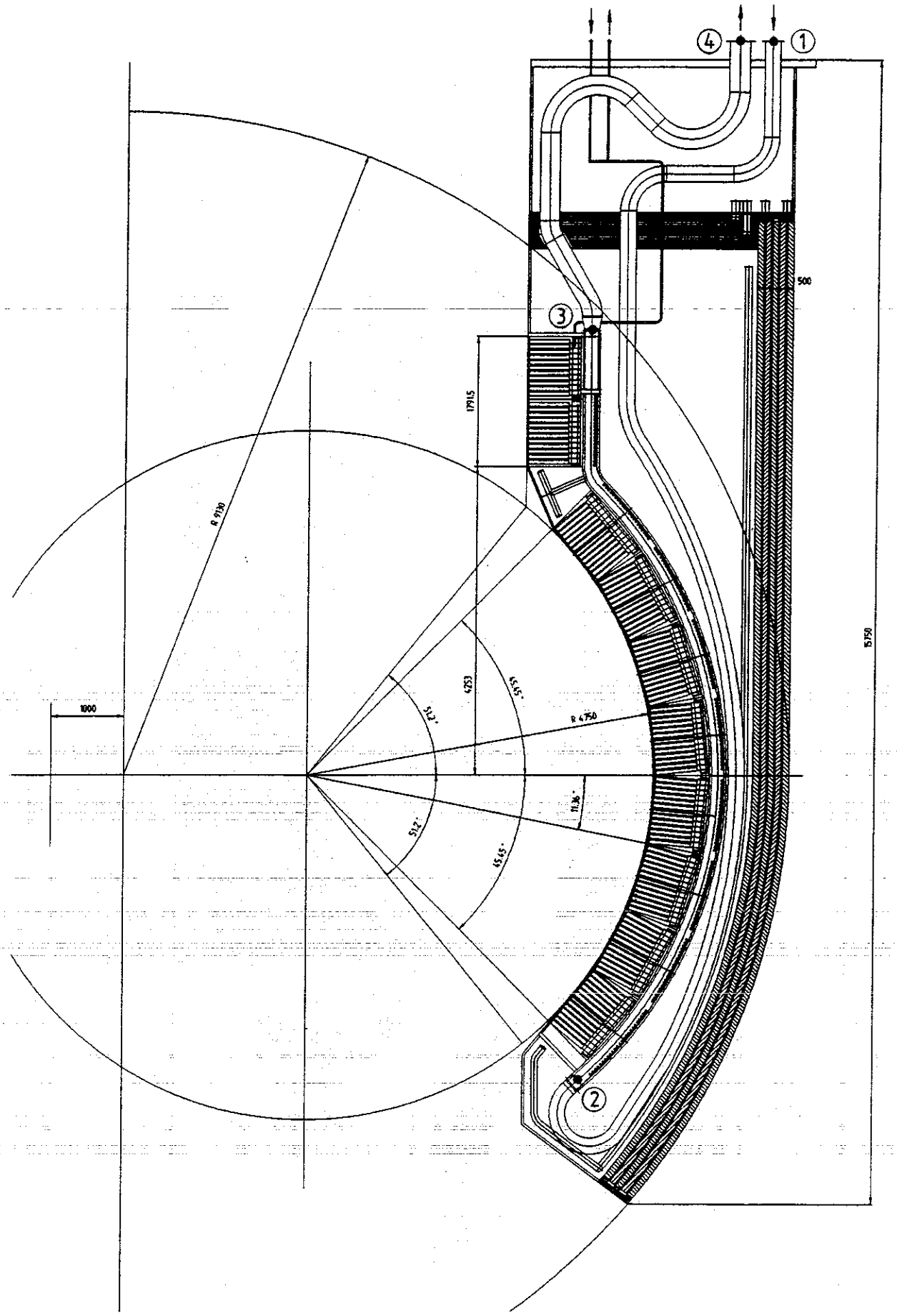

Fig. 2: Radial-poloidal section through an outboard segment.

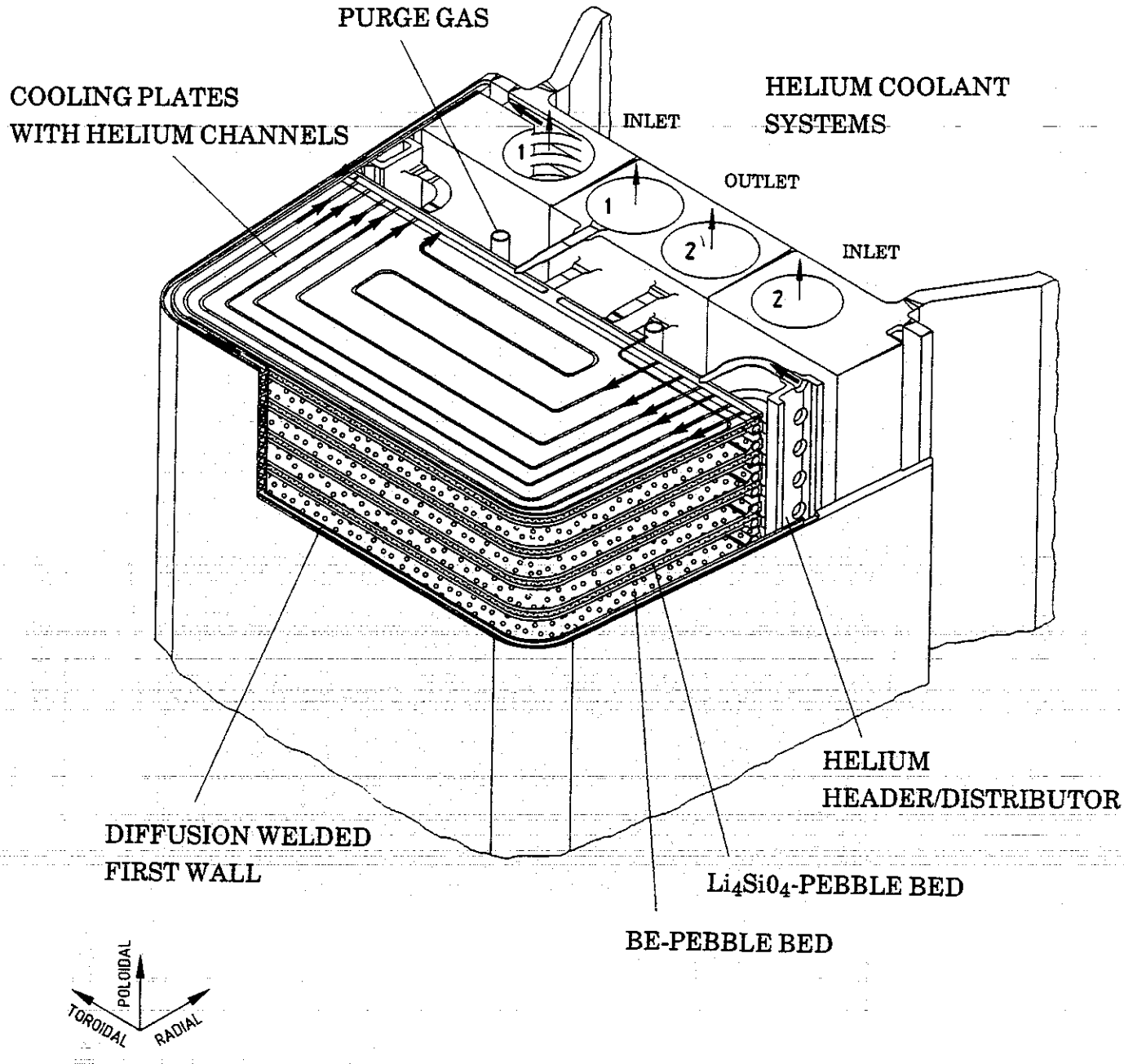

Fig. 3: Layout of an outboard segment in an isometric representation (detail from the central torus zone).

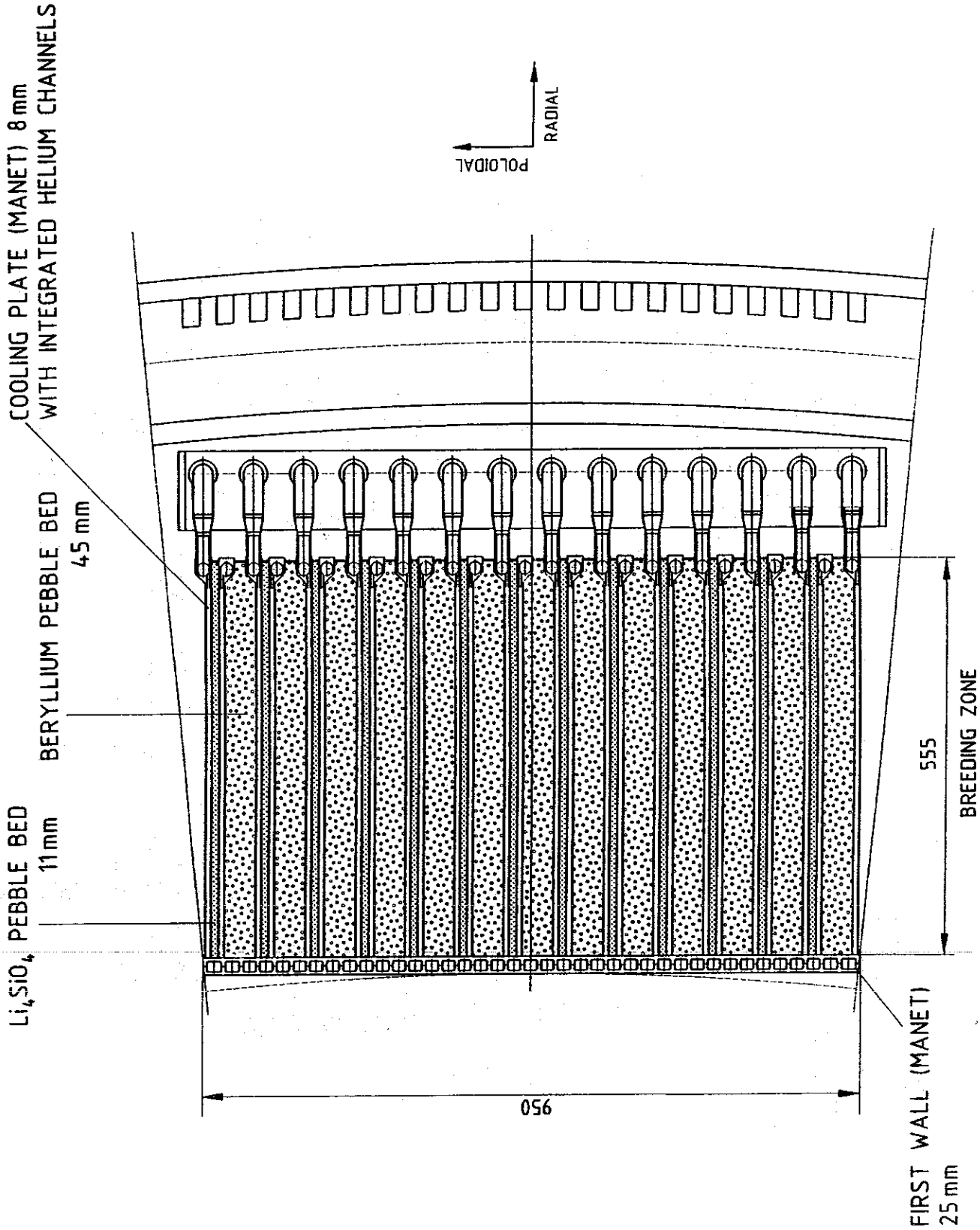

Fig. 4: Radial-poloidal section through the median zone of an outboard segment.

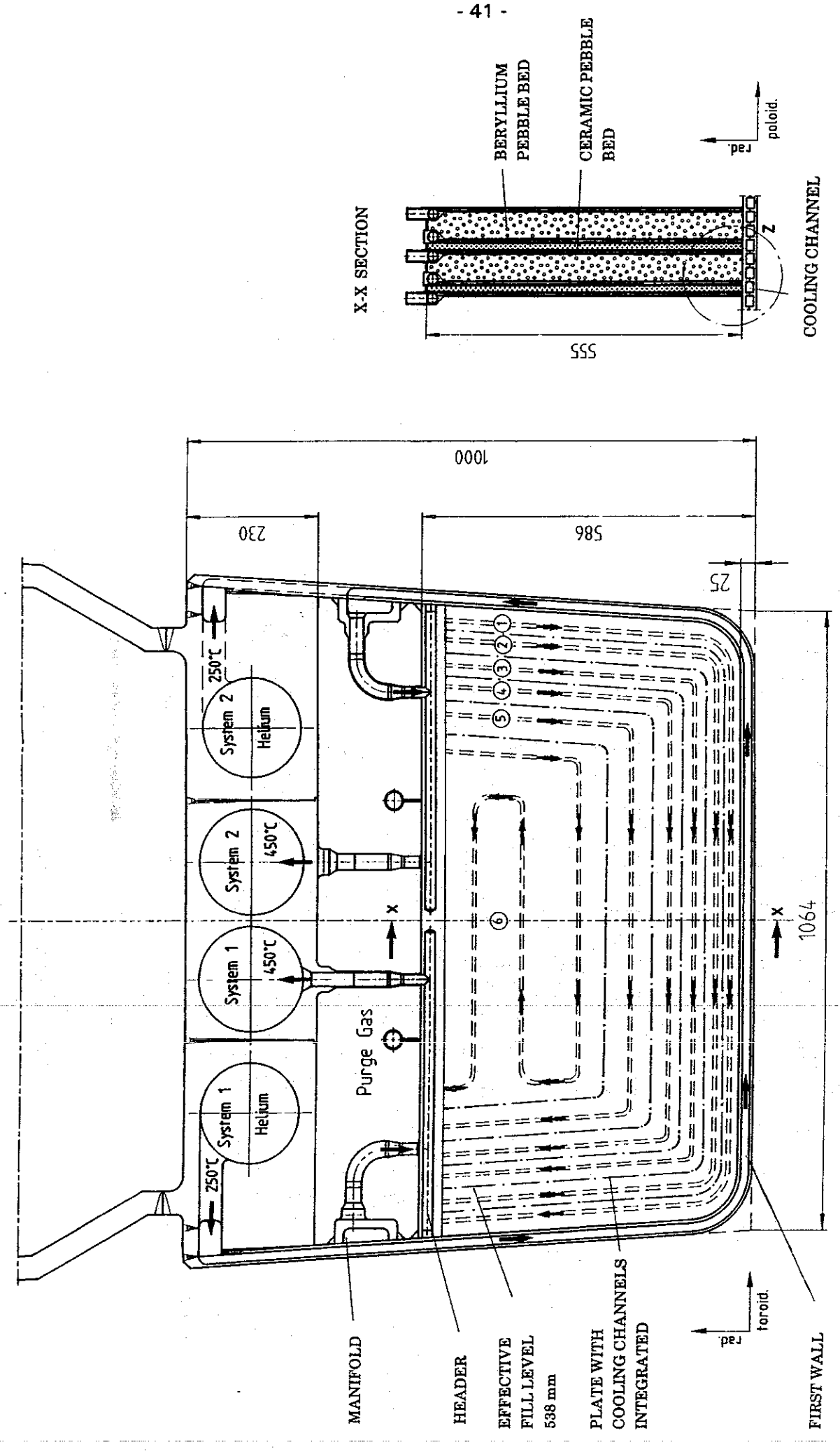

Fig. 5: Radial-toroidal cross section of an outboard blanket segment in the center of the torus.

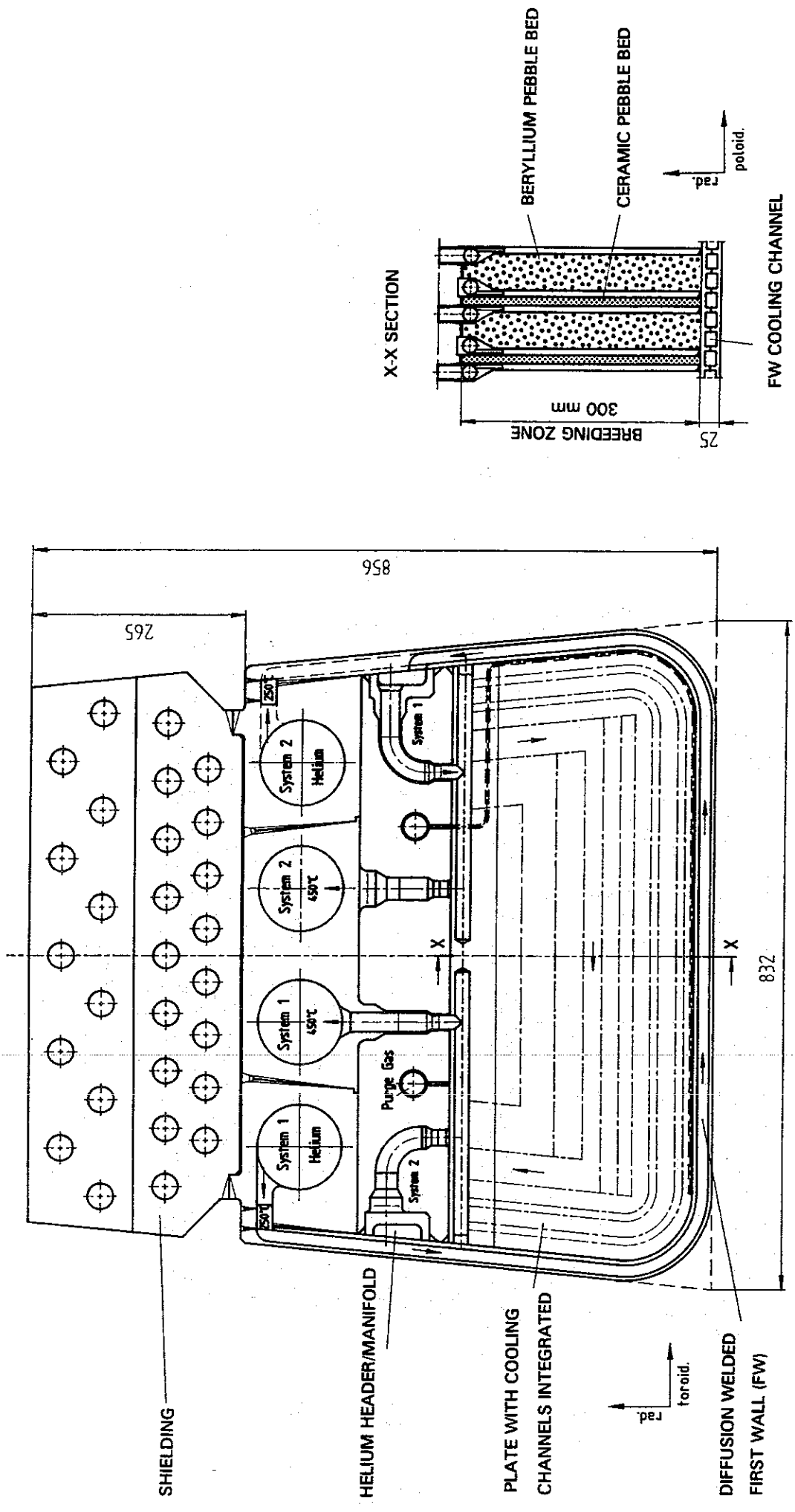

Fig. 5a: Radial-toroidal cross section of an inboard blanket segment in the center of the torus.

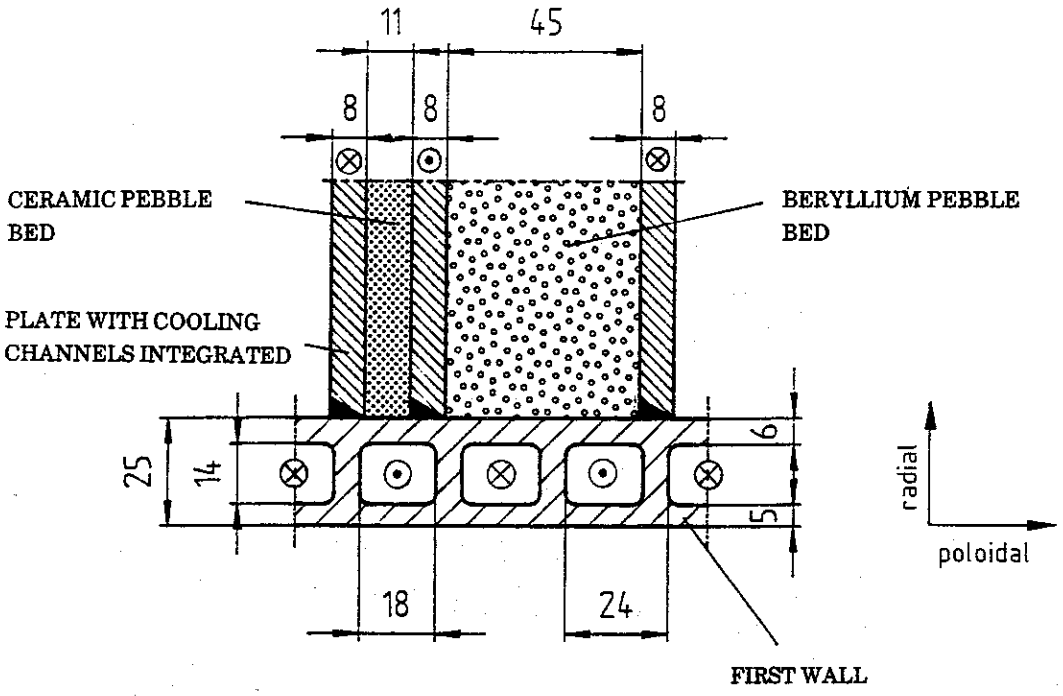

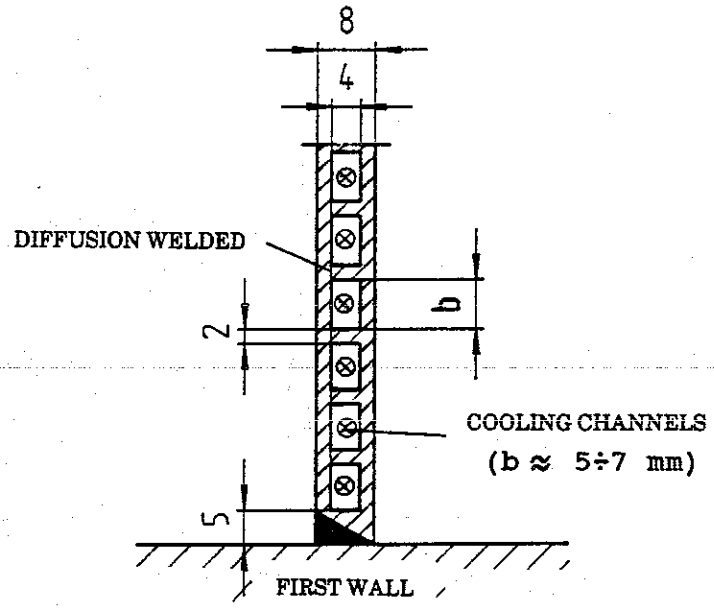

DETAIL - PLATE

Fig. 6: Arrangement of cooling channels in the First Wall and in the cooling plates.

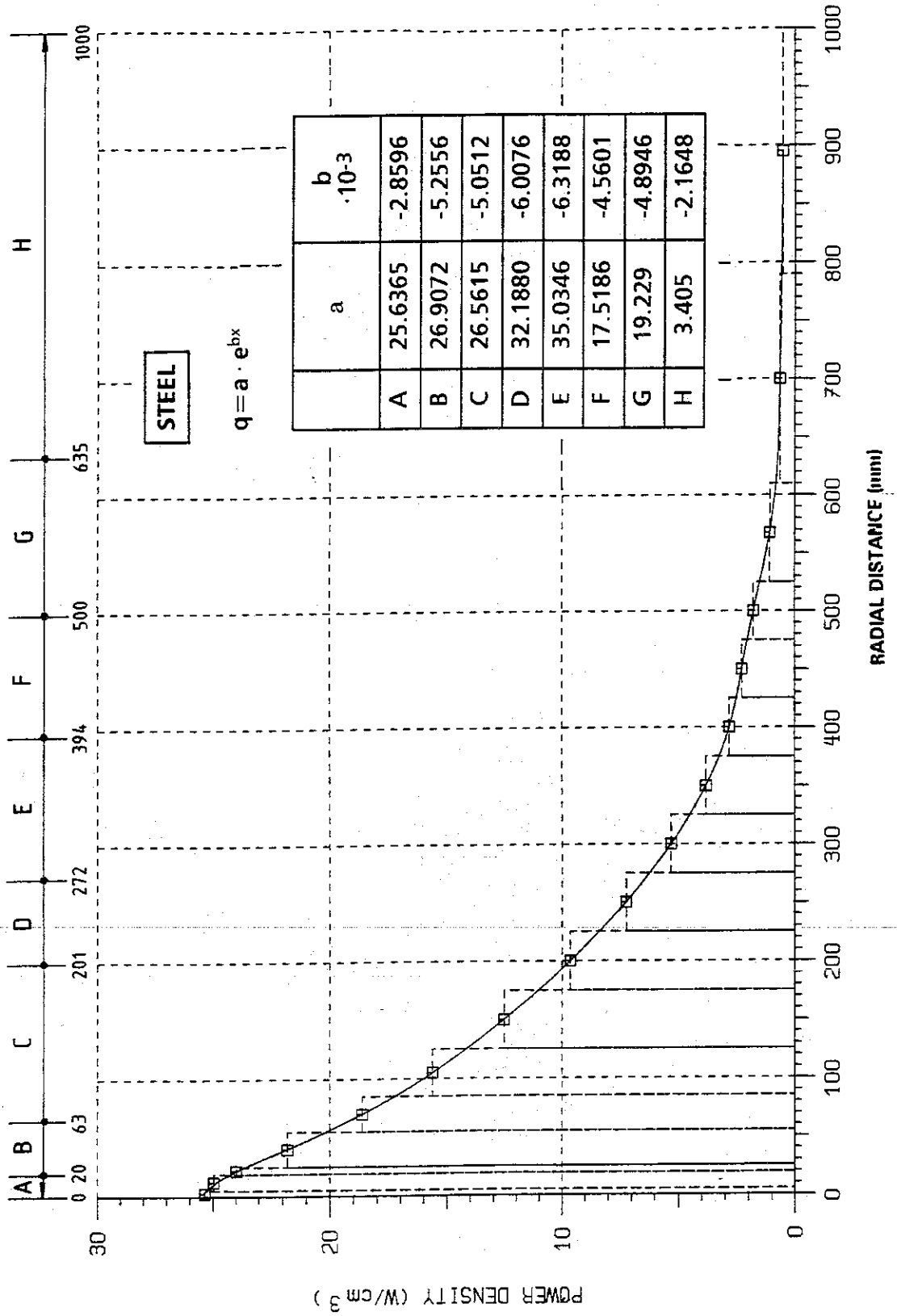

	a	b ·10⁻³
A	25.6365	-2.8596
B	26.9072	-5.2556
C	26.5615	-5.0512
D	32.1880	-6.0076
E	35.0346	-6.3188
F	17.5186	-4.5601
G	19.229	-4.8946
H	3.405	-2.1648

Fig. 7: Radial distribution of power densities in steel in the center of the torus.

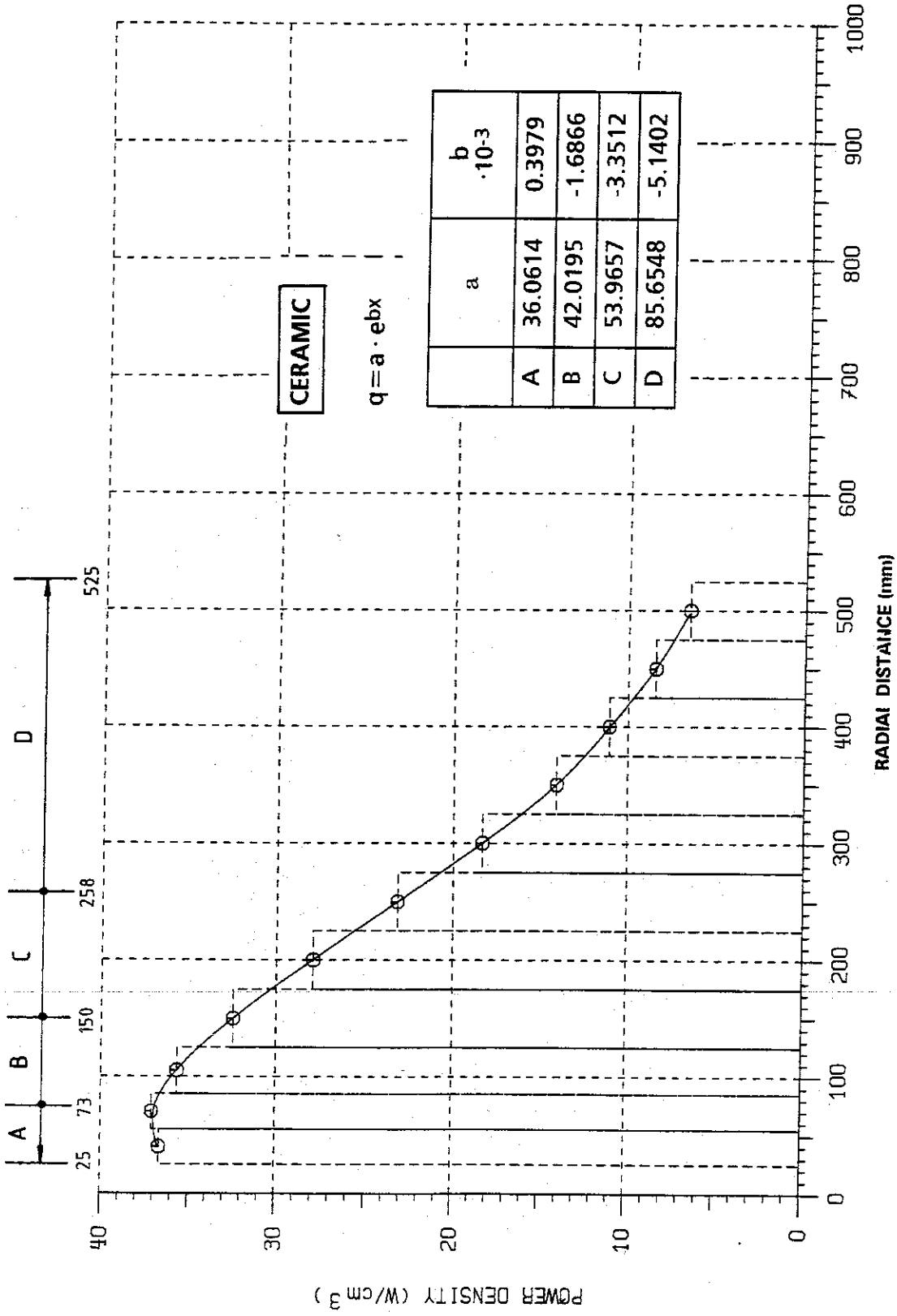

Fig. 8: Radial distribution of power densities in the ceramic in the center of the torus.

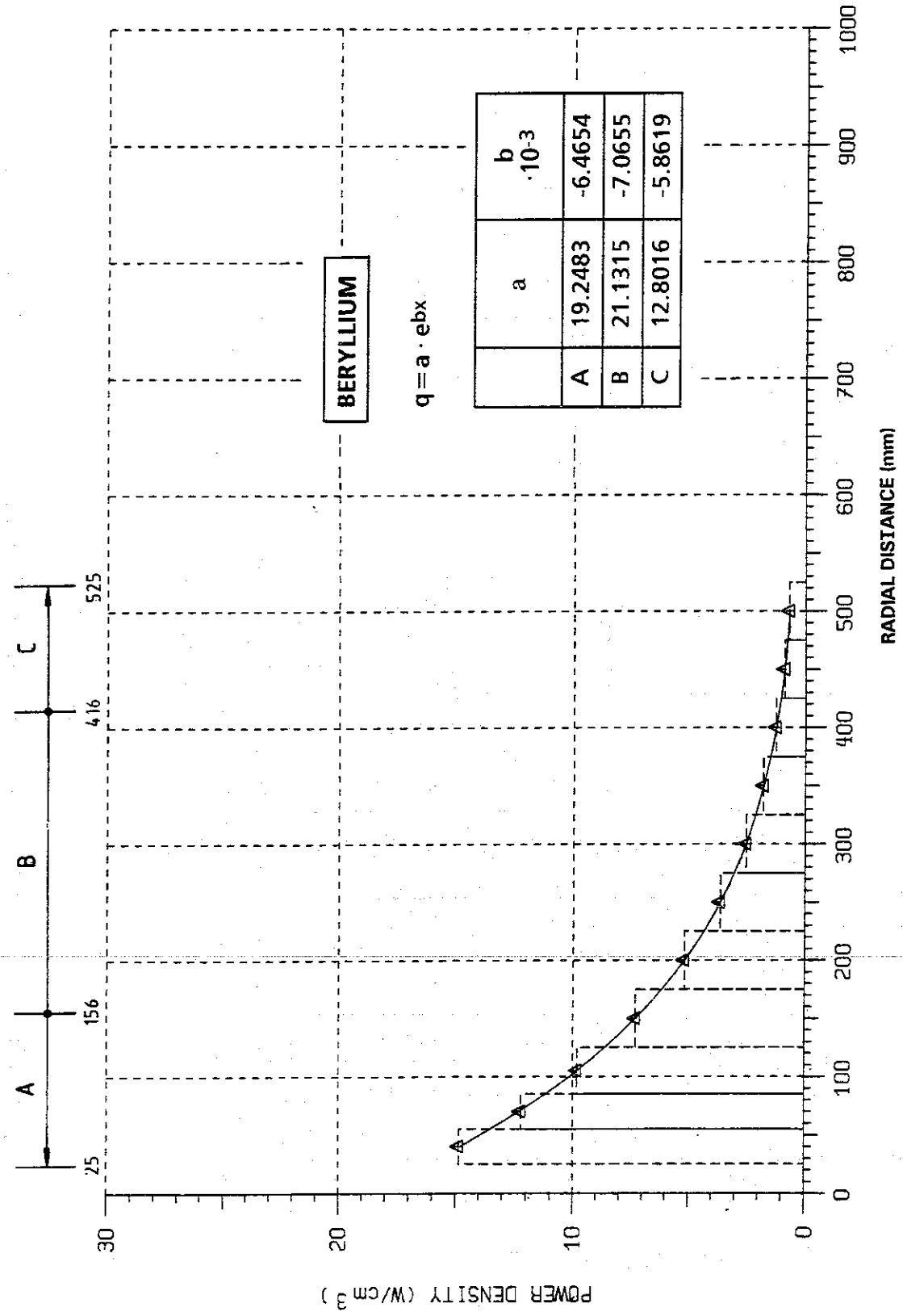

Fig. 9: Radial distribution of power densities in beryllium in the center of the torus.

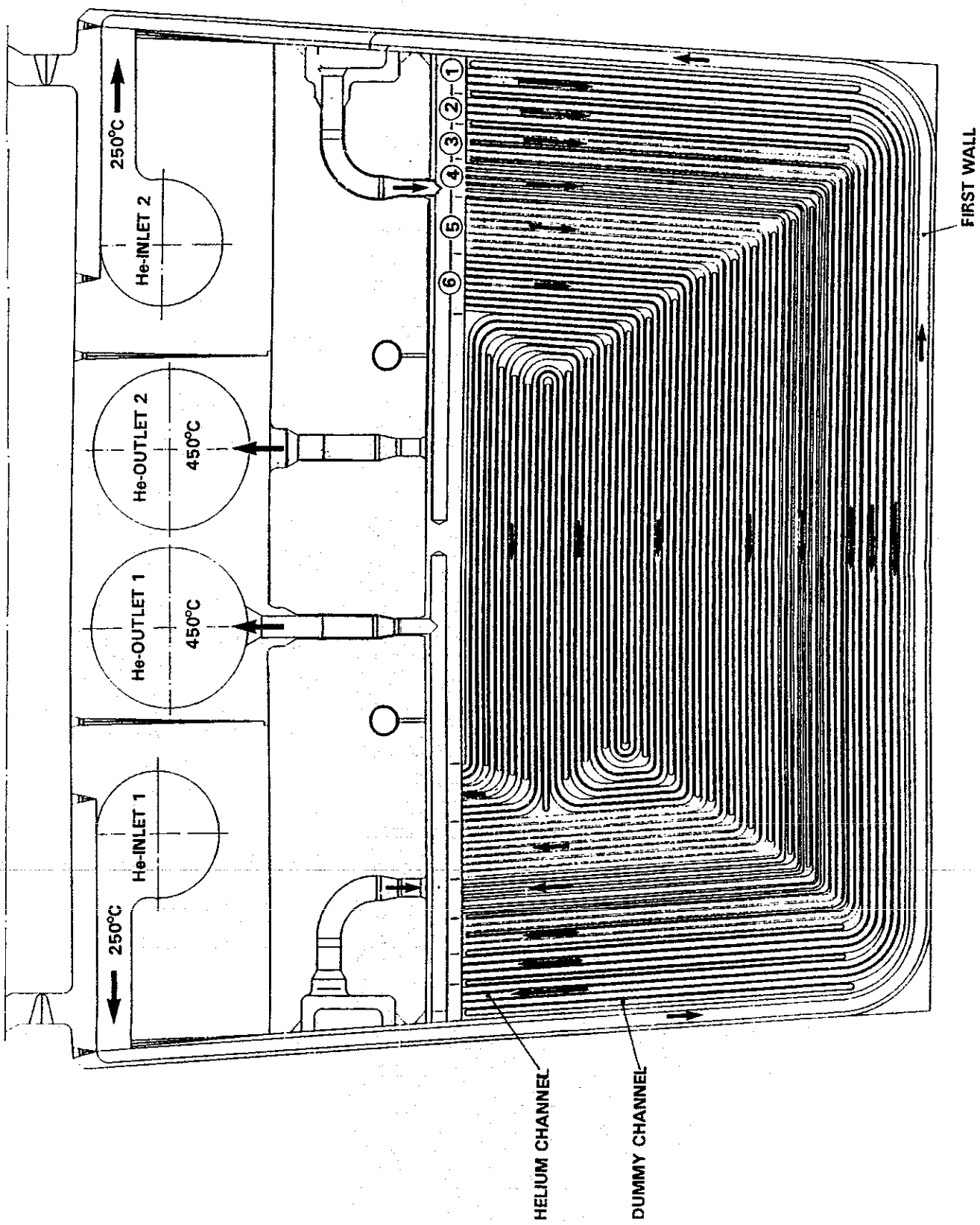

Fig. 10: Arrangement of the cooling channels integrated in the plate.

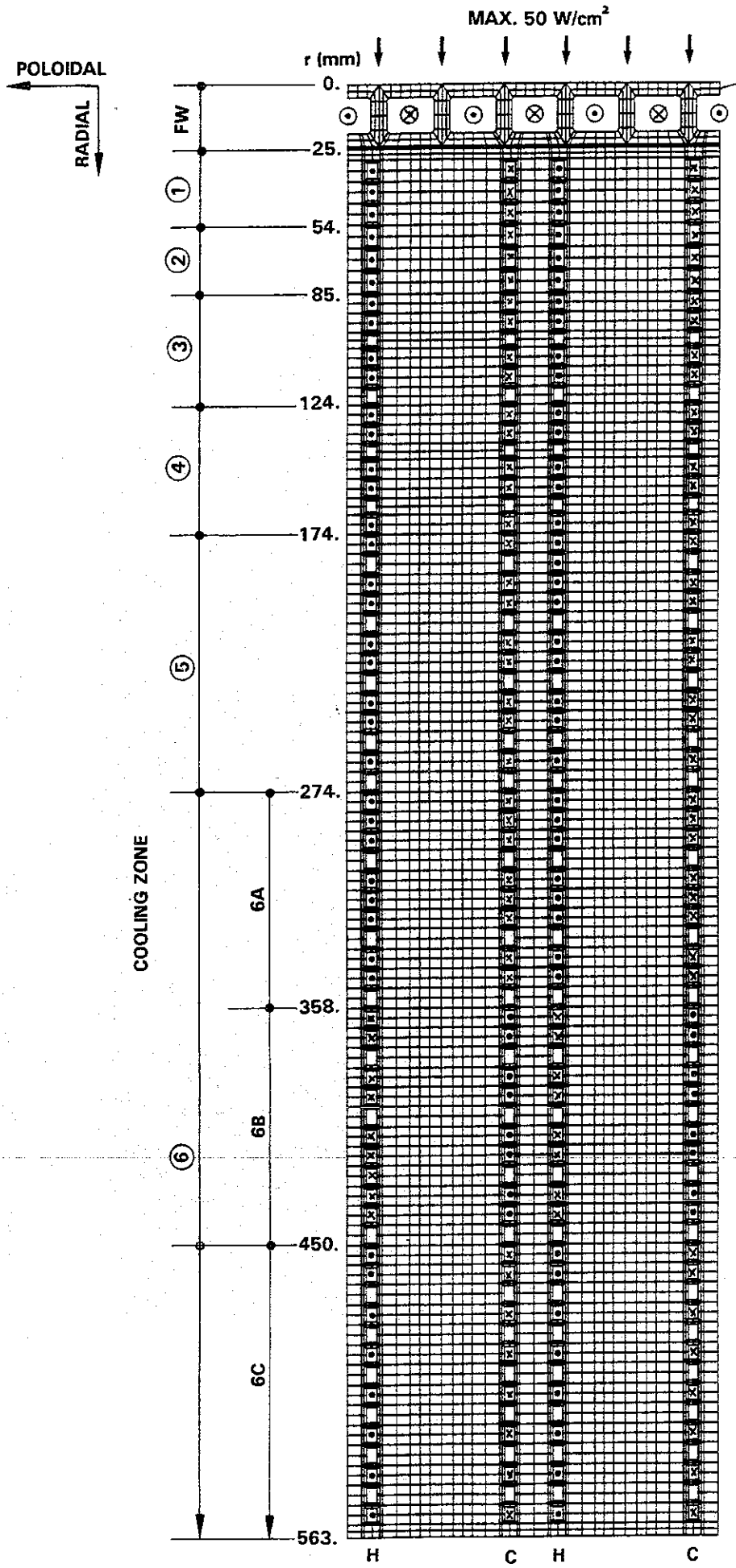

FIRST WALL:

	T_{He} (°C)		α (W/m²k)
	H	C	
	291.2	254.1	5314

COOLING PLATES:

	T_{He} (°C)		α (W/m²k)
	H	C	
ZONE 1	430.9	319.6	6664
ZONE 2	422.6	318.7	6253
ZONE 3	427.0	314.2	5387
ZONE 4	429.6	310.8	4109
ZONE 5	441.6	302.2	3001
ZONE 6	395.0	348.4	2560

H = HOT GAS

C = COLD GAS

Fig. 11: Finite element computation model [8].

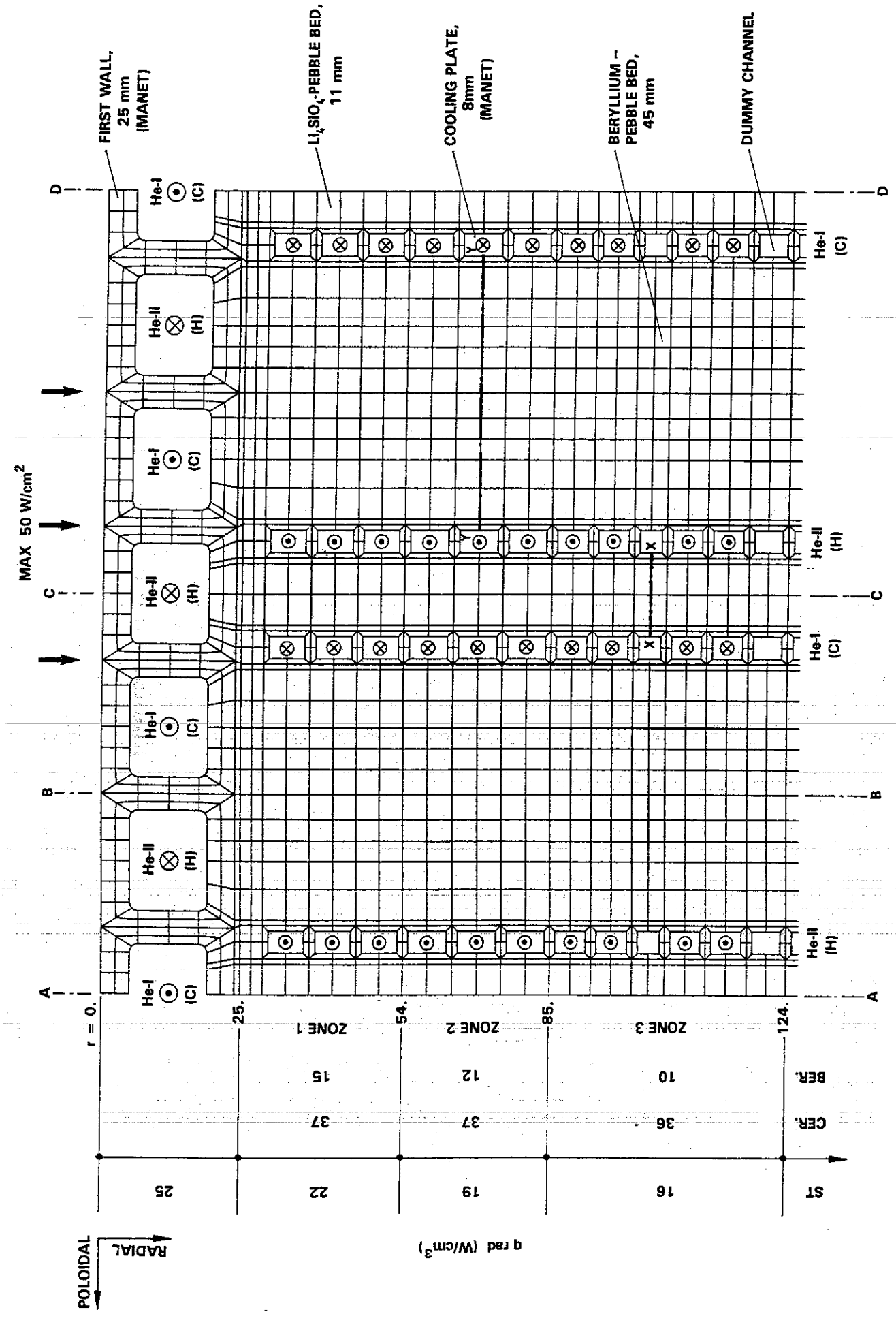

Fig. 11a: Enlarged detail of the front area with the First Wall and three cooling zones, according to Fig 11.

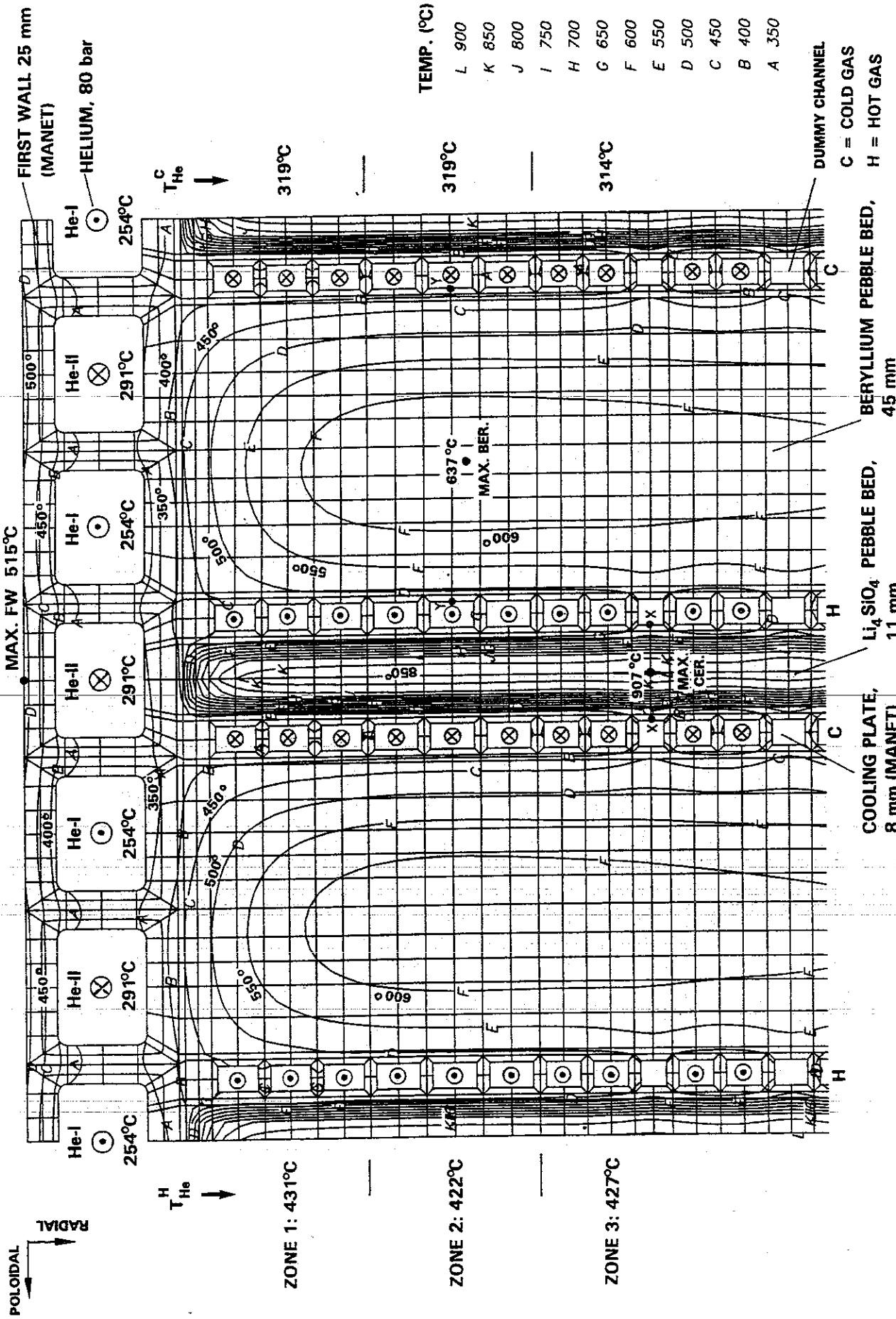

Fig. 12: Temperature distribution in the front area of the breeding zone.

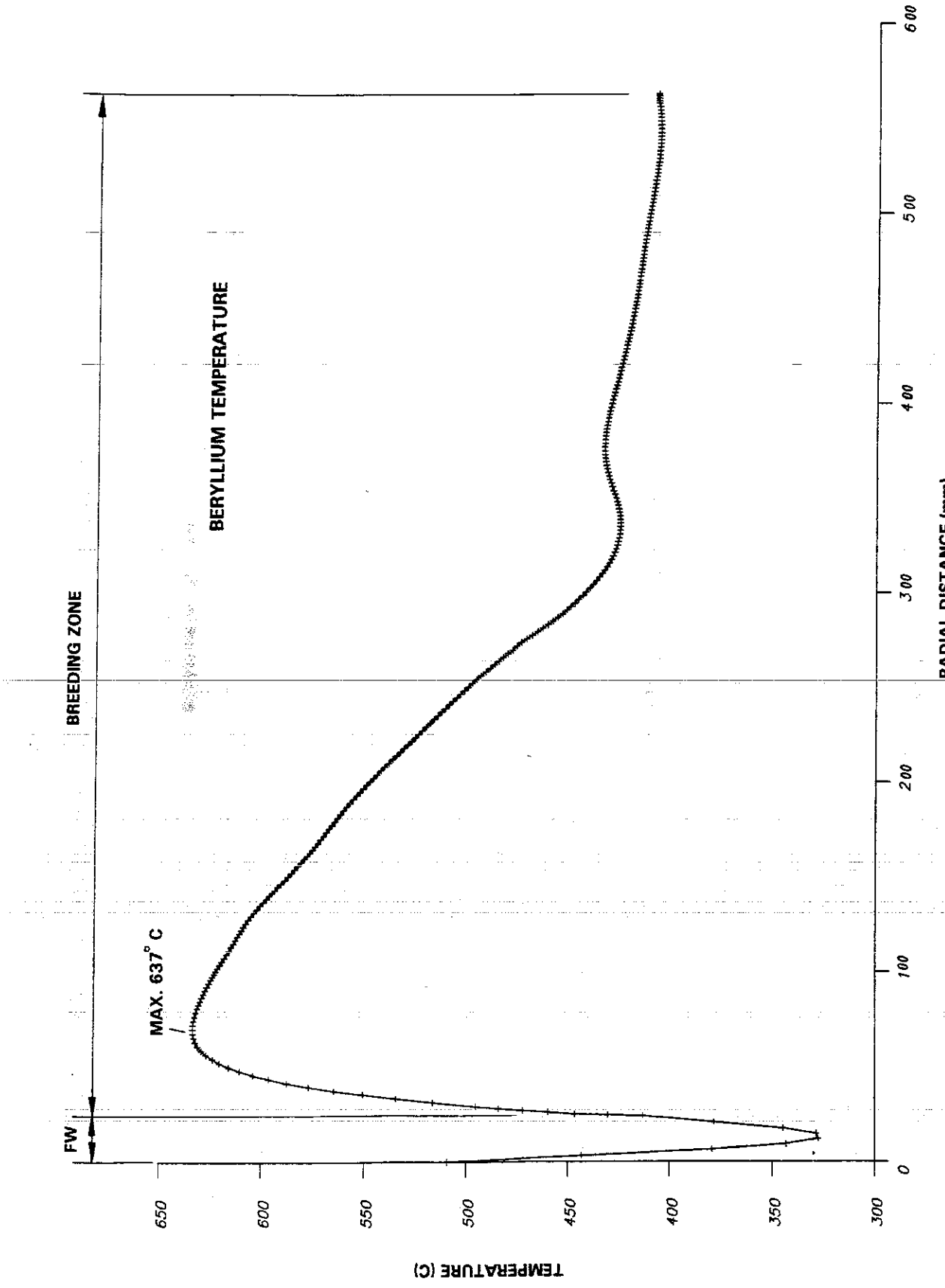

Fig. 13: Radial temperature plot along the mid-plane of the beryllium pebble bed (B - B section, Fig 11a).

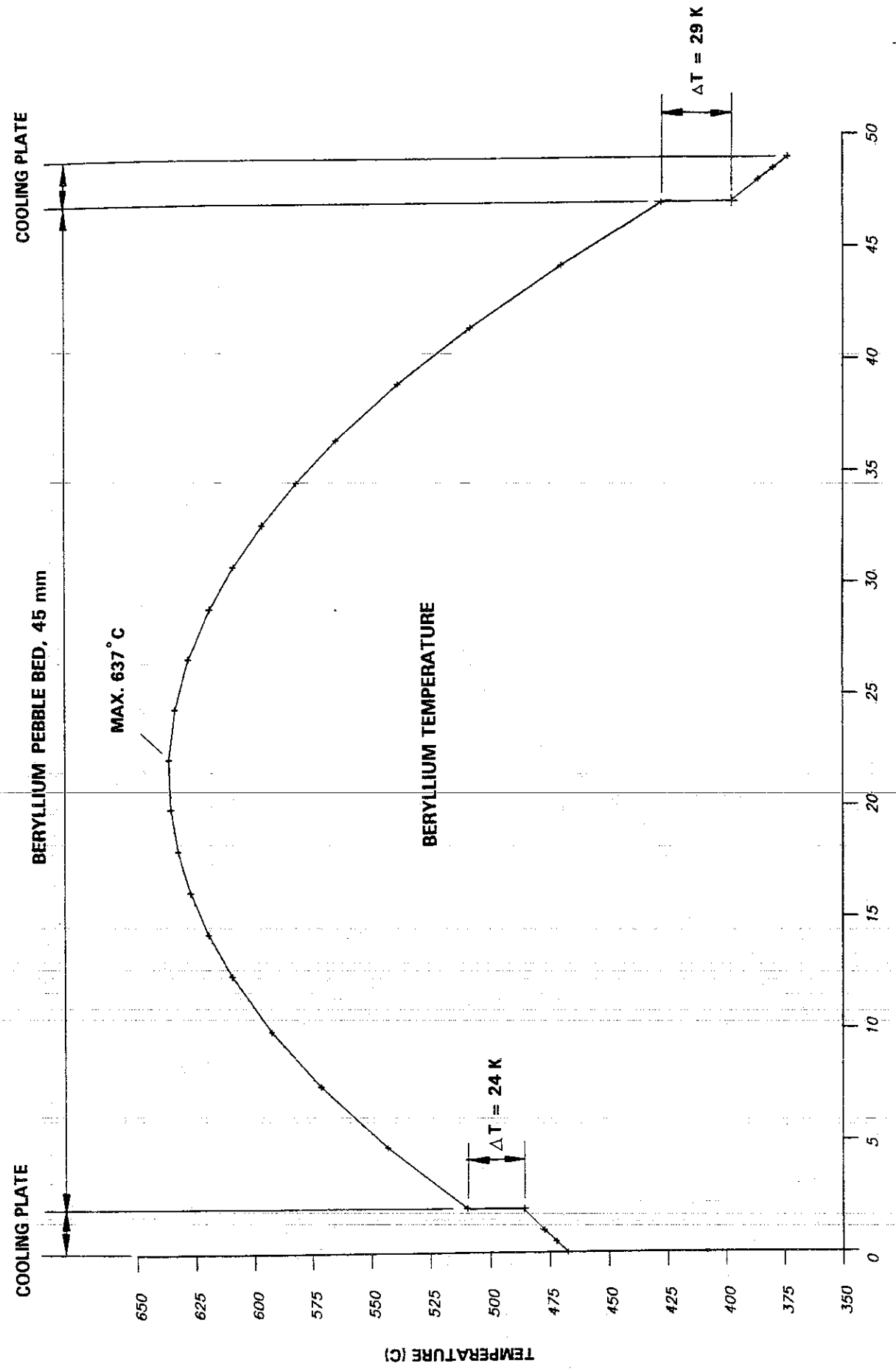

Fig. 14: Poloidal temperature plot in the beryllium pebble bed between two cooling plates along the Y - Y routes in Fig 12.

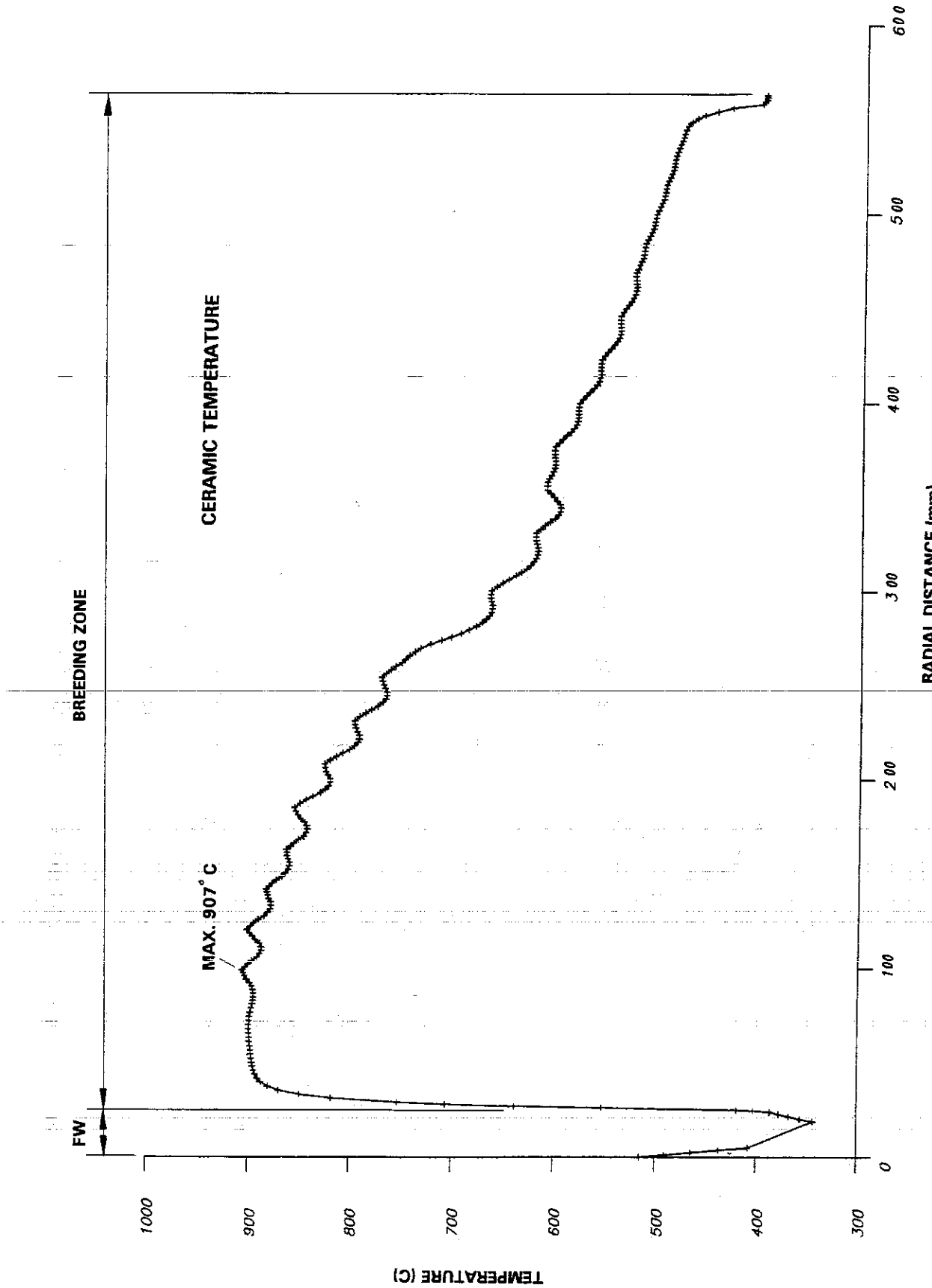

Fig. 15: Radial temperature plot along the mid-plane of the beryllium pebble bed (C - C section, Fig 11a).

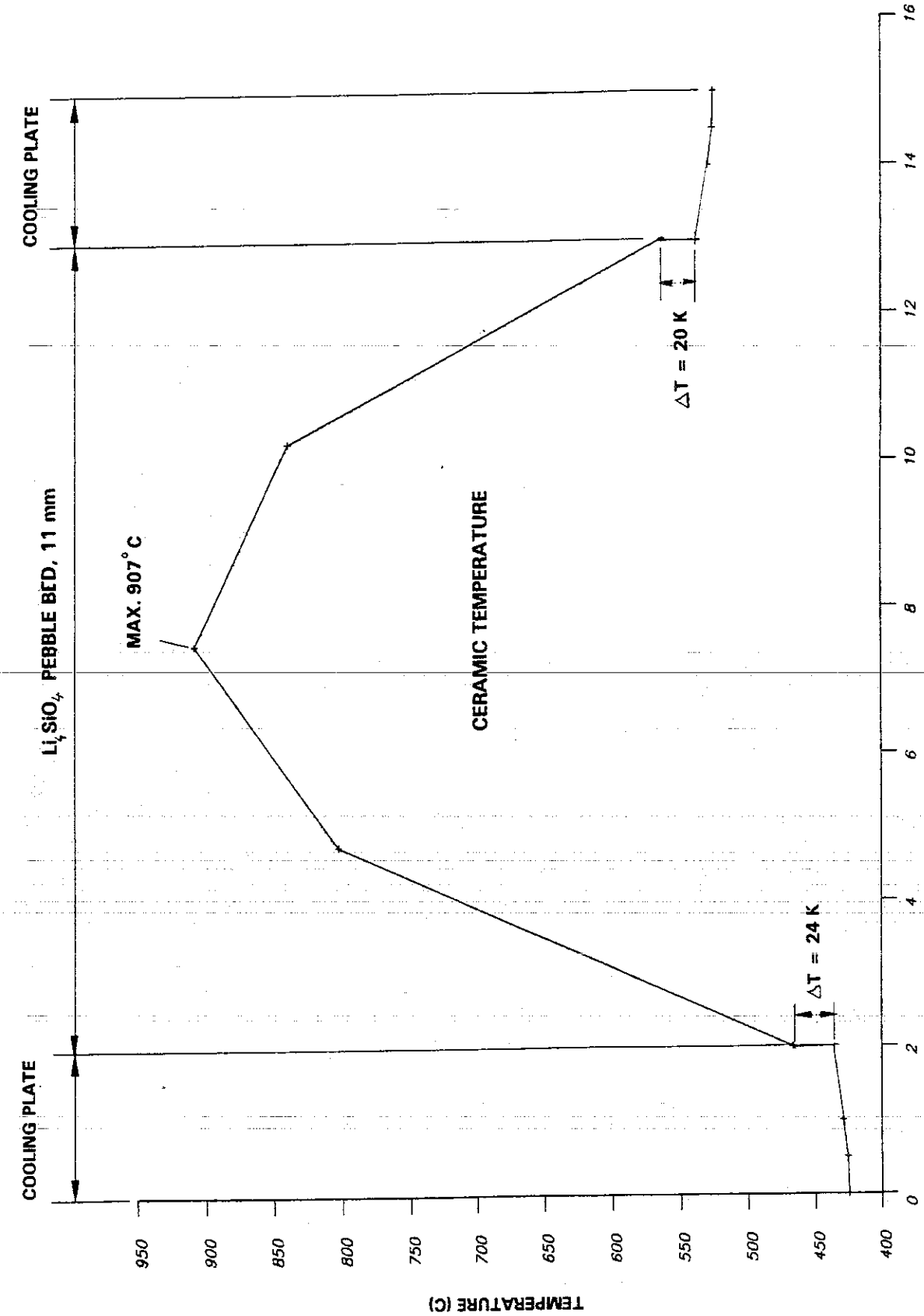

Fig. 16: Radial temperature plot in the ceramic pebble bed between two cooling plates along the X - X routes in Fig 12).

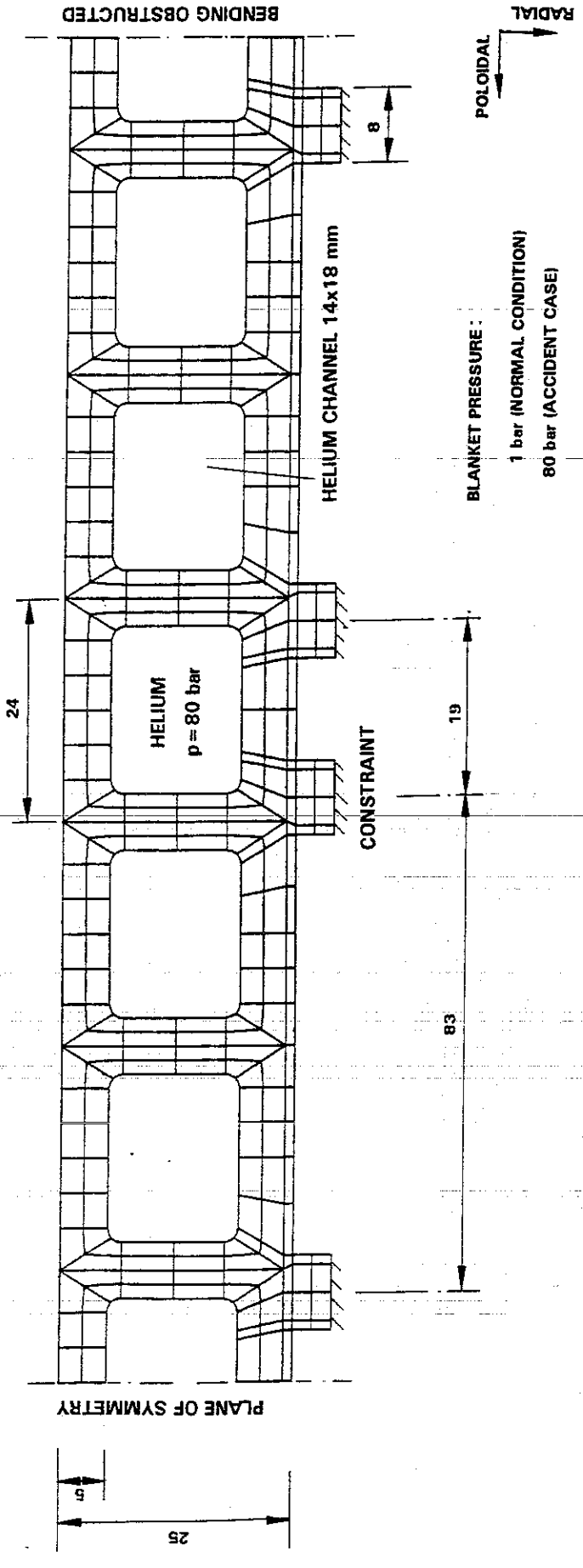

Fig. 17: Finite Element model for the First Wall structure (MANET).

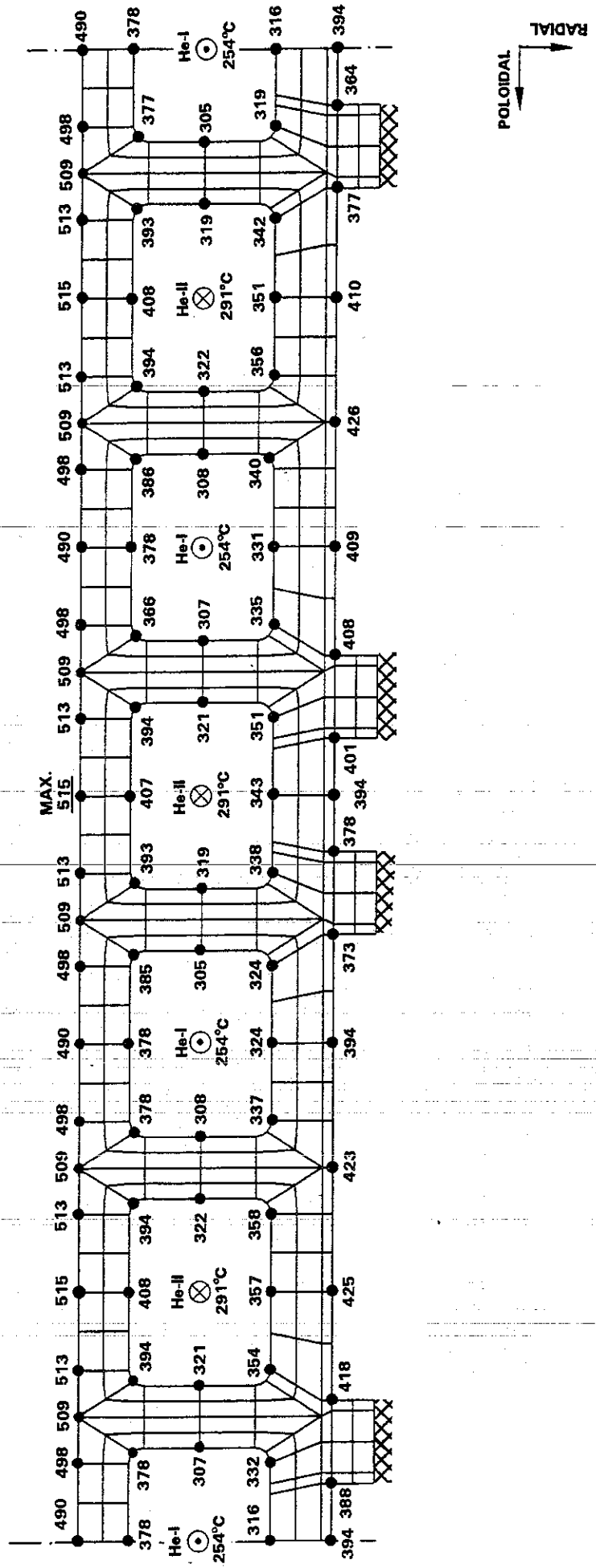

Fig. 18: Temperature distribution in the First Wall structure.

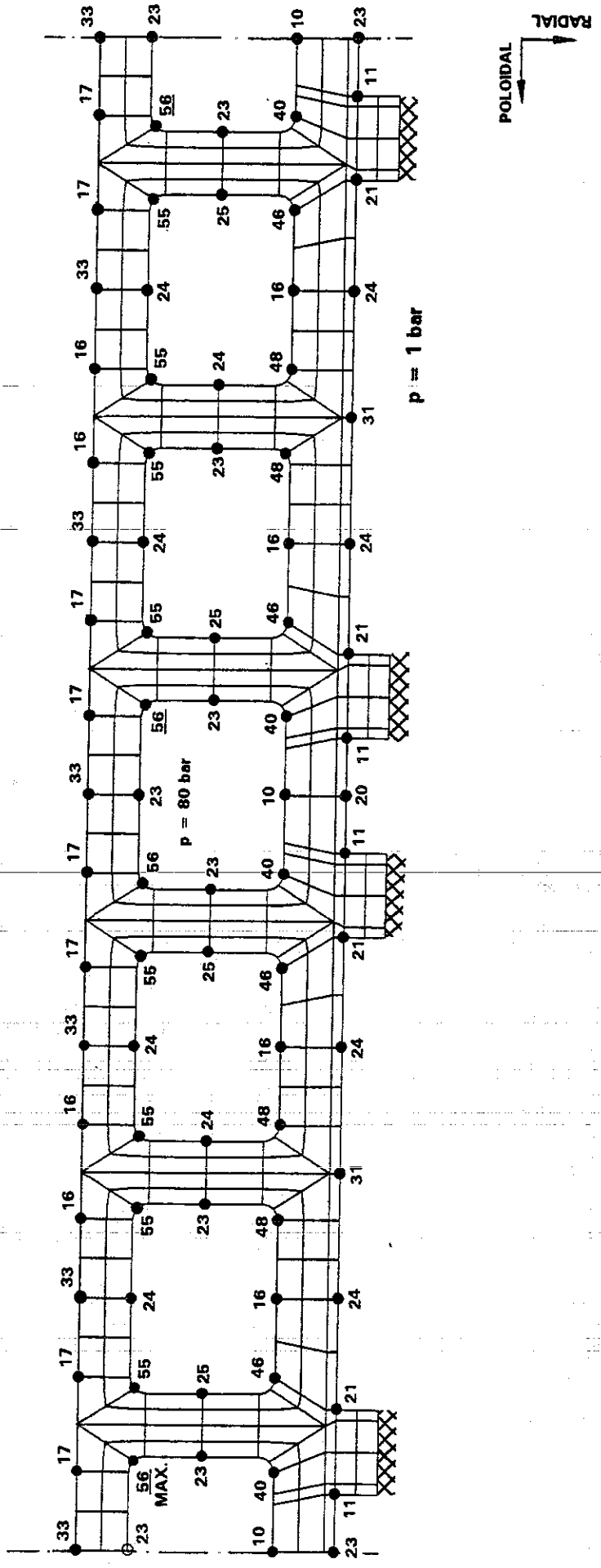

Fig. 19: Von Mises primary stress [MPa] during normal operation of the reactor.

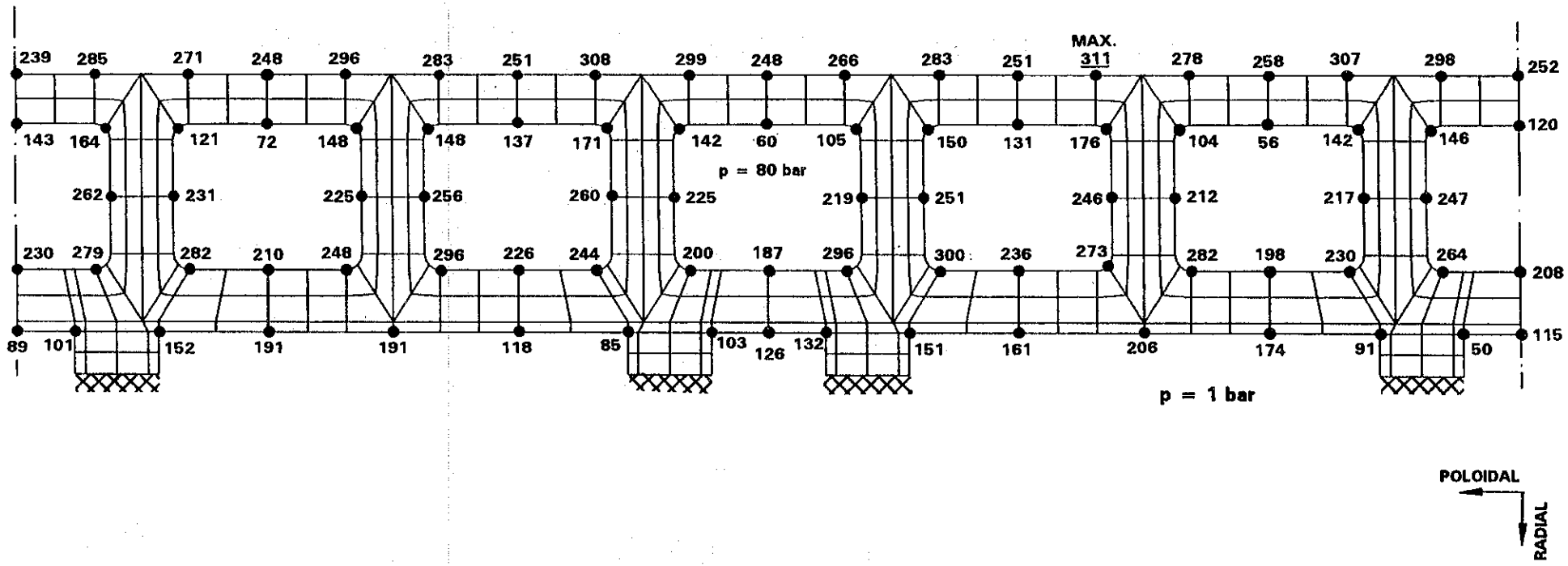

σ_{max} = 311 MPa < σ_{adm}^{500C} = 494 MPa

Fig. 20: Von Mises primary plus secondary stresses [MPa] during normal operation of the reactor.

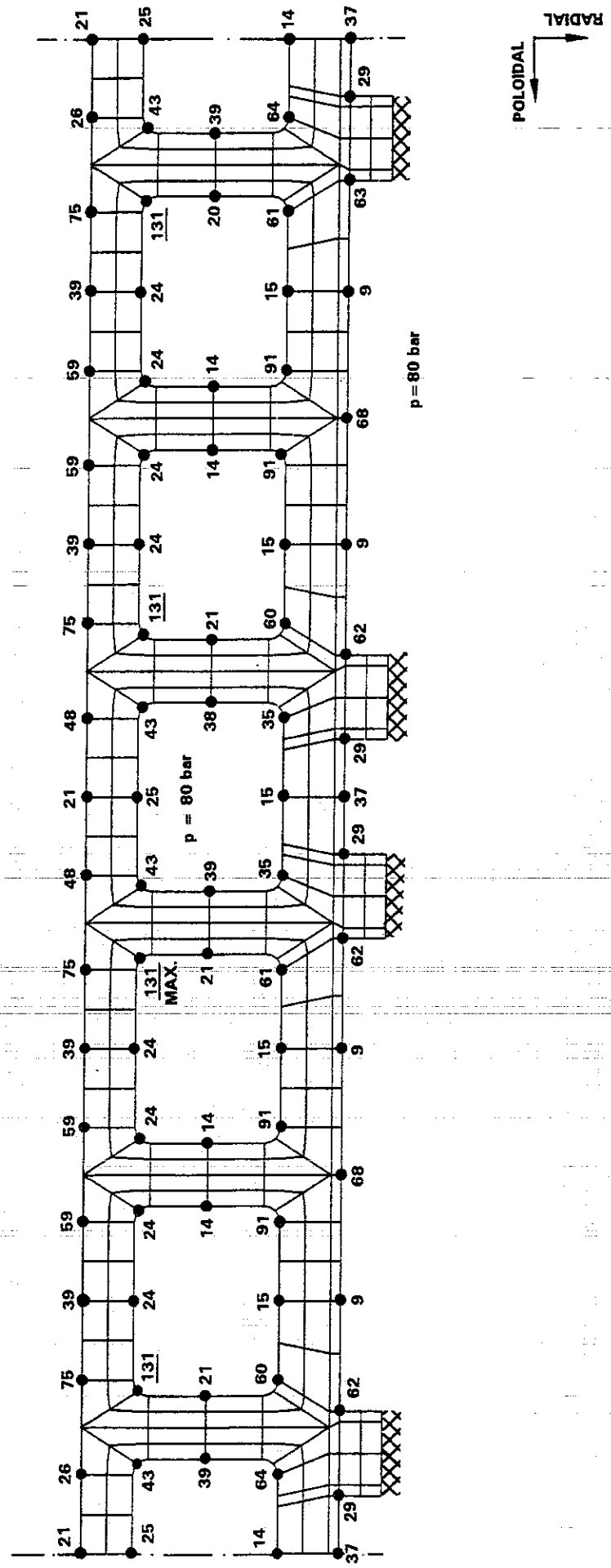

Fig. 21: Von Mises primary stress [MPa] in an accident case.

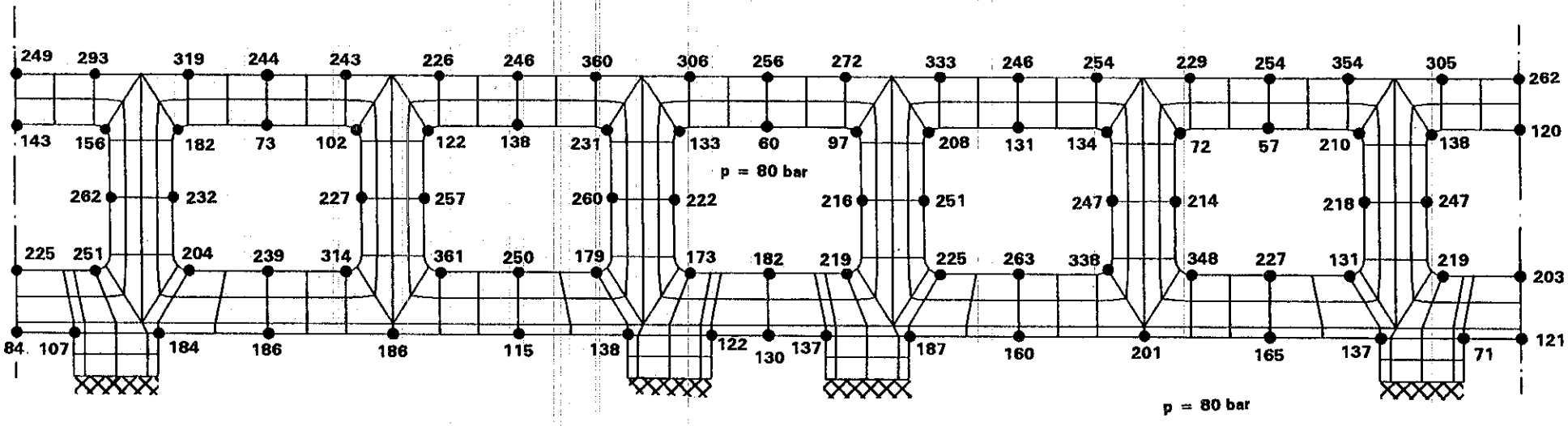

σ_{max} = 361 MPa < $\sigma_{adm}^{500^{\circ}C}$ = 494 MPa

Figure 22: Von Mises primary plus secondary stress [MPa] in an accident case.

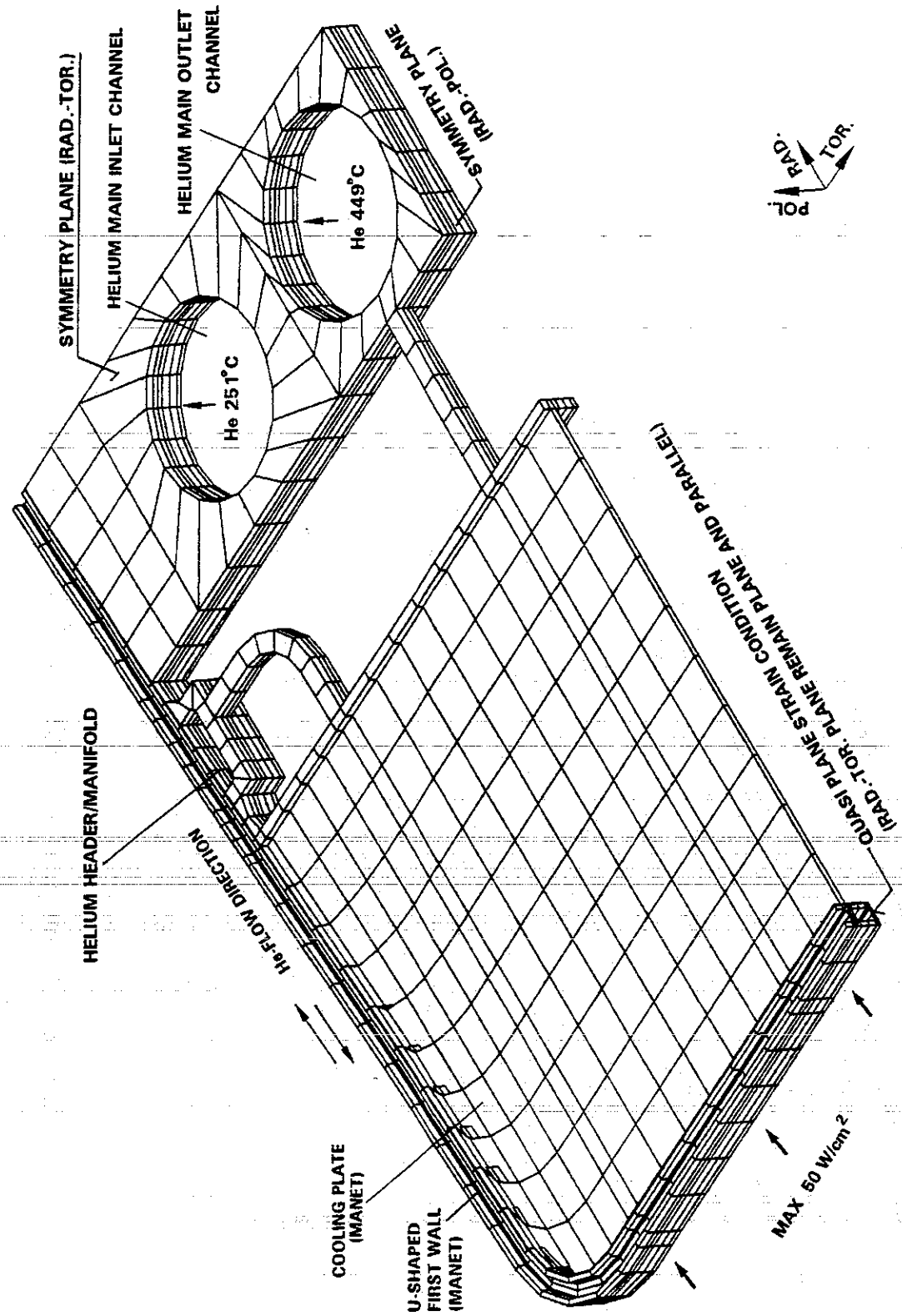

Fig. 23: Finite Element model.

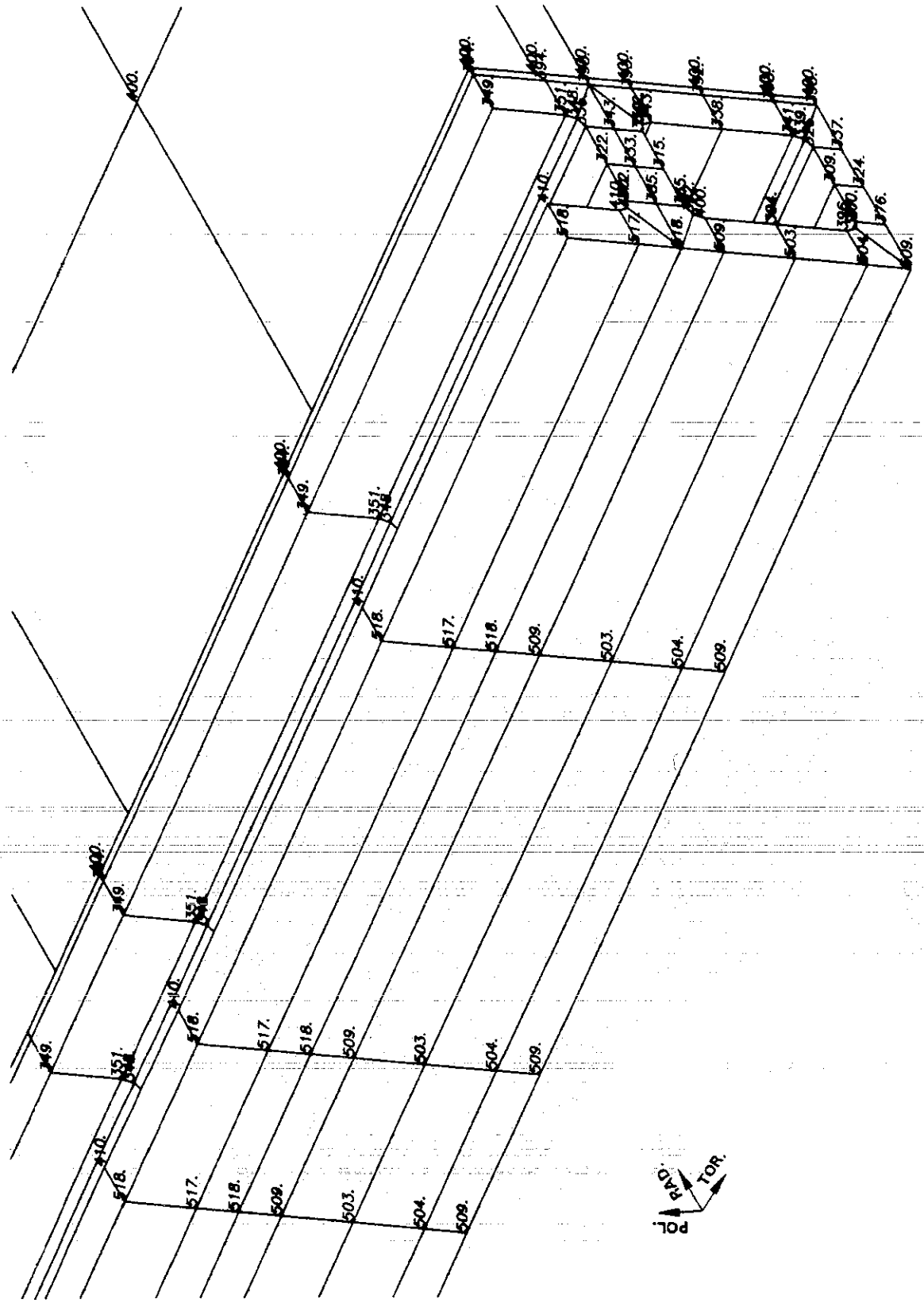

Fig. 24: Temperature distribution in the FW central zone.

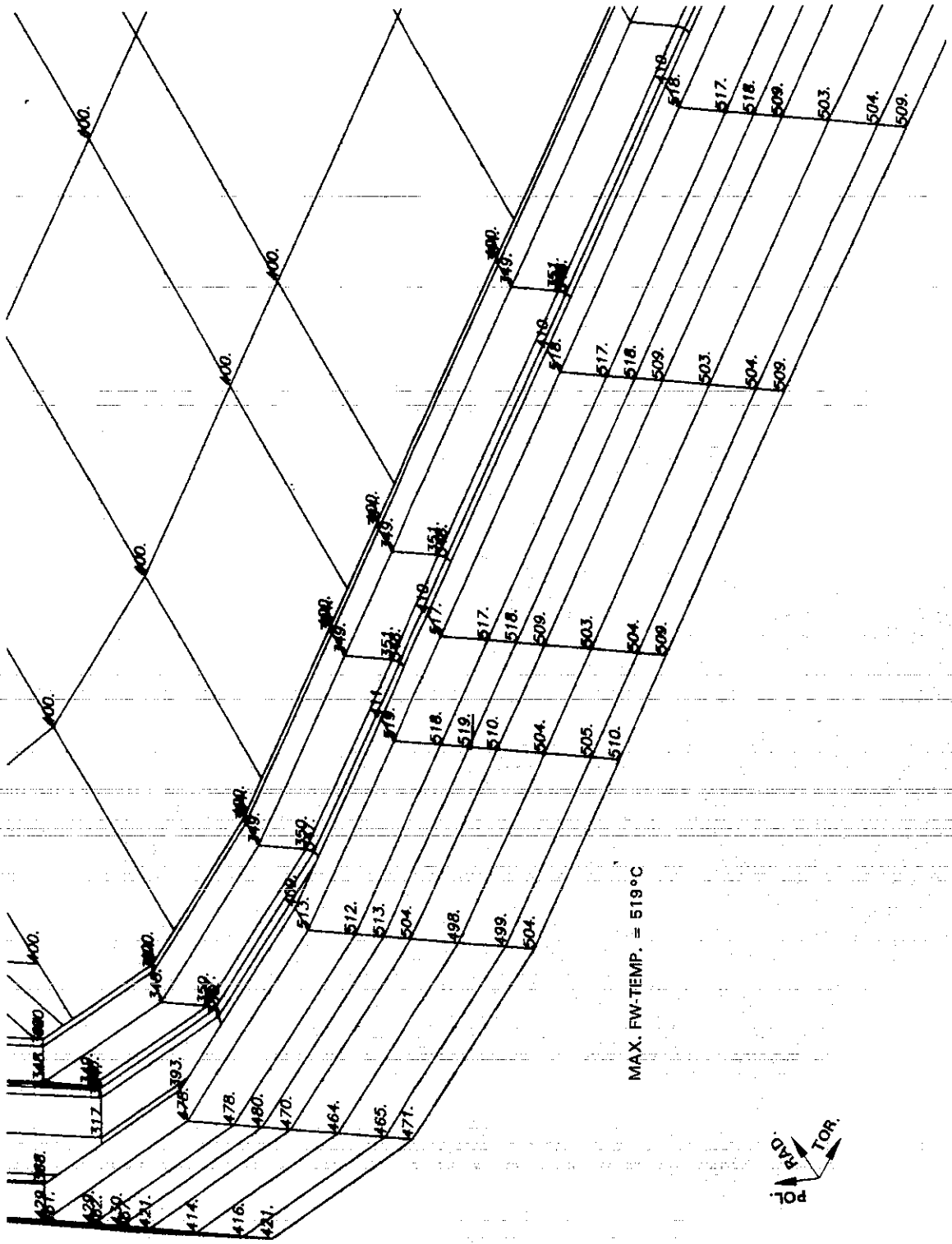

Fig. 25: Temperature distribution in the FW/SW corner zone.

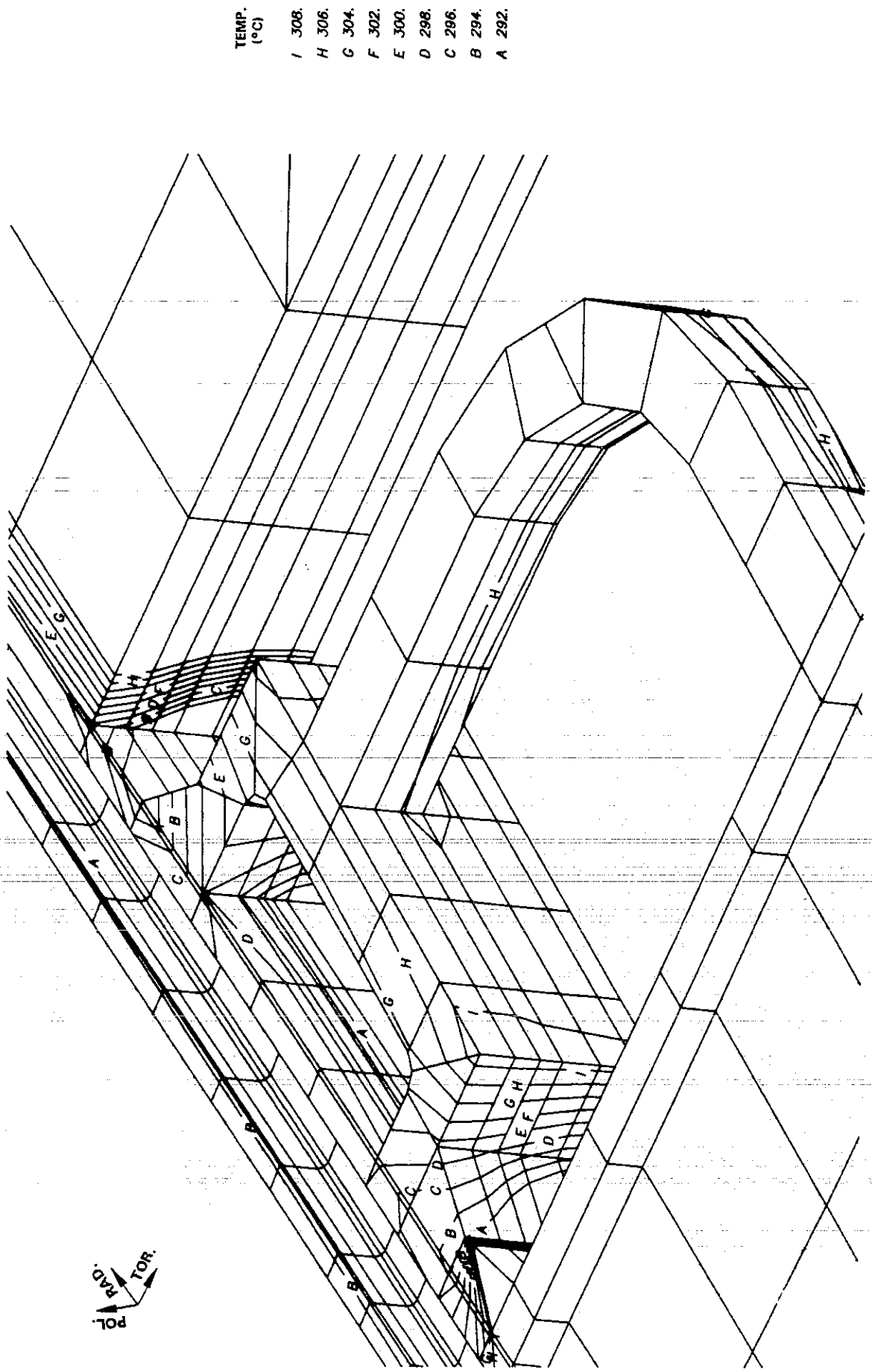

Fig. 26: Temperature distribution in the He header zone.

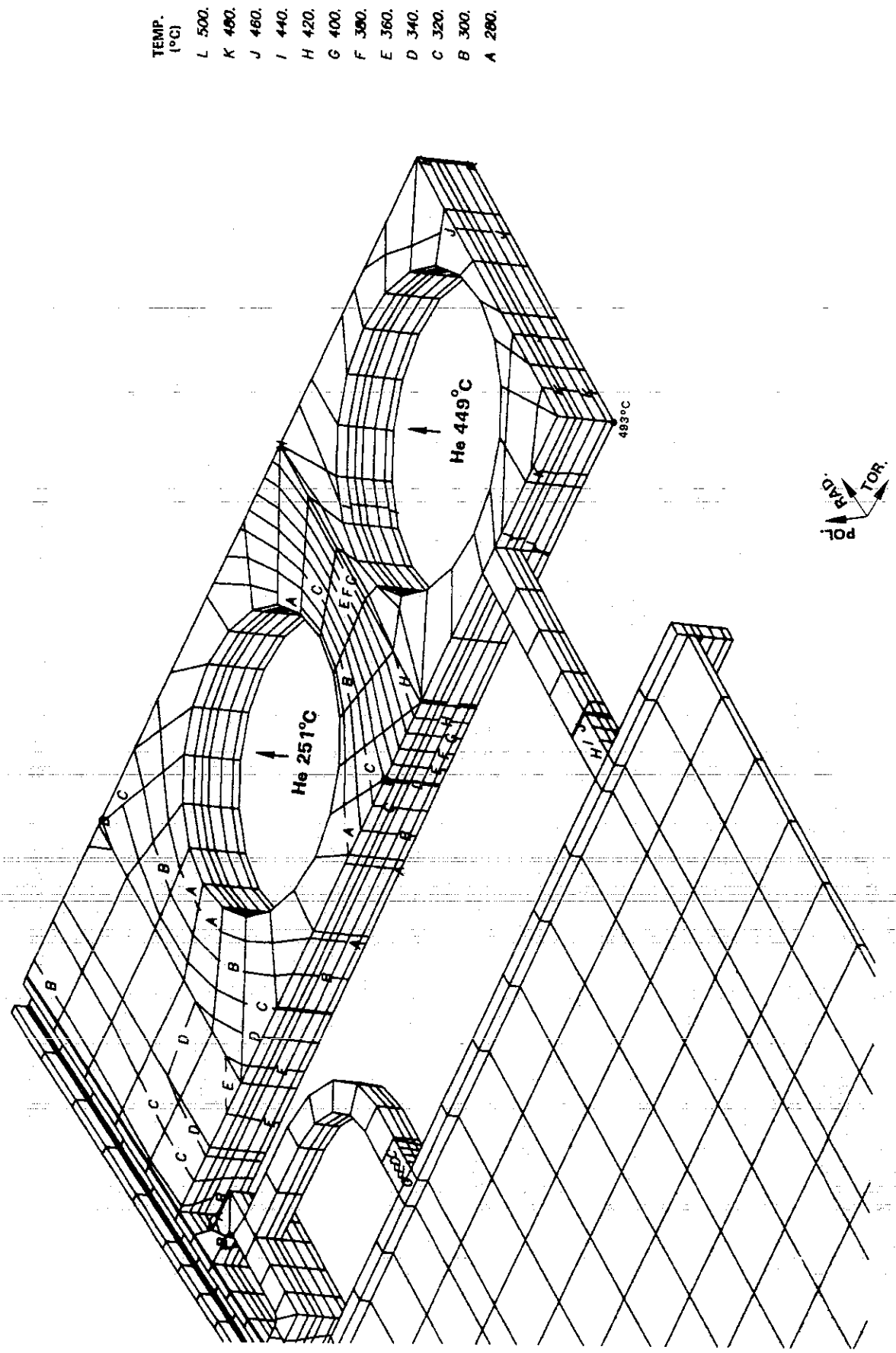

Fig. 27: Temperature distribution in the He main pipe zone.

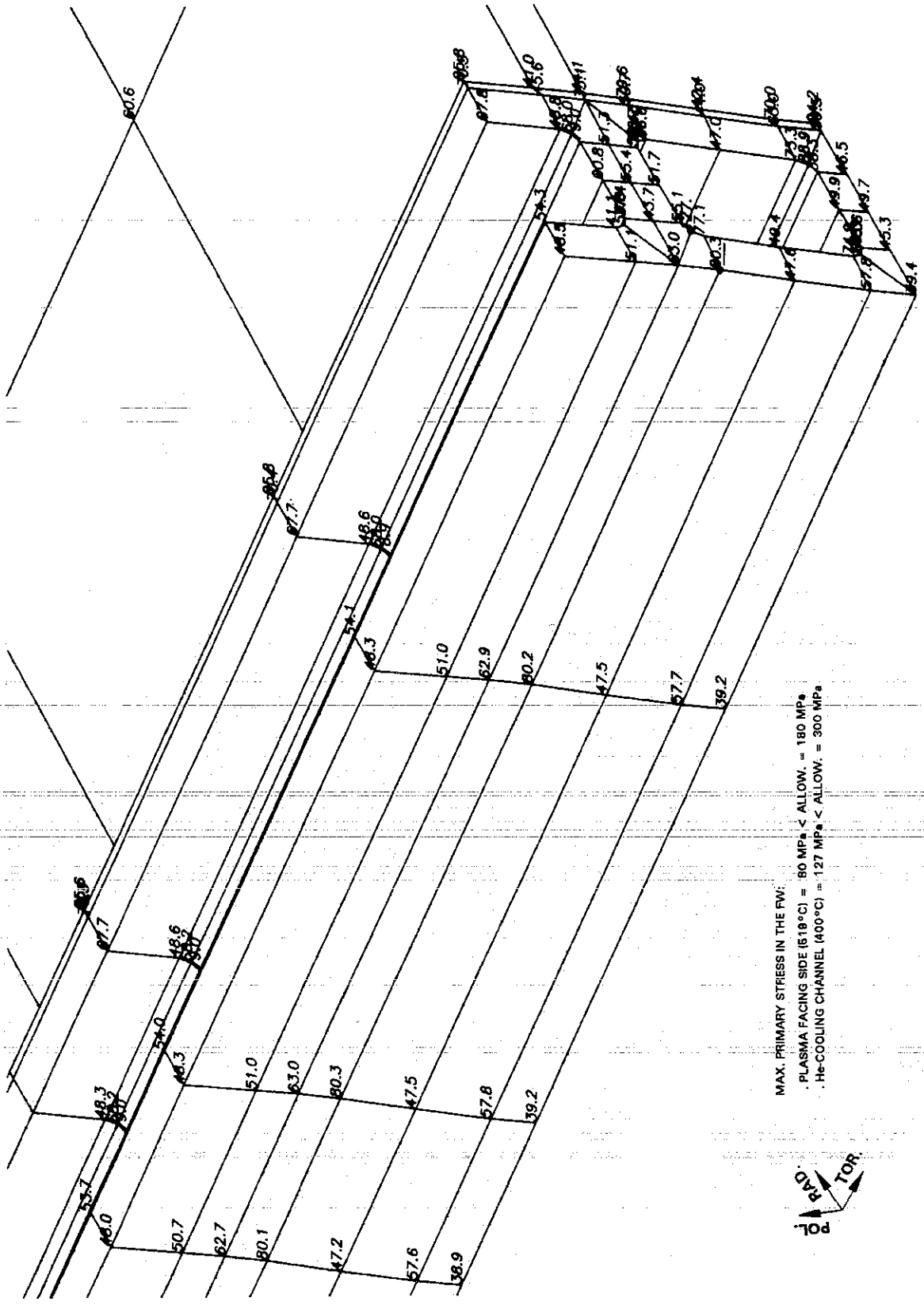

Fig. 28: von Mises primary stresses in the FW central zone.

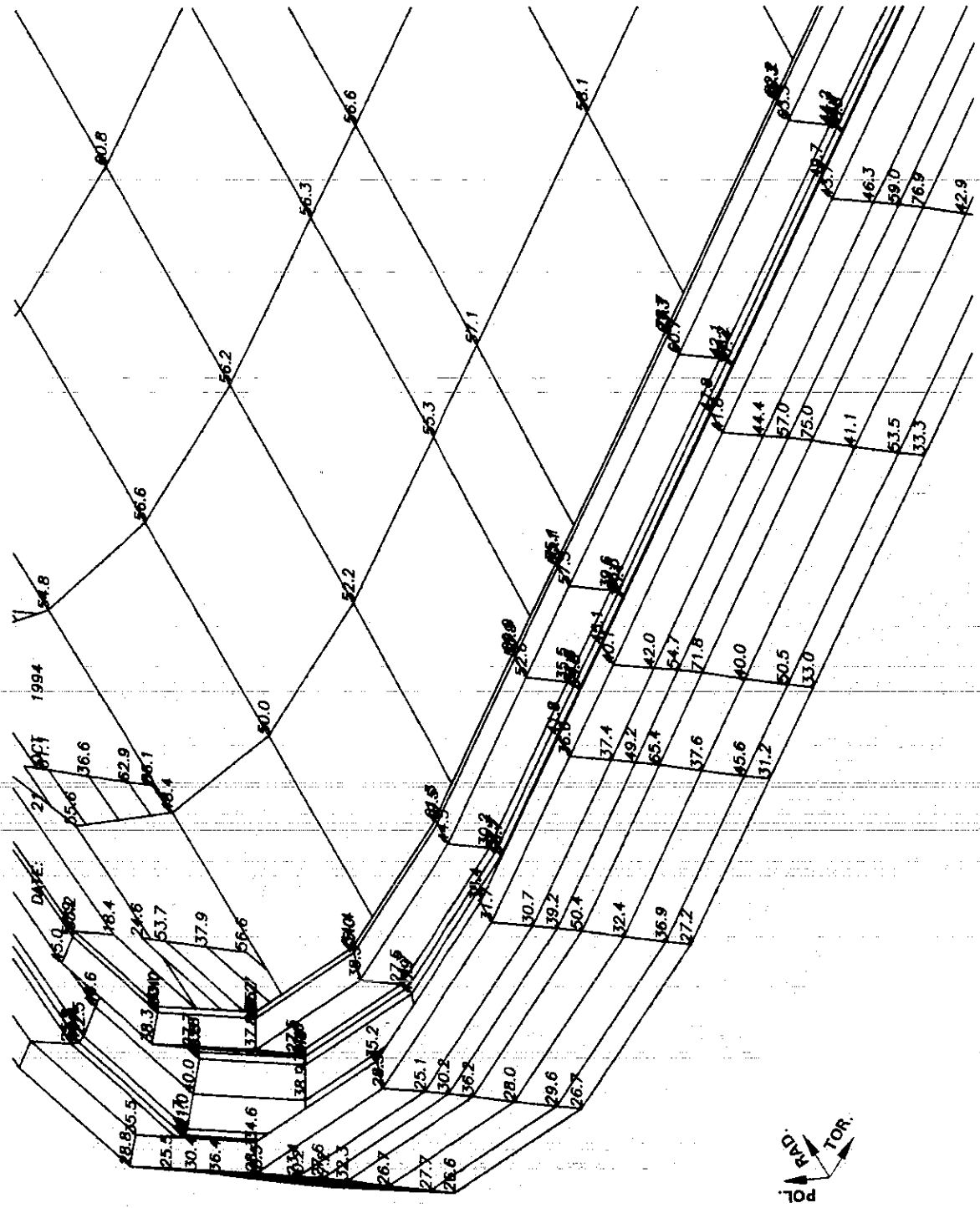

Fig. 29: von Mises primary stresses in the FW/SW corner zone.

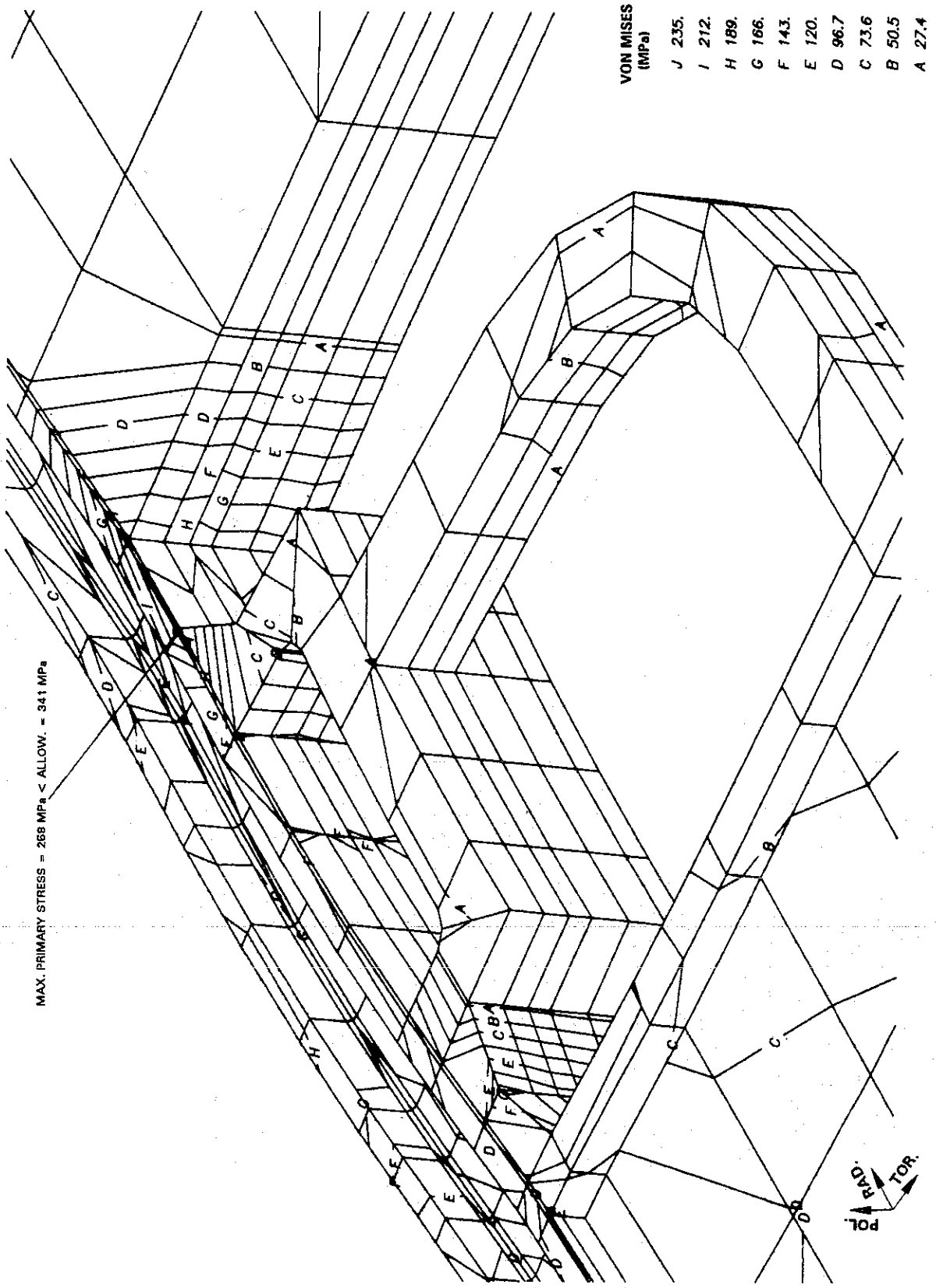

Fig. 30: von Mises primary stresses in the He header zone.

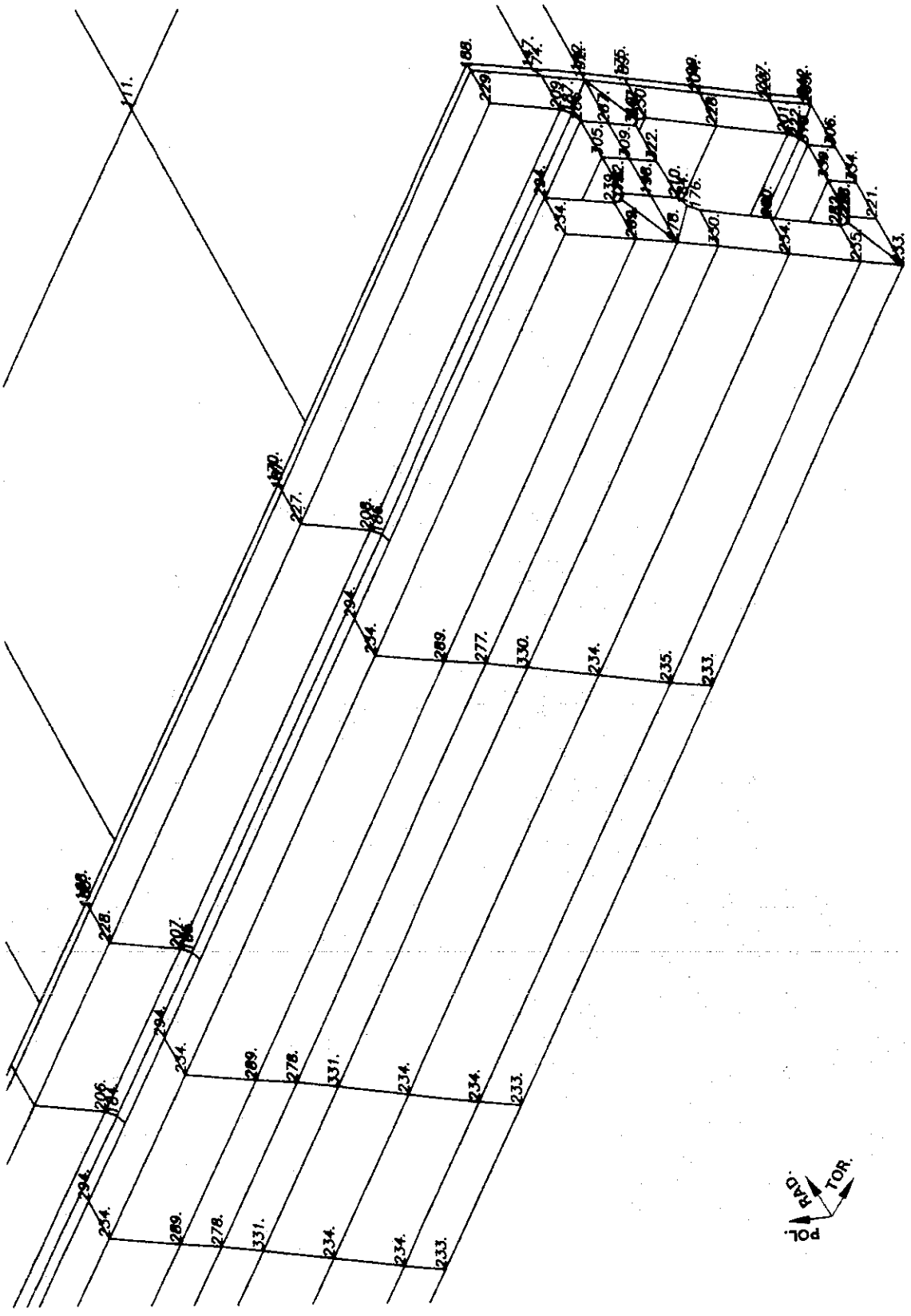

Fig. 31: von Mises primary plus secondary stresses in the FW central zone.

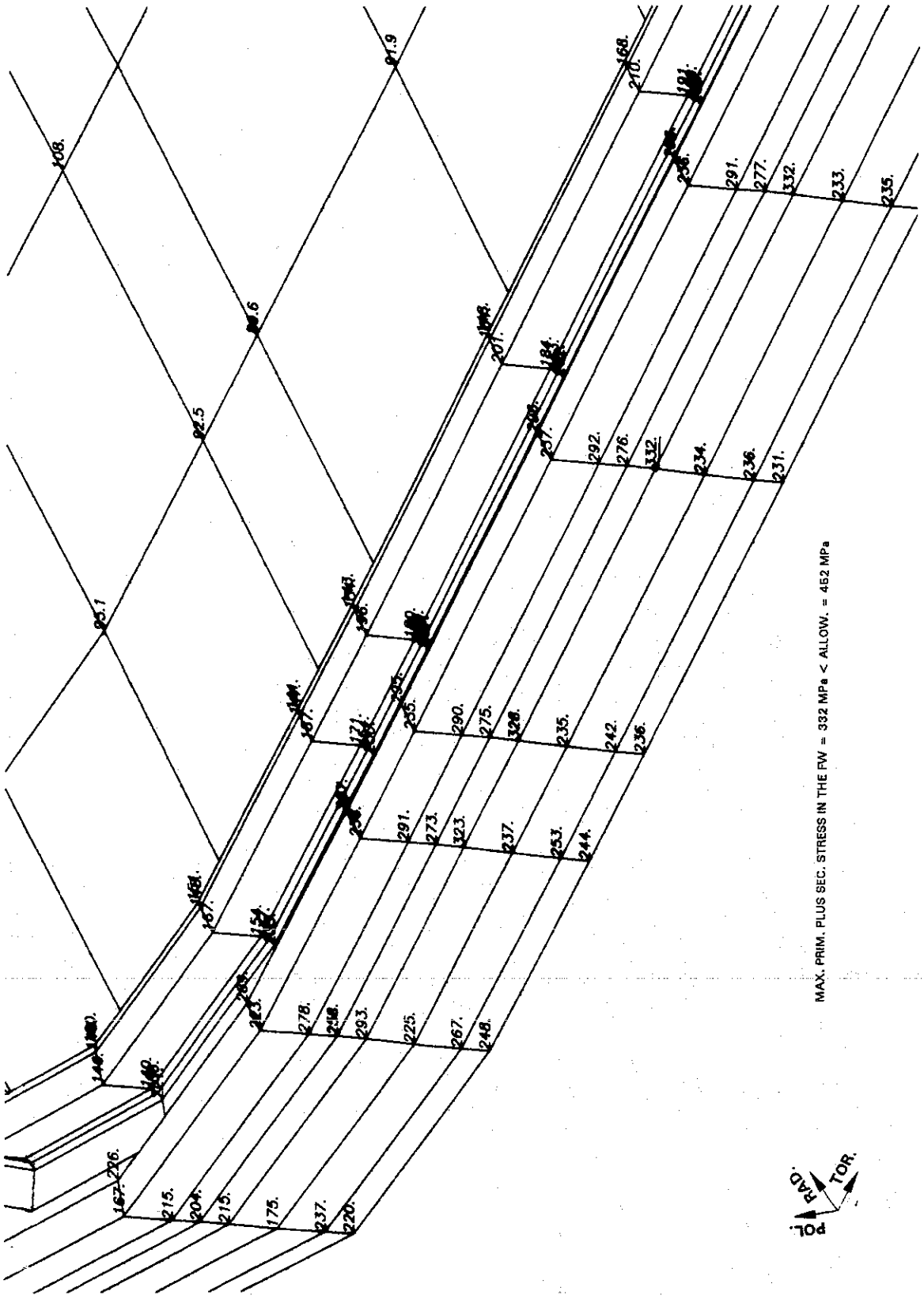

Fig. 32: von Mises primary plus secondary stresses in the FW/SW corner zone.

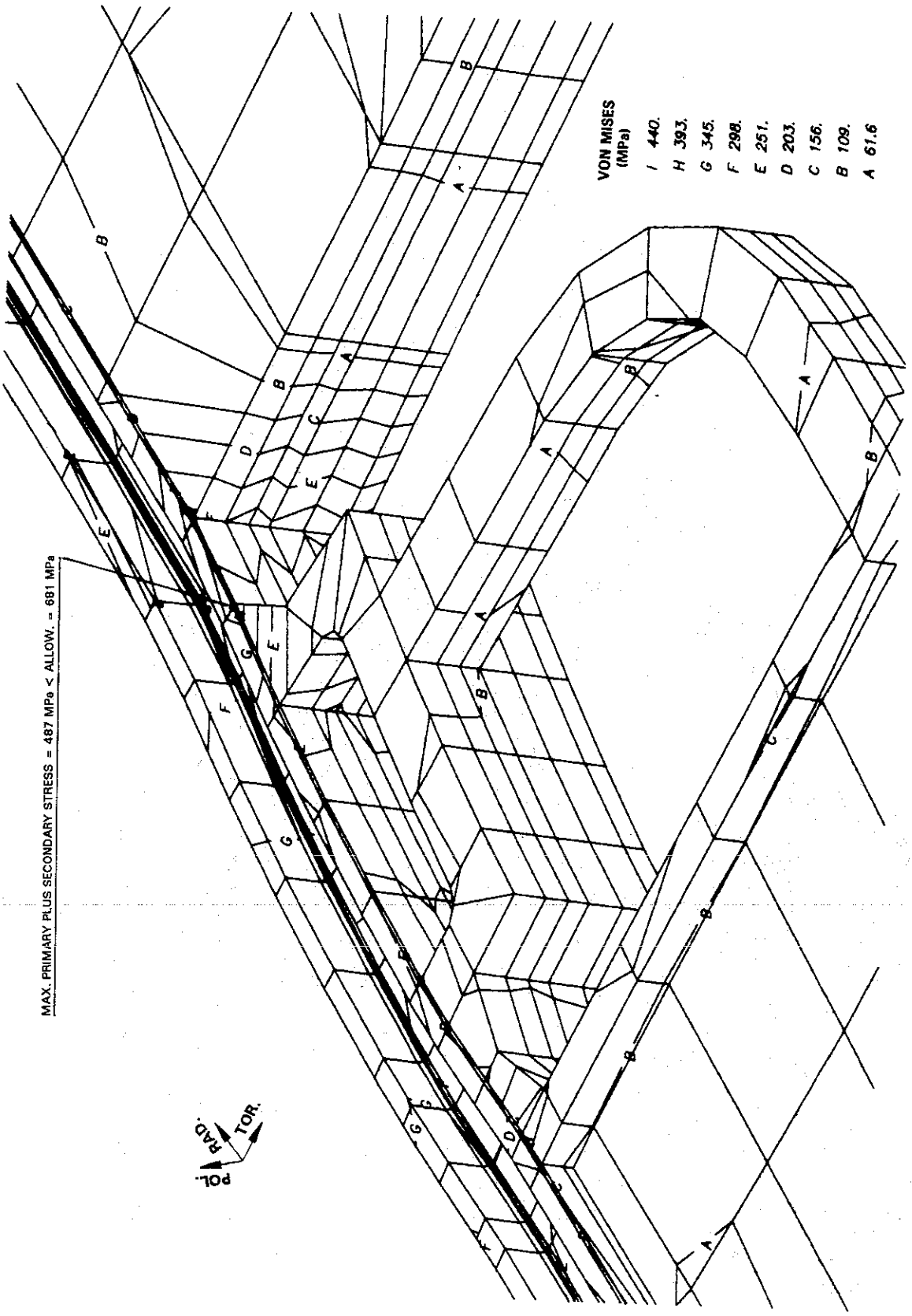

Fig. 33: von Mises primary plus secondary stresses in the He header zone.

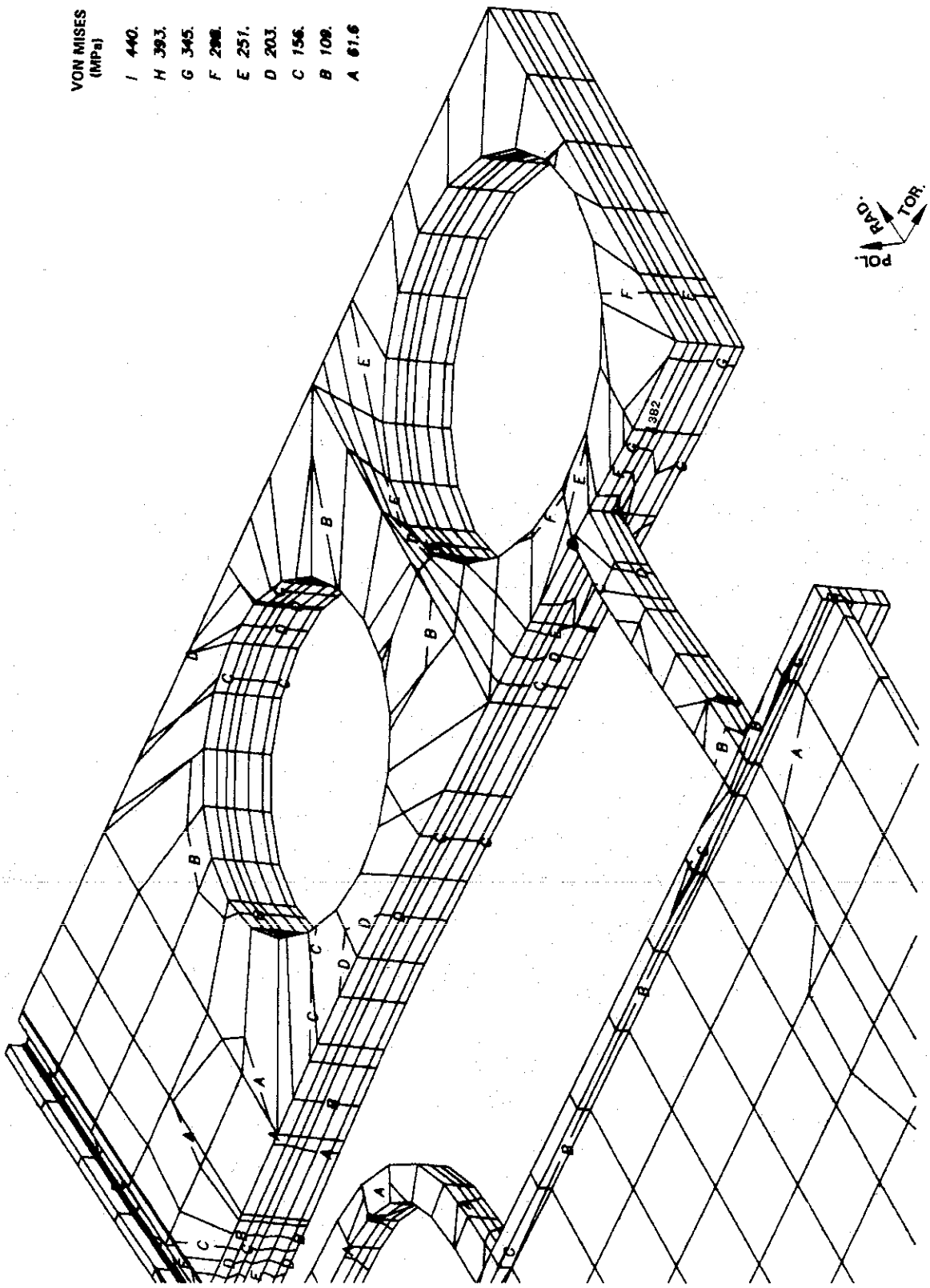

Fig. 34: von Mises primary plus secondary stresses in the He main pipe zone.

Appendix to PART 1

Power balance of an outboard section at the torus center with a poloidal height of 12 mm for a solution with coil of tube and mixed pebble beds [1] (Fig. A1 and A2).

Generated powers [W]:

First Wall	
- volumetric heat power	6906
- surface heat power	6380
Mixed pebble bed including coolant tube:	45726
Sum	59012

Abstracted power [W]:

First Wall channel (one half)	15834
Coolant tube in the breeder zone (one half)	43178
Sum	59012

Helium mass flow m_{He} and temperature rise ΔT_{He}:

	First Wall channel	Coolant tube
$\dot{m}_{He}$ [kg/s]	0.1230	0.0556
$T_{He,\ inlet/outlet}$ [°C]	251/300.5	300.5/450
ΔT_{He} [K]	49.5	149.5

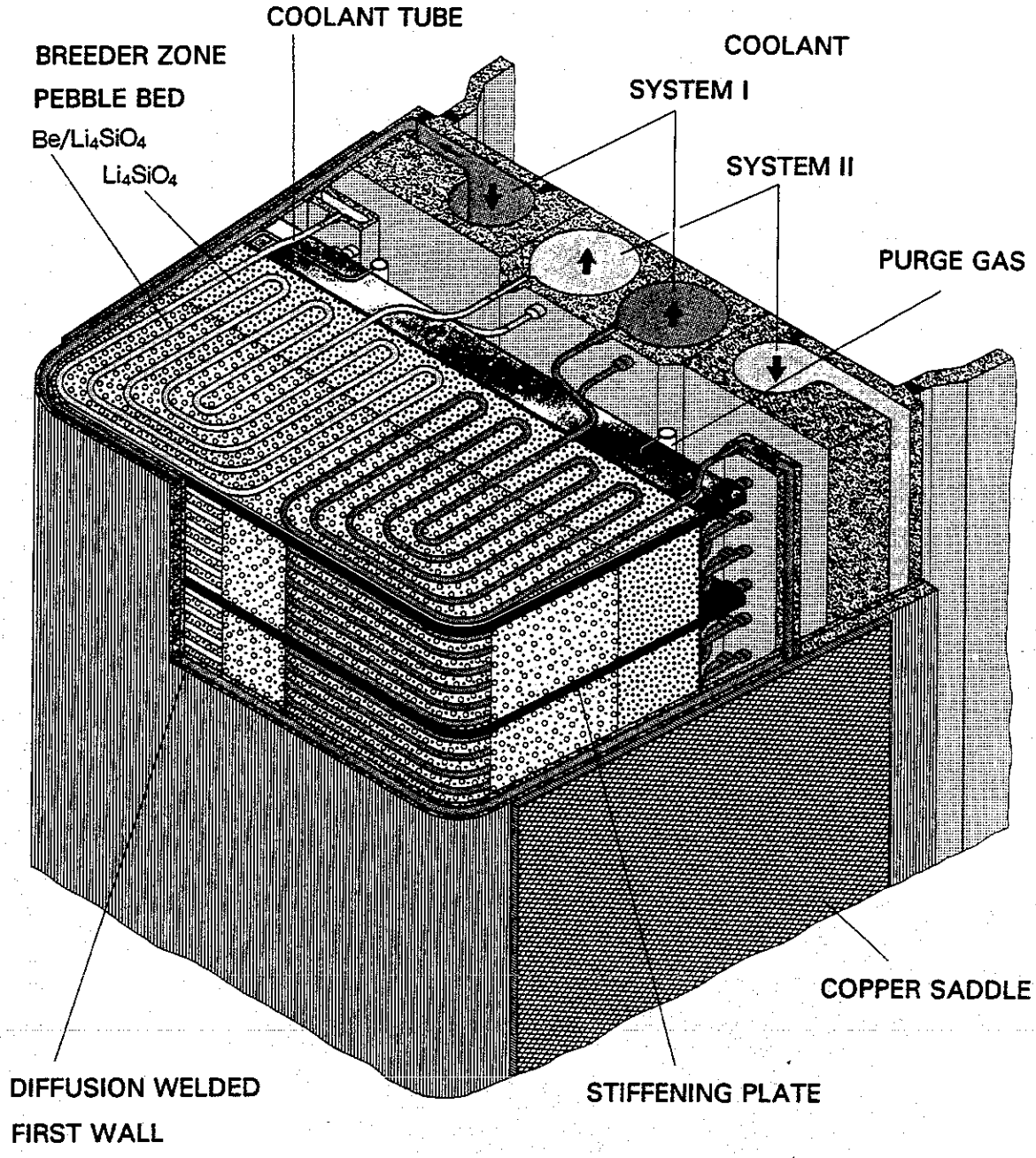

Figure A1: Layout of an outboard blanket segment for a solution with coil of tube and mixed pebble bed [1]

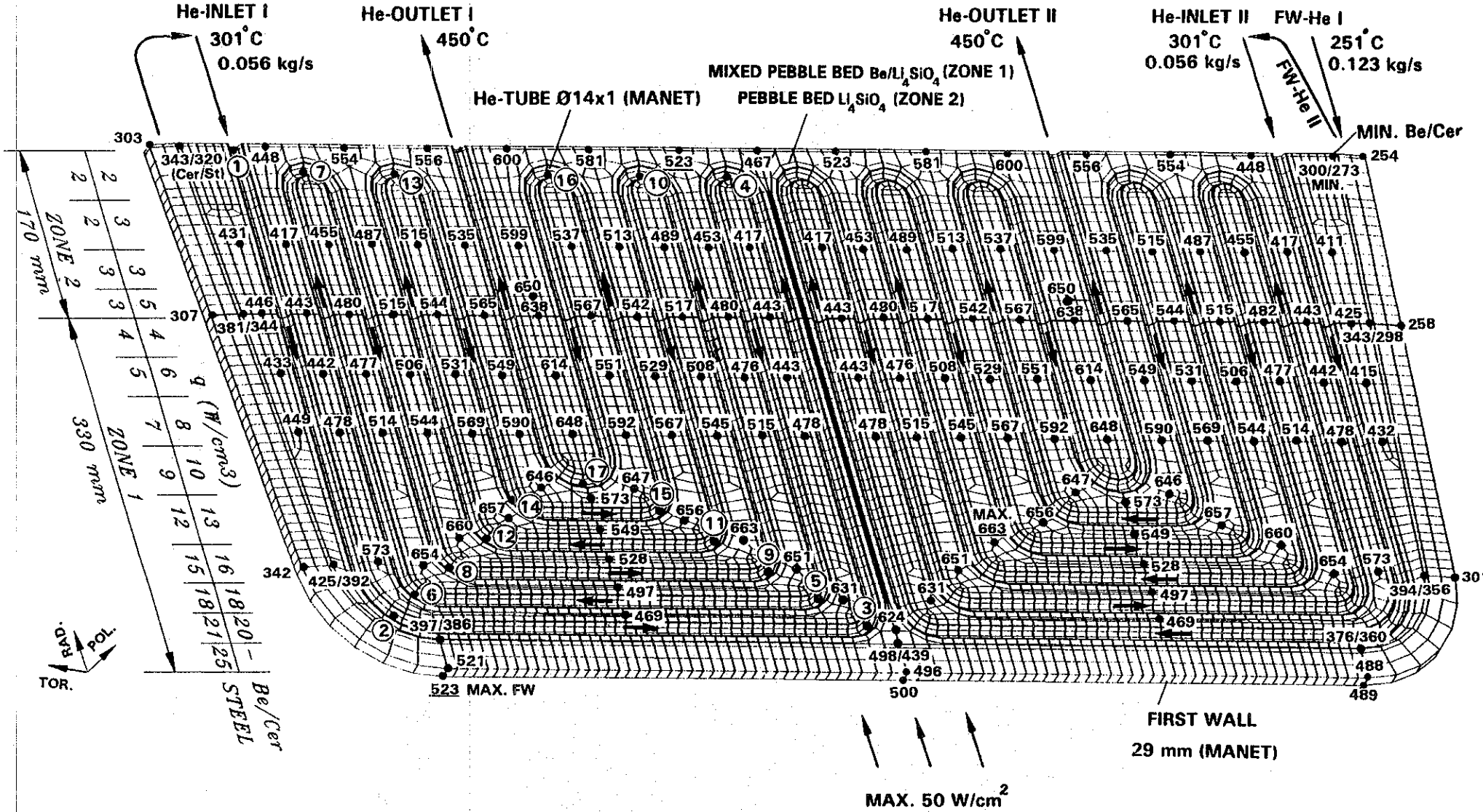

POINT	1	2	3	4	5	6	7	8	9	10	11	12	13	14	15	16	17	18
He-TEMP. (°C)	301	312	326	335	345	358	367	376	386	394	402	410	417	424	429	436	443	450

Helium mass flow: one coil of tube 0.056 kg/s; one First Wall channel 0.123 kg/s

Figure A2: Temperature distribution at the center of an outboard blanket segment for a solution with coil of tube and mixed pebble bed

PART 2

Dual Coolant Self-cooled Liquid Metal Blanket

Contents

Part 2

1 Introduction

Within the framework of blanket development for DEMO a self-cooled liquid metal blanket concept has been elaborated at KfK for some years. The eutectic lead-lithium alloy Pb-17Li has served both as the breeder material and coolant. By use of liquid metal as the coolant the blanket layout can be made relatively simple.

However, this advantage is counteracted by magneto-hydrodynamic (MHD) problems, which are attributable to the interaction of liquid metal flow and the strong magnetic field. Cooling of the First Wall proves to be particularly difficult because faster velocities of the liquid metal are required to remove the high heat flow. This calls for dedicated measures helping to avoid intolerably high MHD pressure losses. Therefore, in the previous reference concept [1] liquid metal flow for cooling of the First Wall is routed parallel to the magnetic field (toroidal) through the respective coolant channels because this direction of flow avoids high MHD pressure losses.

Another solution offers itself as an alternative to this concept, with the First Wall not cooled with liquid metal but with helium [2]. This allows the overall MHD pressure losses to be reduced considerably. Besides avoiding MHD pressure losses, this dual concept offers the following additional advantages:

- Plain layout of the blanket segment.
- Risk of liquid metal leaking into the plasma space nearly excluded by double walled confinement.
- "Leak-tolerant design" not requiring replacement of the blanket segment in case of individual leaks appearing in the weld.
- Removal of all the decay heat feasible both with helium and with liquid metal.

This report deals with the thermohydraulics design of the dual cooling system (helium and liquid metal) for the inboard and outboard segments.

2 General Layout of the Blanket

Figure 1 is a schematic of the layout of the liquid metal blanket in the inboard and outboard segments of the DEMO reactor. On account of the higher magnetic field prevailing in the inboard segment, the inboard blanket is divided into two halves so that the rate of liquid metal flow and consequently the MHD pressure drop can be reduced.

Figures 2 to 4 show the structural design of an outboard blanket segment in an isometric representation with the blanket cross sections at the mid-plane and at the upper end of the blanket. The whole blanket structure is made from 1.4914 martensitic steel (EU designation MANET). The U shape of the First Wall, total thickness 38 mm, consisting of seven diffusion bonded poloidal sections and a straight extension piece, together with the supporting and shielding structure make up a stiff segment box. Within the First Wall parallel coolant channels (□ 25x25 mm) are arranged at the radial toroidal plane with 30 mm channel spacing which are passed by helium gas at 80 bar pressure in alternating directions. The counterflowing coolant gas contributes to achieving a uniform temperature in the external structure and hence to minimizing the thermal stress. Besides, separation of the supply systems I and II guarantees emergency cooling upon failure of a coolant system.

Within the segment box reinforcing plates have been welded together to form grids and have been rigidly welded to the external structure. In the four radial front chambers they form coolant channels for the liquid metal and in the rear chamber poloidal channels for the main helium supply.

The helium coolant gas enters the upper blanket segment at 250 °C, first flows through the rear main supply channels downward while getting but slightly warmed. During diversion at the bottom end of the blanket the helium gas is carried into the parallel coolant channels of the First Wall. By means of a header system it is routed five times in sequence in a meander shaped flow through the segment walls on its way upwards. After the last passage the helium temperature at the upper outlet of the blanket attains a value of 350 °C.

The liquid metal enters the top end of the blanket at a temperature of 275 °C, flows downward through the three rear channel zones, and when it reaches the bottom end of the blanket has been heated to 351 °C. It is then diverted into the front channel zone where it reflows to the top at higher velocity and leaves the blanket again at 425 °C outlet temperature.

For the inboard blanket segment whose horizontal cross section is represented in Fig. 5 the same principle of dual cooling applies as to the outboard blanket segment. On account of the necessity of massive shielding of the magnets placed behind, relatively small liquid metal cooling zones exist there. The two rear channel zones are passed by "cold" and the front channel zone by "hot" liquid metal.

3 Design Method

3.1 Blanket Power

The computations are based on the blanket powers determined by application of the Monte Carlo method [3]. In Figures 6 through 9 the radial power density distributions in steel and lead-lithium are represented for the outboard and inboard blanket segments at the mid and top blanket planes, respectively. The absolute maximum values are 25 W/cm^3 for steel, and 19 W/cm^3 for lead-lithium at the mid-plane of the outboard blanket. These values diminish at the upper end of the blanket, by about 30% in the outboard segment and by about 50% in the inboard segment.

The heat flux density on the surface of the First Wall input by the plasma is assumed to be 40 W/cm^2 on the average and 50 W/cm^2 at the maximum, respectively.

3.2 Design Criteria and Coolant Flows

The necessary lead-lithium flow is determined from the power to be removed from the respective zones of the blanket segment and from the maximum possible enthalpy rise. The latter is limited by the maximum admissible temperature of the interface of steel and liquid metal determined by corrosion. It is approx. 470 °C for MANET steel so that the mean outlet temperature of 425 °C of lead-lithium is assumed. Taking into account the 235 °C fusion point of the Pb-17Li eutectic, the inlet temperature of 275 °C is chosen. Accordingly, the total enthalpy rise for lead-lithium of 150 K is obtained.

The inlet temperature of the helium cooling gas is assumed to be 250 °C, taking into account the DBTT (ductile brittle transition temperature) of MANET steel. The thermal power to be removed by helium is calculated from the heat source power of the First Wall plus side walls and the thermal power on the surface input by the plasma. For the sake of simplification, the power of the heat source in the steel walls separating helium gas from liquid metal is added with half its amount each to the two coolants.

For the First Wall exposed to the highest thermal load the additional criterion holds that the First Wall temperature, taking into account the creep rupture strength of MANET, must not exceed a maximum of approx. 550 °C. The mean outlet temperature of helium is therefore assumed to be 350 °C after adjustment of flow to pressure loss. This corresponds to a total enthalpy rise of the helium coolant gas of 100 K. The mean coolant gas pressure is assumed to be 80 bar.

3.3 Distribution of Coolant Flow

As already said, the whole First Wall is passed as much as five times by helium gas in successive toroidal flows from the bottom inlet to the top outlet (Figs. 10 and 11). In the main blanket part the helium cooling gas already after four passages experiences about 95% of the total enthalpy rise. This is the reason why the helium temperature level, after the fourth passage, is higher by 95 K than that in the bottom blanket zone. This would raise to the same extent the temperature level of the First Wall. To counteract this influence on the First Wall temperature, higher helium velocities are needed in the top blanket zone in order to enhance heat transfer. For this reason, the coolant channel is divided into zones for helium passage in such a way that the helium velocity steadily increases from bottom to top. Such channel divisions for the outboard and inboard segments are represented schematically in Figs. 10 and 11. This allows the First Wall temperatures to be made uniform in poloidal direction.

The radial decrease in power within the blanket cross section (see Fig. 6) results in accordingly lower powers of the heat source for the rear lead-lithium channel zones. This would mean that the lead-lithium in channel zone II experiences much more heating than that in channel zone IV. To compensate for this influence and hence obtain a homogeneous distribution of temperatures in the blanket cross section, it is attempted to achieve identical enthalpy rises of the lead-lithium partial streams in zones II, III and IV. This is feasible, for instance, by throttling of the mass flows at the bottom end of the blanket. The lead-lithium flows for the channel zones indicated in the outboard segment cross section have been entered in Fig. 3. The global temperature distribution of lead-lithium in the outboard blanket is shown in Fig. 12 (see section below).

3.4 Reduction of the Maximum First Wall Temperature by Artificial Roughnesses

The Finite Element computer code ABAQUS [4] is used to determine the temperatures of the First Wall. A local peak heat load of the surface of 50 W/cm^2 is assumed. The constitutive data of helium and the Nusselt relations have been taken from [5]. The Prandtl number is 0.67. The helium counterflows in the neighboring coolant channels and the heat exchange at the partitioning wall to liquid metal are not taken into consideration. In this way one is on the safe side.

The results of computation (see section below) show that the maximum First Wall temperature under the prevailing thermohydraulics conditions exceeds the tolerable value

by about 50 K. An increase in total coolant flow would imply a considerable loss of pressure and deterioration of the thermodynamic efficiency of the reactor. A suitable countermeasure would be artificial roughening of the coolant channel wall facing the plasma. By this, both the maximum First Wall temperature can be effectively lowered and the temperature distribution given a much more uniform pattern. This will decisively reduce the thermal stresses occurring. The associated pressure loss is relatively small because only a specified surface must be roughened. It is referred to [6] in the determination of the conditions of heat transfer and pressure losses on rough surfaces. The result of a comparison computation (see section below) makes evident that the maximum steel temperature is lowered by approx. 70 K in case the heat transfer coefficient is raised by a factor of 2. The total pressure loss increases by about 18% as a result of artificial roughening, and its absolute value is 1.5 bar for the outboard segment and 1.2 bar for the inboard segment. The resistance coefficients in the determination of the losses occurring during diversion are taken from [7].

4 Design Calculation for the Outboard Blanket Segment

4.1 Helium Loop

4.1.1 Thermal Power to be Removed (Poloidal Sum)

Surface power: 40×10^4 W/m^2·8.31 m^2 = 3.324 MW

Power of heat source [MW]:

	First Wall				Side Walls				Helium Main Pipes	Total
	Outside	Center	Inside	Total	Outside	Center	Inside	Total		
Main blanket zone	0.8605	0.8948	$\frac{1.132}{2}$	**2.3213**	0.2875	0.2419	$\frac{0.3261}{2}$	**0.6925**	0.2469	**3.2607**
Extension at top	0.0904	0.0767	$\frac{0.0938}{2}$	**0.2140**	0.0209	0.0163	$\frac{0.0210}{2}$	**0.0478**	0.0218	**0.2836**

Sum of heat source power: **3.5442 MW**

Total (surface + heat source power): **6.8682 MW**

4.1.2 Required Helium Flow

$$\dot{m}_{He} = \frac{Q}{c_p \cdot \Delta T_{He}} = \frac{6.8682\,x\,10^{6}\,W}{5.2\,x\,10^{3}\,\frac{J}{kgK}\cdot(350-250)\,K} = 13.21\,\frac{kg}{s}$$

4.1.3 Number of Parallel Helium Passages (Fig. 10)

n=4 (main blanket zone) + 1 (extension at top)

4.1.4 Coolant Channel Geometry

Channel cross section: 25x25 mm

Poloidal channel spacing: 30 mm

Position of the coolant channels:

	Main Blanket Zone, Section No. (Figs. 10, 12)								Extension at Top	
	1	2	3	4	5	6	7	8	A	B
Height of section [mm]	1080	1050	1050	1050	1050	1050	1050	1080	1200	1250
Number of channels	36	35	35	35	35	35	35	36	40	41
Mean toroidal channel length [mm]	881	967	1026	1057	1057	1026	967	881	881	881
Plasma facing surface [m2]	0.951	1.015	1.077	1.110	1.110	1.077	1.015	0.951	-	-

Total number of coolant channels:

Main blanket zone 282

Extension at top 81

4.1.5 Design of the He Passages (Fig. 10)

n = 4 in the main blanket part + 1 in the extension at top

He Passage	Number of Coolant Channels	Flow Cross Section x 10-4 [m²]	Mean Channel Length [m]			Plasma Facing Surface [m²]	Q x 10³ [W]			ΔT_{He} [K]			T_{He} [°C]				Flow Values at p_{He} = 80 bar			
													Inlet		Outlet					
			FW	SW	Σ		FW 2)	SW	Σ	FW	SW	Σ	SW	FW	FW	SW	ρ 3) [kg/m³]	c 4) [m/s]	Re 5) [-]	Δp_λ 6) [bar]
I	93	581.25	0.93	1.6	2.53	2.6421	1725.0	199.3	1924.3	25.1	2.9	28.0	254.0	255.5	280.6	282.0	7.11	32.0	$1.9 \cdot 10^5$	0.074
II	76	475.0	1.04	1.6	2.64	2.3798	1731.1	232.3	1963.4	25.2	3.4	28.6	282.0	283.7	308.9	310.6	6.76	41.1	$2.3 \cdot 10^5$	0.121
III	62	387.5	1.01	1.6	2.61	1.8752	1305.1	165.6	1470.7	19.0	2.4	21.4	310.6	311.8	330.8	332.0	6.47	52.7	$2.7 \cdot 10^5$	0.187
IV	51	318.75	0.90	1.6	2.50	1.4098	882.9	95.2	978.1	12.9	1.3	14.2	332.0	332.7	345.6	346.2	6.29	65.9	$3.2 \cdot 10^5$	0.273
V 1)	81	506.25	0.83	1.6	2.43	-	214.0	48.0	263.0	3.1	0.7	3.8	346.2	346.6	349.7	350.0	6.19	42.1	$2.0 \cdot 10^4$	0.107

Total: 0.762

1) Extension at top, total He flow

2) Surface and heat source powers

3) $\rho[kg/m^3] = 48.091 \cdot \frac{p\,[bar]}{T\,[K]}$

4) $c\,[m/s] = \frac{\dot{m}}{\rho \cdot A}$; $\dot{m}_{He} = 13.21\ kg/s$

5) $Re = \frac{c \cdot d_h}{\nu} = \frac{c \cdot d_h}{\eta/\rho}$ *with* $\eta = 0.4646 \cdot T_{He}^{0.66}[K] \times 10^{-6}[kg/ms]$

6) $\Delta p_\lambda = \lambda \cdot \frac{l}{d_h} \cdot \frac{\rho}{2} \cdot c^2$ *with* $\lambda = 0.020\ (d_h/k = 1250)$

4.1.6 Pressure Losses due to Diversion

	Pressure Loss Coefficient ζ for One Passage
Inflow (117 dia./25 dia.) normal, rounded (* broken)	0.06 (* 0.25)
2 bends, 120° r/d = 60/25 = 2.4; hydraulically smooth	2·0.09 = 0.18
2 bending edges (FW/SW), 93.75° r/d = 100/25 = 4; hydraulically smooth	2·0.07 = 0.14
Outflow (25 dia./117 dia.), abrupt	0.91
	Total: 1.29

Pressure Loss Portions in One Passage:

Friction pressure loss coefficient:

$$\Sigma\left(\lambda\cdot\frac{l}{d_h}\right)\approx 0.02\cdot\frac{2.6\,m}{25\,x\,10^{-3}\,m}=2.08$$

Diversion pressure loss coefficient:

$\Sigma\zeta = 1.29$

Total pressure loss coefficient $= 2.08+1.29 = 3.37$

$$\textit{Friction pressure loss fraction} = \frac{2.08}{3.37} = 0.617$$

$$\textit{Diversion pressure loss fraction} = \frac{1.29}{3.37} = 0.383$$

Total Pressure Losses in the Coolant Channels (without feed pipes):

$$\Delta p_{\lambda+\zeta} = \frac{0.762\ bar}{0.617} = 1.235\ bar$$

4.1.7 Further Pressure Losses in the Poloidal Helium Feed and Discharge Channels

Geometric Data:

		He header/ manifold (upward)	He main supply (downward)
d_h [m]		117×10^{-3}	178×10^{-3}
l_{tot} [m]	(together with extension at top)	≈ 11	≈ 11
A [m^2]		ca. 298×10^{-4}	644×10^{-4}

Hydraulic Data:

$\dot{m}$ [kg/s] (1 cooling system)	6.605	6.605
T [°C]	300	250
p [bar]	80	80
ρ [kg/m^3]	6.7	7.4
c [m/s]	$\approx 33/2 = 16,5$	16,5
η [kg/ms]	31×10^{-6}	29×10^{-6}
Re [-]	4.2×10^5	5.7×10^{-5}
d_h/k [-] with k = 0.01 mm	11,700	17,800
λ	0.0145	0.014

Estimated Diversion Losses:

Bottom inflow:	$\zeta \approx 0.17 + 0.06 = 0.23$
2x45°diversion: (d/R≈160/480)	$\zeta \approx 2 \cdot 0.03 = 0.06$
7x13° diversion: (d/R≈160/480)	$\zeta \approx 7 \cdot 0.017 = 0.12$
	$\Sigma\zeta = 0.41$

Total Pressure Loss:
Supply system:

$$\Delta p_{\lambda+\zeta} = \left(0.0145 \cdot \frac{11\,m}{117\,x\,10^{-3}\,m} + 0.41 \right) \cdot \frac{7.4}{2} \frac{kg}{m^3} \cdot 15^2 \frac{m^2}{s^2} = 0.015\,bar$$

Discharge System:

$$\Delta p_{\lambda+\zeta} = \left(0.014 \cdot \frac{11\,m}{178\,x\,10^{-3}\,m} + 0.41 \right) \cdot \frac{6.2}{2} \frac{kg}{m^3} \cdot 16.5^2 \frac{m^2}{s^2} = 0.011\,bar$$

Total Helium Pressure Losses between Blanket Inlet and Outlet:

$$\Delta p_{He,tot} = 1.235\,bar + 0.015\,bar + 0.011\,bar = 1.261\,bar$$

4.1.8 Admissible FW Temperature and Increase in Heat Transfer Coefficient by Artificial Roughness

Maximum admissible FW temperature for MANET: 550 °C

4.1.8.1 Heat Transfer Coefficient in the Front FW Coolant Channels

$$Nu = 0.018744 \cdot (Re)^{0,8} \cdot \left(\frac{T_W}{T_E}\right)^{-0.18}$$

$$\alpha = \frac{Nu \cdot \lambda_{He}}{d_h}$$

$$with \ \lambda_{He}[W/mK] = 3.623 \, x \, 10^{-3} \cdot T_{He}^{0.66}[K],$$

T_W[K]: mean inner wall temperature;

T_E[K]: inlet temperature.

For n=4+1 (design Sect. 4.1.5) the following α-values are obtained for the FW coolant channels and the resulting maximum FW temperature according to the computations with ABAQUS (cf. also Table 1):

He Pas-sage	Re_{FW} [-]	Nu [-]	$T_{max,He,FW}$ [°C]	$\lambda_{He,FW}$ [W/mK]	α_{FW} [W/m²K]	$q_{surface}$ x 10^4 [W/m²]	$q_{max.}$ x 10^6 [W/m³]	T_{FW} [°C] Inside	T_{FW} [°C] Max. outside	ΔT_{FW} [K]	$\Delta T_{He/wall}$ [K]
I	1.92x10⁵	302	280.6	0.231	2793	50	22	493	597	104	212
II	2.27x10⁵	349	308.9	0.239	3335	50	24	493	599	106	184
III	2.71x10⁵	406	330.8	0.245	3975	50	23	485	591	106	154
IV	3.23x10⁵	470	345.6	0.250	4698	50	19	473	579	106	127
V	2.01x10⁵	323	349.7	0.253	3267	-	10	365	371	105	20

The maximum FW temperature in this case is 599 °C which exceeds by far the admissible limit.

4.1.8.2 Increase in Heat Transfer Coefficient α_{FW}* by Artificial Roughness

Goal: reduction of the maximum FW temperature to $T_{max,\,FW} \leq 550\,°C$.

Shape and appearance of roughness rib: rectangular, only at plasma facing channel wall, transverse to flow direction.

For a maximum factor $f_\alpha = \alpha^*_{FW}/\alpha_{FW}$ of 2.0 the following values are obtained:

He Pas-sage	Maximum Factor f_α	α_{FW}*	T^*_{FW} [°C]		$\Delta T^*_{max,FW}$ [K]	$\Delta T^*_{He/wall}$ [K]	$f\Delta p$ [-]	Δp^* [bar]
			Inside	Max. outside				
I	2.0	5586	391	509	118	110	1.90	0.098
II	2.0	6670	404	525	121	95	1.90	0.164
III	2.0	7950	410	531	121	79	1.90	0.253
IV	2.0	9396	410	530	120	64	1.90	0.362
V	-	-	-		-	-	-	0.107
							$\Sigma\Delta p^*$	0.984

Increase in pressure loss due to artificial roughness:

(0.984 - 0.762) bar = 0.222 bar

Total pressure loss in the presence of artificial roughness:

$\Delta p^*_{He,tot} \approx (1.261 + 0.222)$ bar = 1.483 bar

4.2 Liquid Metal Loop

4.2.1 Thermal Power to be Removed (Poloidal Sum)

Heat source power [MW] from:

	Steel Components			Pb-Li Coolants, Channel Zone				Total
	First Wall	Side Wall	Partitioning Plates	I	II	III	IV	
Main blanket zone	1.132/2	0.3261/2	0.9839	9.491	6.1689	2.6515	1.3944	21.4188
Extension at top	0.0943/2	0.0211/2	0.0430	0.7996	0.4741	0.2058	0.1082	1.6884

Total heat source power: **23.107 MW**

4.2.2 Required Pb-Li Flow

$$\dot{m}_{PbLi} = \frac{Q}{c_p \cdot \Delta T_{PbLi}} = \frac{23.107 \times 10^6\ W}{189 \frac{J}{kg\,K} (425-275)\ K} = 815 \frac{kg}{s}$$

4.2.3 Flow, Temperature and Velocity Distributions of Pb-Li Coolant Channel Zones I through IV (Fig. 3)

Channel Zone	Flow Cross Section[1] [x 10^{-4} m^2]		Pb-Li Flow [kg/s]	Velocity [1] [m/s]	Removal of Thermal Power[2] [MW]	Enthalpy Rise[2] [K]	Mean Pb-Li Temperature [°C]			
	With insulating coatings on duct wall	With flow channel inserts for electrical insulation					Main Blanket Zone		Extension at Top	
							Inlet	Outlet	Inlet	Outlet
I	1042.5	994.2	815	0.877	11.3851	74	351	419	419	425
II	1779.8	1711.6	503	0.312	7.2232	76	280	351	275	280
III	1857.6	1788.6	202	0.120	2.9067	76	280	351	275	280
IV	1968.5	1898.0	110	0.061	1.5867	76	280	351	275	280

1) Around the blanket center; regarding the top blanket cross section, see Fig. 4.

2) Inclusive of extension at top

5 Design Calculation for the Inboard Blanket Segment

5.1 Helium Loop

5.1.1 Thermal Power to be Removed (Poloidal Sum)

Surface power: 40×10^4 W/m^2·7.072 m^2 = 2.83 MW

Heat source power [MW]:

Inboard Blanket	First Wall				Side Walls				He Main Tubes	Total
	Outside	Center	Inside	Sum	Outside	Center	Inside	Sum		
Upper half	0.2645	0.1967	0.3314/2	**0.6269**	0.0967	0.0647	0.1112/2	**0.2170**	0.3517	**1.1956**
Lower half	0.2494	0.1843	0.3049/2	**0.5862**	0.0874	0.0592	0.1020/2	**0.1977**	0.3121	**1.0960**
Equatorial range of partition-ing	0.0201	0.0158	0.0283/2	**0.0501**	0.0027	0.0019	0.0036/2	**0.0064**	0.0659	**0.1224**
Divertor zone, top	0.0488	0.0356	0.593/2	**0.1141**	0.0199	0.0129	0.0227/2	**0.0441**	0.1184	**0.2766**
Divertor zone, bottom	0.0482	0.0356	0.0610/2	**0.1143**	0.0141	0.0105	0.018/2	**0.0336**	0.1022	**0.2501**

Total heat source power: **2.94 MW**

Total (surface + heat source power): **5.77 MW**

5.1.2 Required Helium Flow

Total flow:

$$\dot{m}_{He} = \frac{Q}{c_p \cdot \Delta T_{He}} = \frac{5.77\,x\,10^6\ W}{5.2\,x\,10^3\ \frac{J}{kgK} \cdot (350-250)\ K} = 11.10\ \frac{kg}{s}$$

For one blanket half: $\dot{m}_{He} = 5.55$ kg/s

5.1.3 Number of Parallel He Passages per Blanket Half

n = 4 (main blanket part) + 1 (divertor zone)

5.1.4 Coolant Channel Geometry

Channel cross section:	20x25 mm
Poloidal channel spacing:	30 mm
Total number of coolant channels:	
Main blanket zone	280
Divertor zones	166

5.1.5 Design of the He Passages (Fig.11)

n = 4 in the main blanket part + 1 in the divertor zone (for one blanket half each)

He Passage	Number of Coolant Channels	Flow Cross Section x 10^{-4} [m^2]	Mean Channel Length [m]			Plasma Facing Surface [m^2]	Q x 10^3 [W]			ΔT_{He} [K]			T_{He} [°C]				Flow Values at p_{He} = 80 bar			
			FW	SW	Σ		FW 2)	SW	Σ	FW	SW	Σ	Inlet		Outlet		ρ 3) [kg/m3]	c 4) [m/s]	Re 5) [-]	Δp_λ 6) [bar]
													SW	FW	FW	SW				
I	42	210	0.77	1.14	1.91	1.07	676.3	85.4	761.7	23.4	3.0	26.4	266.3	267.8	291.2	292.7	6.96	38.0	2.0×10^5	0.082
II	37	185	0.77	1.14	1.91	0.92	544.2	60.5	604.7	18.9	2.1	21.0	292.7	293.7	312.6	313.7	6.68	44.9	2.2×10^5	0.116
III	33	165	0.77	1.14	1.91	0.82	451.4	42.3	493.7	15.6	1.5	17.1	313.7	314.4	330.0	330.8	6.46	52.0	2.4×10^5	0.150
IV	28	140	0.77	1.14	1.91	0.72	369.4	28.9	398.3	12.8	1.0	13.8	330.8	331.3	344.1	344.6	6.30	62.9	2.8×10^5	0.214
V 1)	83	415	0.77	1.14	1.91	-	114.1	44.1	158.2	3.9	1.5	5.4	344.6	345.3	349.2	350.0	6.20	21.6	0.9×10^5	0.025

Total: 0.587

1) Divertor zone, total He flow

2) Surface and heat source power

3) $\rho[kg/m^3] = 48.091 \cdot \frac{p\,[bar]}{T\,[K]}$

4) $c\,[m/s] = \frac{\dot{m}}{\rho \cdot A}$; $\dot{m}_{He} = 5.55\ kg/s$ *per blanket half*

5) $Re = \frac{c \cdot d_h}{\nu} = \frac{c \cdot d_h}{\eta/\rho}$ *with* $\eta = 0.4646 \cdot T_{He}^{0.66}[K] \cdot 10^{-6}[kg/ms]$

6) $\Delta p_\lambda = \lambda \cdot \frac{l}{d_h} \cdot \frac{\rho}{2} \cdot c^2$ *with* $\lambda = 0.020\ (d_h/k = 1250)$

5.1.6 Diversion Pressure Losses

	Pressure Loss Coefficient ζ for One Passage
Inflow(117 dia./22dia.) normal, rounded (*broken)	0.06 (* 0.25)
2 bends, 120° r/d = 60/25 = 2,4; hydraulically smooth	2·0.09 = 0.18
2 bending edges (FW/SW), 86.25° r/d= 105/22.2= 4.7; hydraulically smooth	2·0.07 = 0.14
Outflow (22 dia./117dia.), abrupt	0.91
	Total: 1.29

Pressure Loss Portions in One Passage:

Friction pressure loss coefficient:

$$\Sigma\left(\lambda\cdot\frac{l}{d_h}\right)\approx 0.02\cdot\frac{1.9\ m}{22.2\ x\ 10^{-3}\ m}=1.71$$

Diversion pressure loss coefficient:

$\Sigma\zeta = 1.29$

Total pressure loss coefficient $= 1.71 + 1.29 = 3.0$

Friction pressure loss fraction $= \frac{1.71}{3.0} = 0.57$

Diversion pressure loss fraction $= \frac{1.29}{3.0} = 0.43$

Total Pressure Losses in the Coolant Channels (without supply pipes):

$$\Delta p_{\lambda+\zeta} = \frac{0.587}{0.57} = 1.03\ bar$$

5.1.7 Further Pressure Losses in the Poloidal Helium Feed and Discharge Channels

Geometric Data:

			He header/ manifold (upward)	He main supply (downward)
d_h [m]			$\approx 100 \times 10^{-3}$	$\approx 150 \times 10^{-3}$
l_{tot} [m]	(with divertor part)		≈ 7	≈ 7
A [m^2]		approx.	194×10^{-4}	419×10^{-4}

Hydraulic Data:

$\dot{m}$ [kg/s] (1 cooling system)	2.775	2.775
T [°C]	300	250
p [bar]	80	80
ρ [kg/m^3]	6.7	7.4
c [m/s]	$\approx 21/2 = 10,5$	10,7
η [kg/ms]	31×10^{-6}	29×10^{-6}
Re [-]	2.3×10^5	3.1×10^{-5}
d_h/k [-] with k = 0.01 mm	10,000	15,000
λ	0.016	0.015

Estimated Diversion Losses:

Bottom feed:	$\zeta \approx 0.17 + 0.06 = 0.23$
Diversions:	$\zeta \approx 0.06$
	$\Sigma\zeta = 0.29$

Total Pressure Loss:

Supply System:

$$\Delta p_{\lambda+\zeta} = \left(0.016 \cdot \frac{7\,m}{100\,x\,10^{-3}\,m} + 0.29 \right) \cdot \frac{7.4}{2} \frac{kg}{m^3} \cdot 9.65^2 \frac{m^2}{s^2} = 0.005\,bar$$

Removal System:

$$\Delta p_{\lambda+\zeta} = \left(0.015 \cdot \frac{7\,m}{150\,x\,10^{-3}\,m} + 0.29 \right) \cdot \frac{6.2}{2} \frac{kg}{m^3} \cdot 10.7^2 \cdot \frac{m^2}{s^2} 0.004\,bar$$

Total Helium Pressure Losses between Blanket Inlet and Outlet:

$$\Delta p_{He,\,tot} = 1.03\,bar + 0.005\,bar + 0.004\,bar = 1.04\,bar$$

5.1.8 Admissible FW Temperature and Increase in the Heat Transfer Coefficient as a Result of Artificial Roughness

Maximum admissible FW temperature for MANET: 550 °C

5.1.8.1 Heat Transfer Coefficient in the Front FW Coolant Channels

$$Nu = 0.018744 \cdot (Re)^{0.8} \cdot \left(\frac{T_W}{T_E}\right)^{-0.18}$$

$$\alpha = \frac{Nu \cdot \lambda_{He}}{d_h}$$

$$with \quad \lambda_{He}[W/mK] = 3.623 \, x \, 10^{-3} \cdot T_{He}^{0.66}[K],$$

T_W[K]: mean inner wall temperature;

T_E[K]: inlet temperature.

For n=4+1 (design, Section 5.1.5) the following α-values are obtained for the FW coolant channels and the resulting maximum FW temperature according to the ABAQUS computations (cf. also Table 2):

He Pas-sage	Re_{FW} [-]	Nu [-]	$Tmax_{He,FW}$ [°C]	$\lambda_{He,FW}$ [W/mK]	α_{FW} [W/m²K]	$q_{surface}$ x 10⁴ [W/m²]	$q_{max.}$ x 10⁶ [W/m³]	T_{FW} [°C] Inside	T_{FW} [°C] Max. Outside	ΔT_{FW} [K]	$\Delta T_{He/wall}$ [K]
I	2.0x10⁵	308	291.2	0.234	3245	50	20	473	577	104	182
II	2.2x10⁵	337	312.6	0.240	3643	50	18	473	576	103	160
III	2.4x10⁵	365	330.0	0.246	4035	50	14	471	573	102	141
IV	2.8x10⁵	413	344.1	0.250	4642	50	12	464	566	102	120
V	0.9x10⁵	172	349.2	0.252	1958	--	4	359	361	2	10

The maximum First Wall temperature in this case is 577 °C which is also well above the admissible limit.

5.1.8.2 Increase in Heat Transfer Coefficient α_{FW}^* by Artificial Roughness

Goal: reduction of the maximum FW temperature to $T_{max, FW} \leq 550$ °C

Shape and appearance of roughness rib: rectangular, only at plasma facing channel wall, transverse to flow direction.

For a maximum factor $f_\alpha = \alpha^*_{FW}/\alpha_{FW}$ of 2.0 the following values are obtained:

He Passage	Maximum Factor f_α	α_{FW}^*	T^*_{FW} [°C]		$\Delta T^*_{max,FW}$ [K]	$\Delta T^*_{He/wall}$ [K]	$f\Delta p$ [-]	Δp^* [bar]
			Inside	Max. Outside				
I	2.0	6490	385	503	118	94	1.90	0.112
II	2.0	7286	402	512	110	89	1.90	0.158
III	2.0	8070	402	517	115	72	1.90	0.204
IV	2.0	9284	405	519	114	61	1.90	0.292
V	-	-	-		-	-	-	0.107
							$\Sigma\Delta p^*$	0.766

Pressure loss increase as a result of artificial roughness:

(0.766 - 0.587) bar = 0.179 bar

Total pressure loss in the presence of artificial roughness:

$\Delta p^*_{He,tot} \approx$ (1.040 + 0.179) bar = 1.22 bar

5.2 Liquid Metal Loop

5.2.1 Thermal Power to be Removed (Poloidal Sum)

Heat source power [MW] from:

	Steel Components			Pb-Li Coolants, Channel Zone			Total
	First Wall	Side Wall	Partitioning Plates	I	II	III	
Upper half	$\frac{0.3314}{2}$	$\frac{0.1112}{2}$	0.2254	2.7158	1.1917	0.7688	**5.1230**
Lower half	$\frac{0.3049}{2}$	$\frac{0.1020}{2}$	0.2080	2.4594	1.0945	0.6967	**4.6621**
Equatorial partitioning zone	$\frac{0.0283}{2}$	$\frac{0.0036}{2}$	0.0856	0.2923	0.1380	0.0829	**0.6148**
Divertor zone, top	$\frac{0.0593}{2}$	$\frac{0.0277}{2}$	0.0496	0.8077	0.3979	0.2756	**1.5718**
Divertor zone, bottom	$\frac{0.0611}{2}$	$\frac{0.0180}{2}$	0.0448	0.7718	0.3655	0.2555	**1.4772**

Total heat source power: **13.45 MW**

5.2.2 Required Pb-Li Flow

$$\dot{m}_{PbLi} = \frac{Q}{c_p \cdot \Delta T_{PbLi}} = \frac{13.45 \times 10^6\ W}{189 \frac{J}{kg\,K} (425-275)\,K} = 474.4 \frac{kg}{s}$$

5.2.3 Flow, Temperature and Velocity Distributions of the Pb-Li Coolant Channel Zones I through III

Channel Zone	Flow Cross Section[1] [x 10-4 m2]		Pb-Li Flow [kg/s]	Velocity 1) [m/s]	Thermal Power Removal 2) [MW]	Enthalpy Rise[2] [K]	Mean Pb-Li Temperature [°C]			
	With insulating coatings on duct wall	With flow channel inserts for electrical insulation					Main Blanket Zone		Extension at Top	
							Inlet	Outlet	Inlet	Outlet
I	730.7	712.3	237.2	0.357	3.935	87.8	337.2	406.0	406	425.0
II	700.0	667.5	143.6	0.227	1.688	62.2	289.6	337.2	275	289.6
III	680.0	648.0	93.6	0.153	1.101	62.2	290.5	337.2	275	290.5

1) see Fig. 5

2) inclusive of divertor zone

6 Power Requirements of the Helium Blower and the Liquid Metal Pump

The adiabatic power of a helium blower can be determined with the following equation:

$$P_{ad} = \dot{m} \cdot \frac{\chi}{\chi\text{-}1} \cdot R \cdot T \cdot \left[\left(\frac{p_2}{p_1} \right)^{\frac{\chi\text{-}1}{\chi}} - 1 \right]$$

with the helium gas constants R = 2078.75 J/kgK and $\chi = 5/3$.

The pressure losses in an outboard segment and an inboard segment, as determined in the preceeding chapters, amount to round 1.5 bar and 1.2 bar, respectively.

Assuming additional pressure losses in the heat exchanger and other components of about 0.5 bar, the total pressure losses in the whole helium loop will be round 2.0 bar in an outboard segment and 1.7 bar in an inboard segment, respectively. With an aver-

age system pressure of 80 bar we obtain for the outboard $p_1 = 79.0$ bar, $p_2 = 81.0$ bar and for the inboard $p_1 = 79.15$ bar, $p_2 = 80.85$ bar. For a given helium mass flow of 13.21 kg/s in an outboard segment and 11.10 kg/s in an inboard segment at T = 513 K the adiabatic blower power amounts to 0.3540 MW in an outboard segment and to 0.2526 MW in an inboard segment. Thus, the total blower power required for the whole reactor will be: (48x0.3540/0.8 + 32x0.2526/0.8) MW = (21.2 + 10.1) MW = 31.3 MW, if a blower efficiency of 0.8 is assumed.

The power of a circulation pump for liquid metal can be determined as

$$P_{LM} = \dot{m}_{LM} \cdot \frac{\Delta p_{MHD}}{\rho}$$

with $\dot{m}_{LM}$, the liquid metal mass flow, equal to 815 kg/s for the outboard and 474 kg/s for the inboard, Δp_{MHD}, the MHD pressure losses [2], equal to 4 bar for the outboard and 1.3 bar for the inboard, ρ, the density of lead-lithium, equal to 9.53×10^3 kg/m^3 at 275 °C. In this case the flow pressure drop can be neglected because the velocity of the liquid metal is very low. Thus, the power of a circulating pump amounts to 0.0342 MW for an outboard segment and to 0.0065 MW for an inboard segment. The total circulating pump power for the whole reactor, with a pump efficiency of 0.8 assumed, sums up to (48x0.0342/0.8 + 32x0.0065/0.8) MW = 2.312 MW.

7 3D Temperature und Stress Calculation for the Outboard Blanket Box

7.1 Generation of the 3D Finite Element Model

In the following computations the ABAQUS Finite Element computer code [3] will be used. To generate the three-dimensional (3D) network [8], the CAD system BRAVO3 [9, 10] will be referred to. For this, the GRAFEM program package will be used which, being a part of the graphics editor, is available in the BRAVO3 system.

First, the editor generates the wire models of the components to be computed which models are needed as initial geometries for generating the three-dimensional network using GRAFEM. At the same time, the geometrical model is converted into a mathematical model by dividing the object into a multitude of nodes and elements which have to be interconnected.

Several mapping techniques of the GRAFEM software can be used for network generation, which will be done by the following steps.

- Generation of boundary lines by having coincide individual circuits of algebraic curves of the wire model.
- Generation of surfaces/planes, which are defined by an external and, maybe, several internal boundary lines.
- Generation of volumes/bodies defined by 12 boundary lines.
- Generation of nodes with variable densities on the boundary lines.
- Generation of the network of solid elements, starting from a plane or a volume.

Thus, the geometric features of the Finite Element models are described if the nodes and elements have been designated and their mutual assignments interconnected; their locations are determined by the x/y/z coordinates. Each element is provided in addition with information, e. g. address, type, material, etc.

In the next step the various loadings and their boundary conditions are specified which have to be assigned to individual groups of nodes and elements. GRAFEM supports data formats of several Finite Element codes, e. g. ABAQUS in the case considered here.

Figure 13 shows the CAD generated Finite Element model of the steel structure used for the stress computations. The model has a poloidal dimension of 30 mm corresponding to a coolant channel pitch. The symmetric radial-toroidal boundary planes run all through the center of the cooling channel ligament.

Knowledge of the temperature distribution is needed to be able to determine the thermal stresses occuring in the steel structures. The network ofr lead-lithium is generated in addition to allow the temperature distribution to be calculated (Fig. 14). On account of the countercurrent flows in the helium coolant channels, the two neighboring radial-toroidal coolant channel mid-planes are chosen as the symmetriy planes. In this way, two helium half-channels with countercurrent flows are added to the model of temperature computation. The poloidal height of the model displaced by 1/2 pitch remains unchanged (30 mm). Moreover, the steel shielding is not taken into account in the temperature computation because that shielding will be provided with an independent coolant system still to be designed. Therefore, in the subsequent computations the temperature of the shielding is assumed to be constant which, however, in the later design of the coolant system has to be set at an optimum value.

7.2 Material data and Admissible Limit of Loading

In Table 3 the thermal conductivity values, the strength values and the thermal expansion coefficient of MANET steel as a function of the temperature have been compiled. The values of thermal condutivity indicated in Table 4 are applicable to lead-lithium. The thermal conductivity of steel and of lead-lithium increases with rising temperature. At 500 °C the value for steel is 26 W/mK and for lead-lithium about 17 W/mK.The regulation according to the ASME code [11, 12] apply in the assessment of stresses:

σ_{adm} = $1 \cdot Sm, t$ for primary membrane stresses ($\sigma_{p.m}$), average taken over the cross-section;

σ_{adm} = $1.5 \cdot Sm,t$ for primary membrane plus bending stresses ($\sigma_{p,m+b}$);

σ_{adm} = $3 \cdot Sm$ for primary and secondary stresses ($\sigma_{p,m+b} + \sigma_s$);

with $S_m = \min (\frac{2}{3} \cdot \sigma_{0.2}, \frac{1}{3} \cdot \sigma_u)$ und $S_{m,t} = \min (S_m, \frac{2}{3} \cdot \sigma_{R,t}, 1 \cdot \sigma_{1,t})$.

where $\sigma_{0.2}$ is the 0.2 offset yield stress, σ_u is the tensile strength, $\sigma_{R,t}$, is the creep resistance, $\sigma_{1,t}$ is the 1% creep strain limit, and t is the time to failure, with $t = 2 \times 10^4$ h for steady-state DEMO operation. A relatively strong decrease of creep resistance of MANET above 500 °C is clearly visible from Table 3.

The equivalent stress intensity used in the comparison with the admissible stress (σ_{adm}) is the von Mises stress derived according to the yielding criterion:

$$\sigma_v = \sqrt{\frac{(\sigma_1-\sigma_2)^2 + (\sigma_2-\sigma_3)^2 + (\sigma_3-\sigma_1)^2}{2}} \qquad (22)$$

with σ_1, σ_2, σ_3 as the principal stresses. The superposition of primary and secondary stresses is made at the stress component level.

7.3 Distribution of Power

The radial distribution of power densities for steel and lead-lithium according to [3] constitutes the basis of calculation of the temperature distribution. The plots of the power density for the mid-plane of the outboard blanket have been traced in Fig. 6. Ac-

cordingly, the maximum power density in steel is about 25 W/cm^3 and in lead-lithium about 19 W/cm^3. These values decrease in poloidal direction towards the blanket ends. At the top blanket end (Fig. 7) the maximum value of steel is as low as 17.5 W/cm^3 and for lead-lithium only 13.5 W/cm^3, respectively. Therefore, a poloidal power distribution, as indicated in the table below, will be assumed in the following computation:

Location (s. Fig. 10)	Poloidal Power Factor	
	Steel	Lead-Lithium
A (bottom end)	0.7144	0.7448
B	0.8856	0.9139
C (mid-plane)	1,0	1,0
D	0.8966	0.9023
E (top end)	0.6730	0.7010

The thermal surface load of the First Wall is on the average 40 W/cm^2 and at the maximum 50 W/cm^2, respectively.

7.4 Method of Computation

7.4.1 Computation of Temperature

In the case of blanket cooling lead-lithium, in addition to its own high heat source power, must accommodate also high thermal powers originating in the adjoining structures. Considering the relatively poor thermal conductivity, strong temperature gradients, normal to the flow direction, develop in the blanket, above all in the wall-facing zones which, in turn, has an impact on the temperature level of the adjoining structures.

Considering the lack of combined solid/fluid codes, the simultaneous determination of the temperature distribution in the steel structure and in the liquid metal flow is feasible on simplifying assumptions only. In the following temperature computation the method of the moving system of coordinates will be applied (see also [15]). The following assumptions are made:

- The liquid metal adopts the pattern of a slug flow. This means that the flow rate in the coolant channels is uniformly distributed over the whole cross-section and has no elements normal to the direction of flow. Consequently, cross mixing of

the flow does not occur implying that normal to the direction of flow heat is transported solely by thermal conduction.

- Axial heat transport in the direction of flow is neglected.
- The liquid metal temperature at the inlet of the respective coolant channel is distributed homogeneously over the cross-section by complete mixing of flows.
- Thermal barriers between the First Wall coolant channels and the liquid metal flow due to MHD insulating coatings or flow channel inserts as another backup solution are neglected.

Quasi-steady state computations are made over the calculated time of fluid movement. The specific heat of the adjoining solid structure is set zero.

The different flow directions (Fig. 14) necessitate in addition to compute separately in a first step the temperatures of some subzones and then - following temperature averaging at the interfaces (ABC, ADC, AE and CG) - to repeat the computation.

7.4.2 Computation of Stresses

In accordance with the ASME rules (Item 7.2) the stresses are computed in two steps. In the first step only blanket loading by internal pressure is taken into account to determine the primary stresses. In a conservative approach a maximum internal pressure in the whole blanket of 80 bar is assumed; it corresponds to the pressure of the helium coolant system and occurs only in an accident case of a large leak between the helium and the Pb-17Li systems. In the second step thermal loading is superposed to the already existing internal pressure loading according to the temperature distribution from 7.4.1

The generalized plane strain boundary condition is used in stress computations. This means that the cutting planes represented in Fig. 13 remain plane and parallel with respect to each other implying that the differential thermal linear expansions in the whole blanket cross-section are taken into account in poloidal direction.

The stresses are calculated solely for the blanket mid-plane of an outboard blanket because in this zone the thermal loadings are maximum. The mean temperature of the shielding structure is conservatively assumed to be 285 °C in order to simulate the greatest possible temperature difference with respect to the front hot First Wall.

7.5 Result

7.5.1 Temperature Computation

Figures 15 through 23 show the temperature distributions for the bottom, middle and top blanket zones at a mean thermal surface loading of 40 W/cm^2. The development of the temperature field in the rear liquid metal zones can be well recognized at the bottom end of the blanket (Fig. 15). The liquid metal temperature in the front chamber is supposed to be homogeneous due to flow mixing in the process of liquid metal flow reversal. Figure 16 shows details of the temperature distribution in a cutout of the front right corner of the First Wall. The mean liquid metal temperature in the first chamber, 348 °C, is slightly below the global design value of 351 °C in Fig. 12 which is a result of heat exchange with the First Wall. The temperature at the point of contact between liquid metal and steel reaches a maximum of 415 °C in the second chamber. On account of the relatively low helium temperature, the temperature of the First Wall is still low in the bottom blanket zone where it attains a maximum of 474 °C. In Fig. 17 a weak temperature gradient can be noticed in the rear liquid metal zone corresponding to the lower power density. On the whole, a smaller fraction of the thermal power generated in the liquid metal is removed via the First Wall. This will lead to an additional temperature rise of the helium gas of approximately 10 K, if all thermal barriers between the First Wall and the liquid metal as mentioned above are neglected. Thus, the uncertainty of the calculated First Wall temperature can be estimated to +10 K at the top and about + 5 K at the center of the blanket which is well covered by the safty margin.

Figure 18 shows the corresponding temperature distribution on the blanket mid-plane. An intensive heat exchange between the liquid metal counterflows can be well recognized. The maximum First Wall temperature determined in this zone is 490 °C (Fig. 19). A weak temperature gradient is also measured in the rear liquid metal zone (Fig. 20). The temperature distribution is almost homogeneous.

At the upper end of the blanket (Fig. 21) the liquid metal experiences full enthalpy rise. This means that the temperature field has fully developed. The maximum temperature of contact between the liquid metal and steel measured here is 443 °C (Fig. 22) which means that it is well below the admissible value of 470 °C. The absolute maximum of 505 °C is also attained here for the First Wall temperature; this value is still far below the limit of 550 °C. The liquid metal temperature at the inlet of the main blanket part via the rear chambers is 280 °C and supposed to be homogeneous (Fig. 23).

In Figs. 24 and 25 the temperature distributions in the steel structure of the blanket center have been represented for mean and maximum thermal surface loadings of

40 W/cm^2 and 50 W/cm^2, respectively. These values serve as a basis for determination of the secondary stress in a further step.

7.5.2 Stress Computation

7.5.2.1 Primary Stress

In Fig. 26 the von Mises stresses in the blanket structure have been represented for a primary internal pressure loading of 80 bar. For the sake of transparency, only the maximum values attained by the respective structural sections have been entered. Besides, for symmetry reasons, they have been represented for only one half of the blanket. The figure makes also evident the corresponding deformation of the structure in a twenty-times enlargement. It makes clearly visible a heavier deformation occurring in the side walls compared with that in the First Wall due to the larger spacings between plates. In Figs. 27 and 28 the stresses have been represented for some structural cross-sections of the First Wall and of the side wall together with the peak values measured.

The resulting maximum stress in the side wall zone is 178 MPa in the ligament separating the channels. It is far below the 1·Sm value at 300 °C of 227 MPa (Table 3), with the stress in the ligament separating the channels conservatively considered to be predominantly a primary membrane stress. The maximum primary membrane plus bending stresses attain here 158 MPa which is also well below the 1.5·Sm limit.

In the First Wall zone the maximum primary membrane plus bending stresses attain 120 MPa which, considering the maximum temperature prevailing there, should be considered as much more critical. Taking into account a maximum thermal surface loading of 50 W/cm^2, a maximum temperature of the First Wall of 527 °C is obtained (Fig. 25). Accordingly, the 1.5·Sm limit value is 176 MPa and hence clearly higher than the existing stress.

The maximum primary membrane stress of 161 MPa in the ligament separating the channels is at that point also far below the admissible 1·Sm value at 330 °C of 220 MPa.

In the interior of the blanket a maximum temperature of contact between the liquid metal and steel of 443 °C was measured, as described in 7.5.1. The corresponding 1·Sm limit value is 185 MPa which is not exceeded at any point of the reinforcing plates in the liquid metal zones. In the helium header zones all stresses are well below the admissible values because the temperature prevailing there is relatively low.

In Fig. 29 the toroidal developments of the primary stresses along the flow path have been represented for the channel interior and the plasma facing side of the straight First Wall section. The bending load in the spacings of the reinforcing plates can be recognized well.

7.5.2.2 Primary plus Secondary Stresses at Mean Heat Flux Density of 40 W/cm^2

In Fig. 30 the distribution of the von Mises stress in the case of primary plus secondary stresses superimposed has been represented for a mean surface heat current density of 40 W/cm2. The maximum stress in the First Wall measured at the point of maximum temperature, 490 °C, is 402 MPa. It is still far below the admissible 3·Sm value of 505 MPa (Table 3). Figure 31 shows in detail the stress distributions for three First Wall cross-sections at the locations A, B and C along the flow direction. The absolute maximum of stress measured on the inner channel wall in the cross-section C is 441 MPa. With the local temperature of 388 °C (Figure 32), the admissible stress 3·Sm is 610 MPa which provides for a sufficiently large safety margin. Figure 33 shows the stress distribution for two side wall cross-sections. Considering the lower stresses and the lower temperatures (Fig. 34), the safety margin available here is adequate. In Fig. 35 the toroidal stress developments on the inner side of the First Wall channel and on the plasma-facing side along the flow direction from A to B have been plotted. An increase in stress with the rising helium coolant gas temperature along the flow path is well visible here. A comparison of the results with the results obtained for primary stresses (Fig. 29) shows that the secondary stress is dominating.

7.5.2.3 Primary plus Secondary Stresses at Maximum Heat Flux Density of 50 W/cm^2

In the thermohydraulics design of the First Wall coolant system mean values were used of the flow variables, e. g. helium flows, helium temperatures, etc., for the respective flow passages. It is clearly visible in Fig. 10 that a single helium flow passage, No. II, with 76 cooling channels, covers a large zone of the blanket center of approximately two sections. It is supposed that a maximum thermal surface loading of 50 W/cm2 can be expected to occur on the equatorial plane of the blanket. To be able to adapt cooling accordingly, the distribution of helium flow within a section must be determined in detail, e. g. by throttling of the boundary zones.

In a simplified and conservative approach the stress will be calculated now for the extreme case of a maximum heat flow density of 50 W/cm^2, albeit at a mean helium flow distribution (without throttling of the boundary channels). The resulting stresses are evident from Fig. 36. Also a maximum von Mises stress of 470 MPa can be determined at the point of maximum thermal loading of the First Wall (Figs. 36 and 37).

At the temperature of 525 °C (Fig. 38) the admissible stress (3·Sm) which can be taken from Table 1 is 463 MPa. It is slightly exceeded here by less than 2%. This peak stress occurs only at the point of transition between the straight part of the First Wall and the bend. Figure 39 shows the toroidal development of stress on the inner and external sides of the First Wall. It appears that all the other stresses occurring are still below the admissible limit. However, this minor excessive of stress can be reduced by suitable flow distribution in the coolant channels during a flow passage, as already mentioned before. Moreover, the temperature of the rear shielding can be set at an even higher value so that the thermal stress in the First Wall is reduced.

Figure 40 shows, e.g. the respective toroidal development of stress in the First Wall upon a slight increase in temperature, from 285 °C to 300 °C, of the shielding structure. It appears from that figure that the 470 MPa stress peaks occuring at the external wall (represented in Fig. 39) are reduced to 450 MPa, at the inner wall from 517 MPa to 494 MPa. Thus, all stresses are now well below the admissible limit value.

The absolute maximum of stress on the inner cooling channel wall, 517 MPa (Fig. 37), also remains well below the 3·Sm limit of 596 MPa because the temperature is lower, namely 404 °C (Fig. 38).

In the side wall zones and in the mid-plane reinforcing structures the stresses attain approximately the same level as in the case in which the heat flux density is 40 W/cm^2. A slight stress relief in the side walls and a minor increase in stress in the shielding, compared with the previous case, are attributable to the larger temperature difference between the front First Wall and the rear shielding structure.

The maximum values of temperature and stress analyses have been compiled in Table 5.

8 Summary of Main Design Data

A) **Thermohydraulics**	outboard segment	inboard segment
First wall heat flux [MW/m²]		
- maximum	0.5	0.5
- average	0.4	0.4
Max. power density [MW/m³]		
- MANET	23.9	20.3
- Pb-17Li	19.4	17.1
Total Power (nuclear-power + surface heat flux) [MW]	30	19.2
Helium cooling:		
- power to be extracted [MW]	6.9	5.8
- pressure [MPa]	8	8
- temperature inlet/outlet [°C]	250/350	240/350
- mass flow rate [kg/s]	13.2	5.55*
- max. velocity [m/s]	66	63
- pressure drop in segment [MPa]	0.15	0.12
- total pressure drop in the whole helium loop, approx. [MPa]	0.20	0.17
- blower performance, adiabatic ** [MW] (total for one reactor: 31.3 MW)	0.443	0.316
Liquid metal cooling:		
- power to be extracted [MW]	23.1	13.4
- temperature inlet/outlet [°C]	275/425	275/425
- mass flow rate [kg/s]	815	237 *
- max. velocity [m/s]	1.1	0.4
- max. interface temperature (struct./breeder) [°C]	443	430
- MHD pressure drop [MPa] [2]		
. with insulating coatings (reference case)	0.4	0.13
. with flow channel inserts (backup solution)	4.3	1.9
- power requirements for LM circulating pump ** [MW] (total for one reactor: 2.3 MW)	0.043	0.008

*) for one blanket half
**) blower and pump efficiency of 80 % is assumed.

B) Mechanical stresses in the mid-plane of outboard segment, calculated for average and maximum surface heat load	
Boundary conditions:	
- internal pressure [MPa]	8
- FW surface heat load [MW/m^2], average/maximum	0.4/0.5
- temperature of shield [°C]	285 (300)
Max. FW temperature [°C] (external plasma side of FW)	490 (527) *
von Mises stresses [MPa]:	
- primary membrane (web plate between FW channels)	161
limit given by ASME	220
- primary membrane + bending (external plasma side of FW)	120
limit given by ASME	176
- primary + secondary (external plasma side of FW)	402 (450) *
limit given by ASME	505 (463) *
max. allowable internal pressure in the segment box during operation (extrapolated) [MPa]	11

*) Values calculated for maximum surface heat load with $T_{shield} = 300$ °C

Acknowledgements

This work has been performed in the framework of the Nuclear Fusion Project of the Forschungszentrum Karlsruhe and is supported by the European Union within the European Fusion Technology Program.

9 References

[1] S. Malang, J. Reimann, H. Sebening (ed.)
DEMO-relevant Test Blanket for NET/ITER, Part 1: Self-cooled Liquid Metal Breeder Blanket
Vol. 1 and 2, KfK 4907 and 4908 (1991).

[2] S. Malang, E. Bojarsky, L. Bühler, H. Deckers, U. Fischer, P. Norajitra, H. Reiser
Dual-coolant Liquid Metal Breeder Blanket
17th SOFT, Roma, Italy, Fusion Technology, 1424-1428, 1992

[3] U. Fischer
Die neutronenphysikalische Behandlung eines (d,t)-Fusionsreaktors nach dem Tokomakprinzip (NET)
KfK 4790, Oktober 1990.

[4] Hibbitt, Karlsson Sorensen
ABAQUS User's Manual Version 4.9, Providence, R.I., USA.

[5] M. Dalle Donne, S. Dorner, S. Taczanowski
Conceptual Design of Two Helium Cooled Fusion Blankets (Ceramic and Liquid Breeder) for INTOR
KfK-Bericht 3584, August 1983.

[6] M. Dalle Donne
Wärmeübergang von rauhen Oberflächen
KfK-Bericht 2397, p. 220 ff., January, 1977.

[7] W. Kalide
Einführung in die technische Strömungslehre
Carl Hanser Verlag, München, 1971.

[8] P. Norajitra, K. Müller
Internal KfK report, March 1995, unpublished.

[9] BRAVO3 GRAFEM User's Guide
Document No. A-22240-003
Applicon/Schlumberger, May 1984.

[10] BRAVO3 GRAFEM Command Reference Guide
Document No. 23718-006, Revision A, October 1989
Schlumberger CAD/CAM, Michigan, USA.

[11] ASME Code III, edition 1986.

[12] E. Zolti, et al.
Interim Structural Design Criteria for Predesign of the NET Plasma Facing Components
NET/IN/86-14, March 1986.

[13] K. Ehrlich
Internal KfK report, May 1986, unpublished.

[14] U. Jauch, G. Hasse, V. Karcher, B. Schulz
Thermophysical Properties in the System Li-Pb
Kfk 4144, September 1986.

[15] P. Norajitra
Temperature and Stress Analysis of the Self-cooled DEMO Liquid Metal Blanket (Option A)
KfK 4657, February 1990.

10 Nomenclature

A [m^2]	flow cross section
A_o [m^2]	surface
α [W/m^2K]	heat transfer coefficient
b [mm]	roughness profile width
c [m/s]	velocity
c_p [J/kgK]	specific heat capacity
Δ_p [bar]	pressure drop
ΔT [K]	enthalpy rise
d_h [m]	hydraulic diameter
fα [-]	ratio of heat transfer coefficients
h [mm]	depth of roughness profile
k [-]	pipe roughness
l [m]	length
λ [W/mK]	thermal conductivity
λ [-]	pipe friction coefficient
$\dot{m}$ [kg/s]	mass flow
n [-]	number of helium passages
Nu [-]	Nusselt number
η [kg/ms]	dynamic viscosity
P´ [mm]	roughness profile pitch
P [W]	Power
p [bar]	pressure
Re [-]	Reynold's number
q [W/m^3]	heat source density
$q_{surface}$ [W/m2]	surface heat flow density
Q [W]	heat flow
R [J/kgK]	gas constant
T [K]	temperature
ρ [kg/m^3]	density
T [°C]	temperature
v [m^2/s]	kinematic viscosity

Subscripts:

ad	adiabatic
FW	First Wall
He	helium
λ	pipe friction
LM	liquid metal
max	maximum
Pb-Li	lead-lithium
SW	side wall
tot	total
ζ	flow resistance
η	efficiency

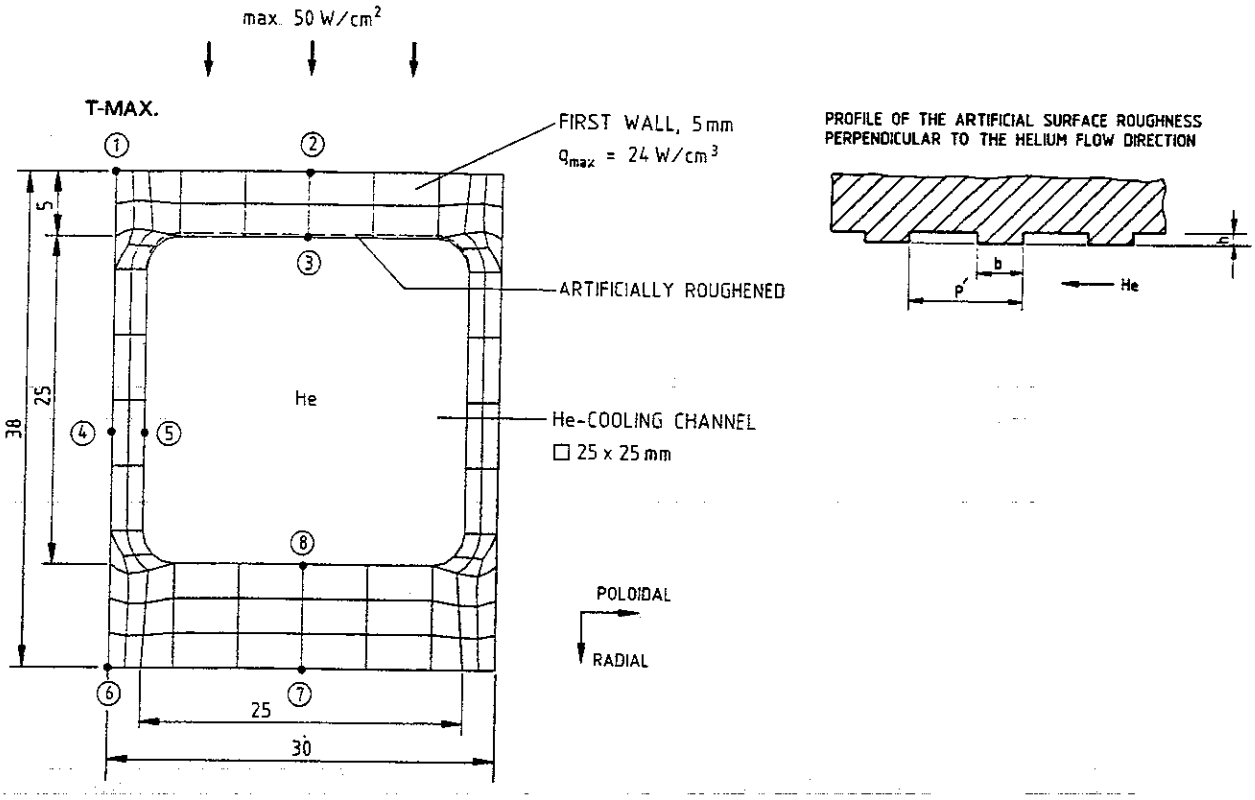

Table 1: Temperature distribution [°C] in the First Wall of the outboard blanket at the coolant channel end of the respective He passage.

Item	Without Roughening					With Roughening $f_a = 2.0$[1)]			
	I	II	III	IV	V	I	II	III	IV
1	589	595	590	579	371	509	525	531	530
2	597	599	591	577	370	499	513	518	517
3	493	493	485	473	365	391	404	410	410
4	318	343	354	363	359	314	340	352	362
5	314	338	350	360	357	310	336	348	359
6	359	393	394	396	376	359	393	394	396
7	358	391	392	395	375	358	391	392	395
8	335	363	369	374	367	334	363	369	374

1) $P' = 2.58$ mm, $b = 1.0$ mm, $h = 0.25$ mm

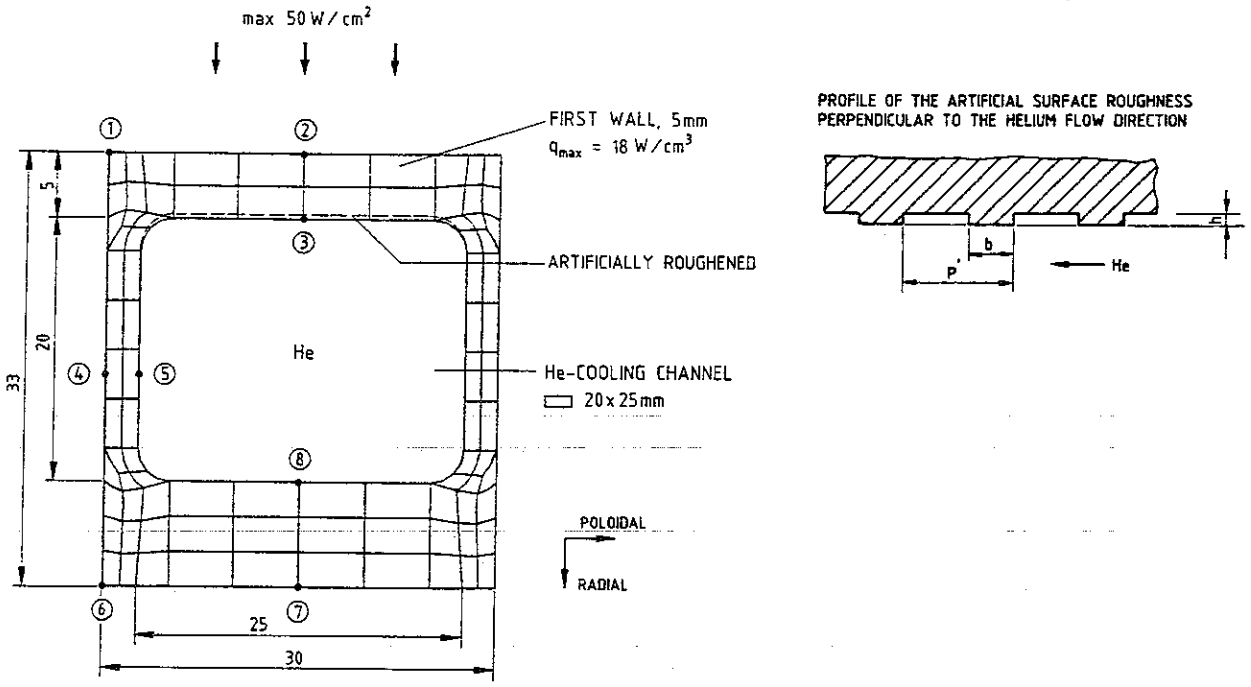

Table 2: Temperature distribution [°C] in the First Wall of the inboard blanket at the coolant channel end of the respective He passage

Item	Without Roughening					With Roughening $f_a = 2.0$[1]			
	I	II	III	IV	V	I	II	III	IV
1	583	591	585	574	374	511	527	531	530
2	597	599	591	577	370	500	513	519	517
3	493	493	485	473	365	392	404	410	410
4	364	387	387	391	370	353	378	380	386
5	347	368	371	377	365	338	361	366	373
6	390	425	418	417	385	388	424	417	417
7	366	399	397	399	377	365	398	397	398
8	340	368	392	376	368	340	368	372	376

1) $P' = 2.29$ mm, $b = 0.89$ mm, $h = 0.22$ mm

Table 3: Material data for 1.4914 steel (MANET) [13]

T [°C]	λ [W/mK]	E x10³ [MPA]	v [-]	α_{EXP}/20 °C x10⁻⁶ [1/K]	$\sigma_{0.2}$ 1) [MPa]	σ_u 2) [MPa]	Sm [MPa]	$S_{m,2x10^4\,h}$ [MPa]
20	24.2	217	0.27	10.11	614	773	258	258
50	24.4	215	0.27	10.23	619	773	258	258
100	24.7	213	0.28	10.46	623	767	256	256
150	24.9	209	0.28	10.70	621	755	252	252
200	25.2	206	0.28	10.95	612	737	246	246
250	25.4	202	0.28	11.20	597	712	237	237
300	25.6	199	0.28	11.45	575	681	227	227
350	25.7	195	0.29	11.68	548	644	215	215
400	25.9	190	0.29	11.90	513	600	200	200
450	26.0	186	0.30	12.09	473	550	183	183
500	26.2	181	0.30	12.24	426	494	165	135
550	26.3	176	0.30	12.34	373	431	144	98
600	26.5	171	0.31	12.40	313	362	121	41

1) corresponds to designation $R_{p0,2}$ according to DIN 50145

2) corresponds to designation R_m according to DIN 50145

Table 4: Thermal conductivity λ [W/mK] of lead-lithium

Material	Temperature [°C]							Source
	20	100	200	300	400	500	600	
Pb-17Li	(26.3) *	(28,7) *	(31,6) *	13.2	15.1	17.1	19.1	[14]

Table 5: Maximum values obtained from the temperature and stress analyses of the outboard blanket

Temperature Analysis	Maximum Temperature [°C]	Location	Design Basis Limit
- First Wall			
. at $q = 40$ W/cm^2	505	top end of blanket	550
. at $q = 50$ W/cm^2 1)	527	blanket mid-plane	550
- PbLi/steel interface	443	top end of blanket	470

1) assuming mean helium flow distribution

Stress Analysis Primary Stress	Maximum von Mises Stress [MPa]	Location	Admissible Stress
a) Primary stress ($p = 80$ bar)		blanket mid-plane	
First Wall			
. external plasma side ($T = 527$ °C)	120		176
. ligament ($T = 330$ °C)	161		220
. side wall ($T = 300$ °C)	178		227
b) Primary plus secondary stresses ($q = 40$ W/cm^2, $T_{Shield} = 285$ °C)		blanket mid-plane	
. First Wall			
- external plasma side ($T = 490$ °C)	402		505
- inside wall ($T = 388$ °C)	441		610
- side wall ($T = 300$ °C)	184		681
c) Primary plus secondary stresses ($q = 50$ W/cm^2, $T_{Shield} = 285/300$ °C)		blanket mid-plane	
. First Wall			
- external plasma side ($T = 525$ °C)	470/450 2)		463
- inside wall ($T = 404$ °C)	517/494		596
. side wall ($T = 300$ °C)	173/162		681

2) values for average shielding temperature of 285 °C and 300 °C, respectively

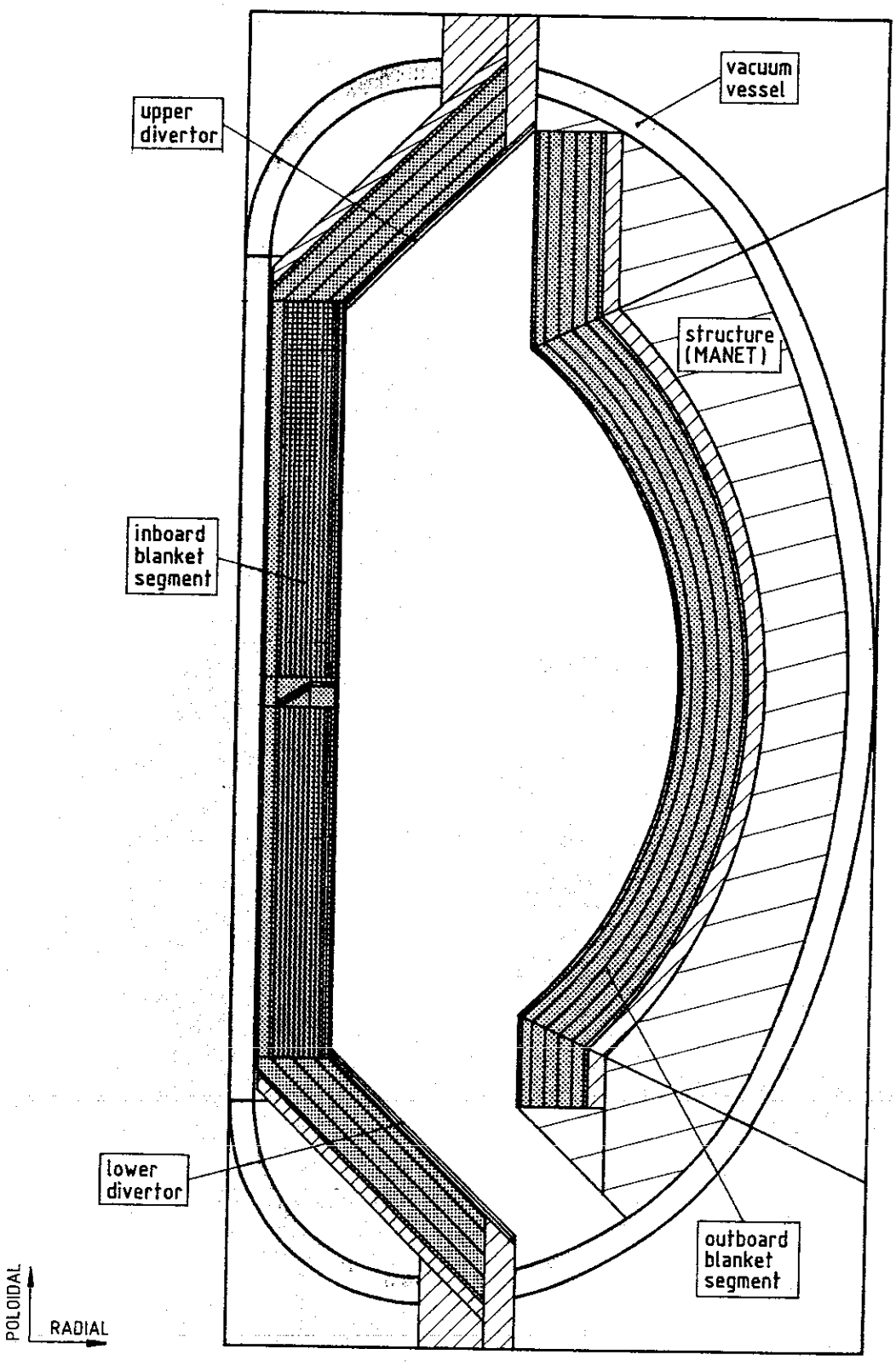

Fig. 1: Radial-poloidal section through the torus, schematic.

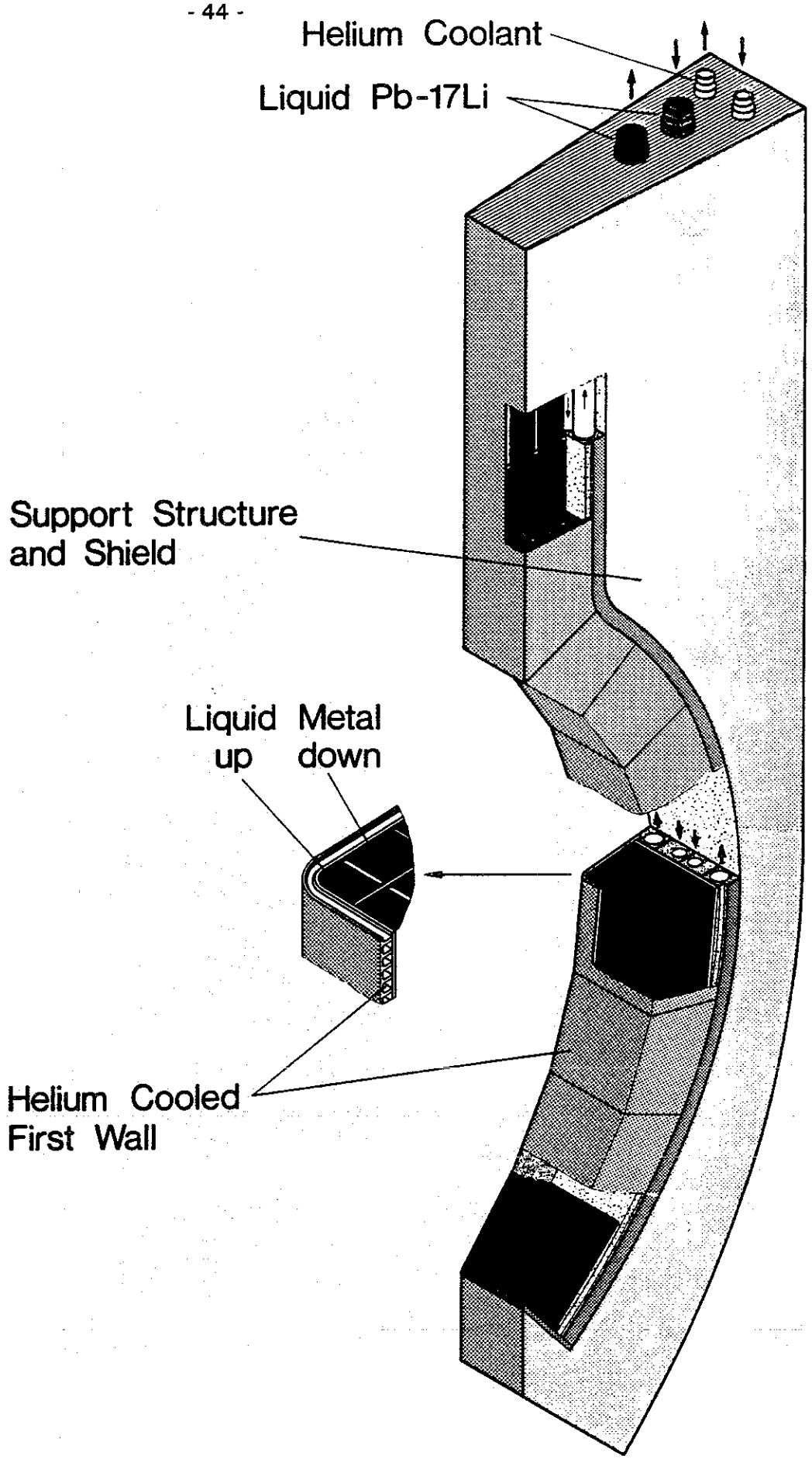

Fig. 2: Isometric representation of an outboard blanket segment.

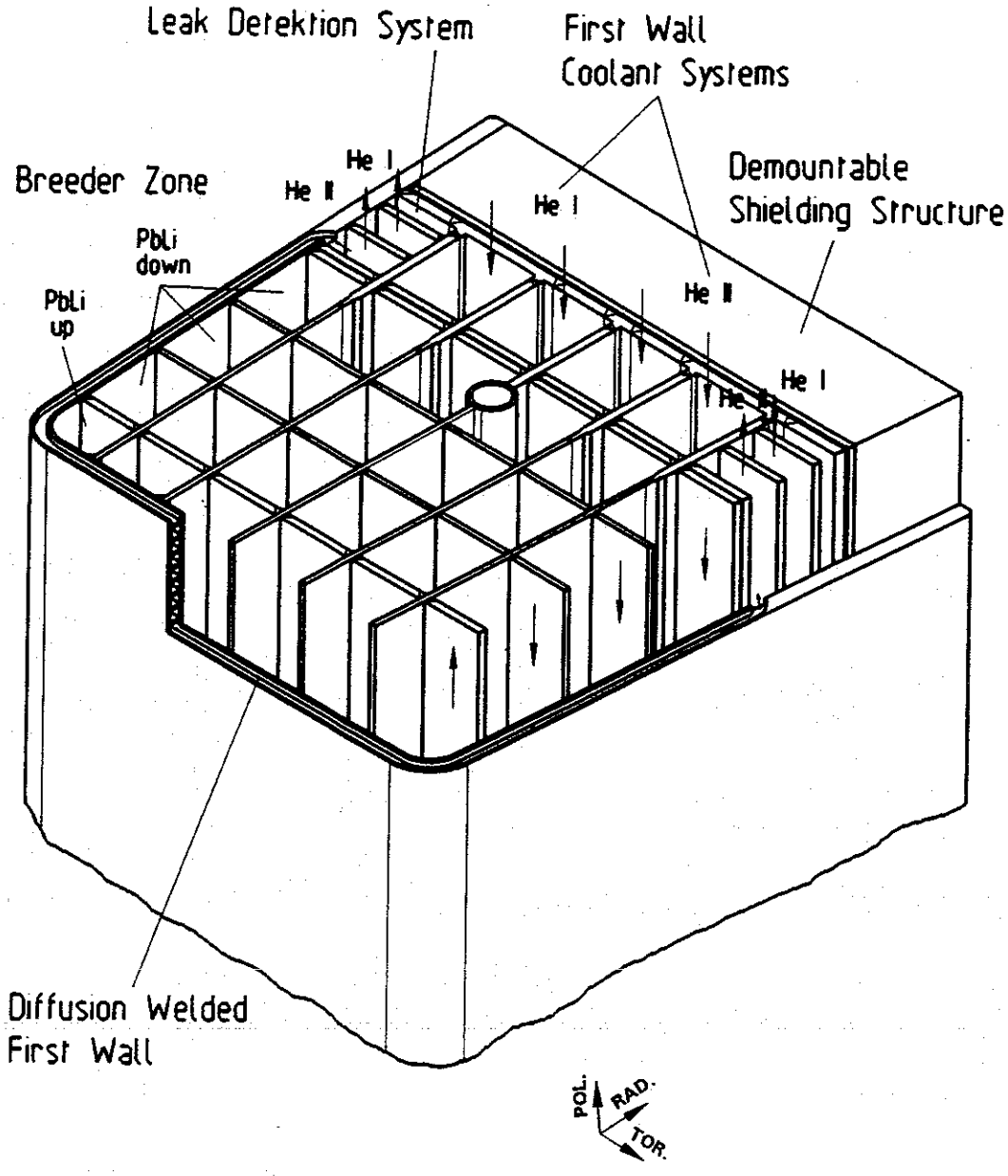

Fig. 2a: Layout of an outboard segment in an isometric representation (detail from the central torus zone).

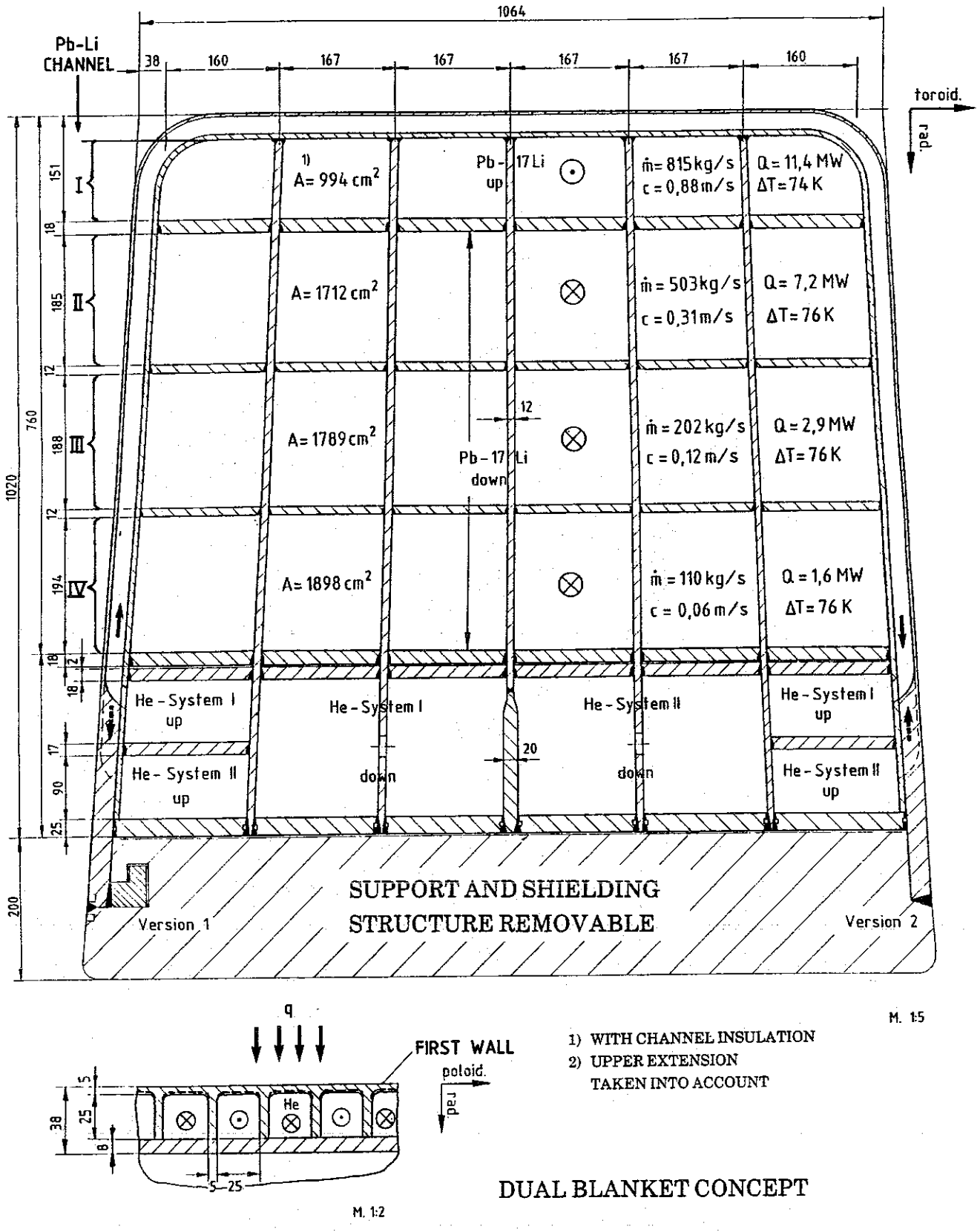

Fig. 3: Equatorial cross section of an outboard blanket segment.

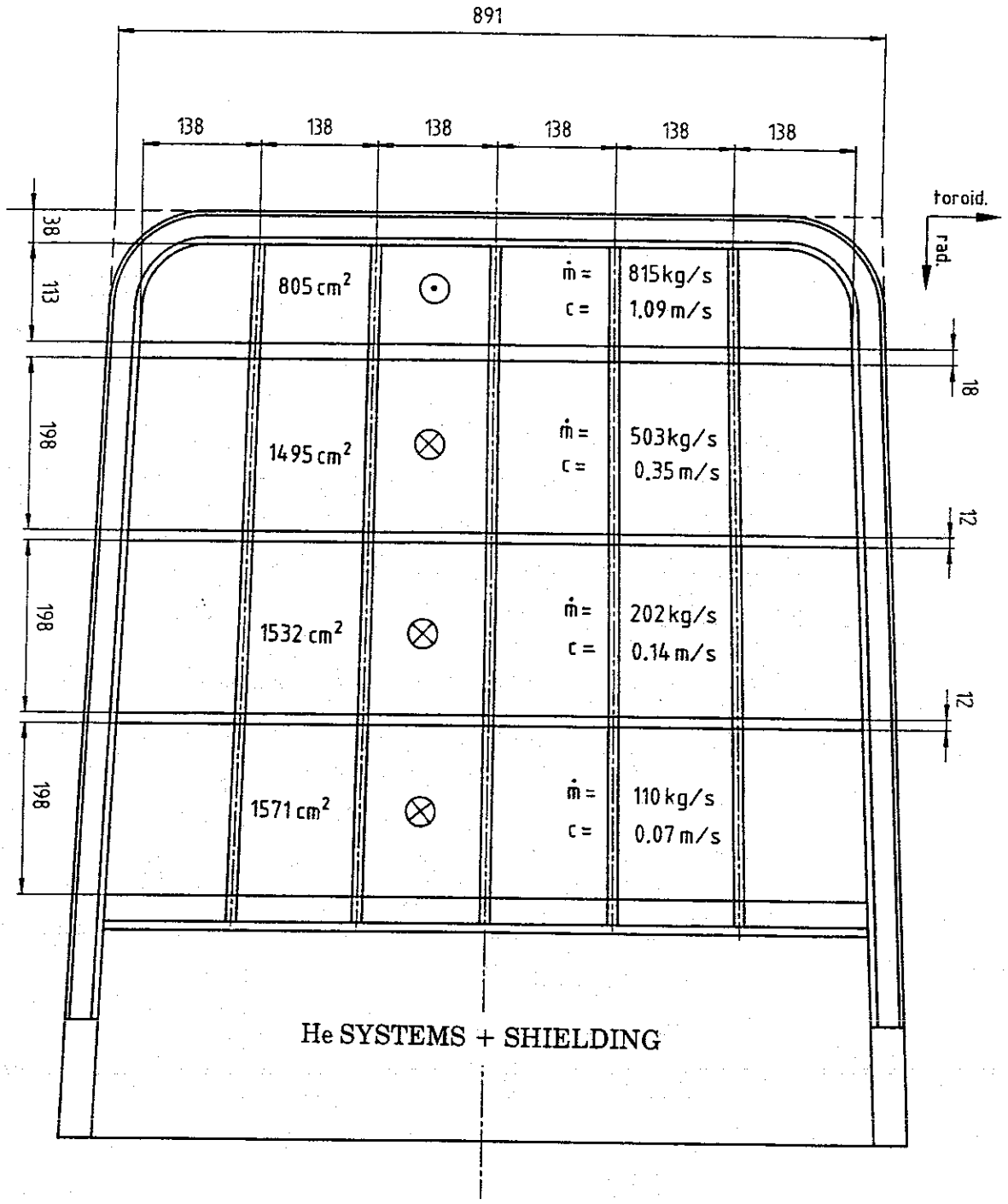

Fig. 4: Cross section at the top end of an outboard blanket segment.

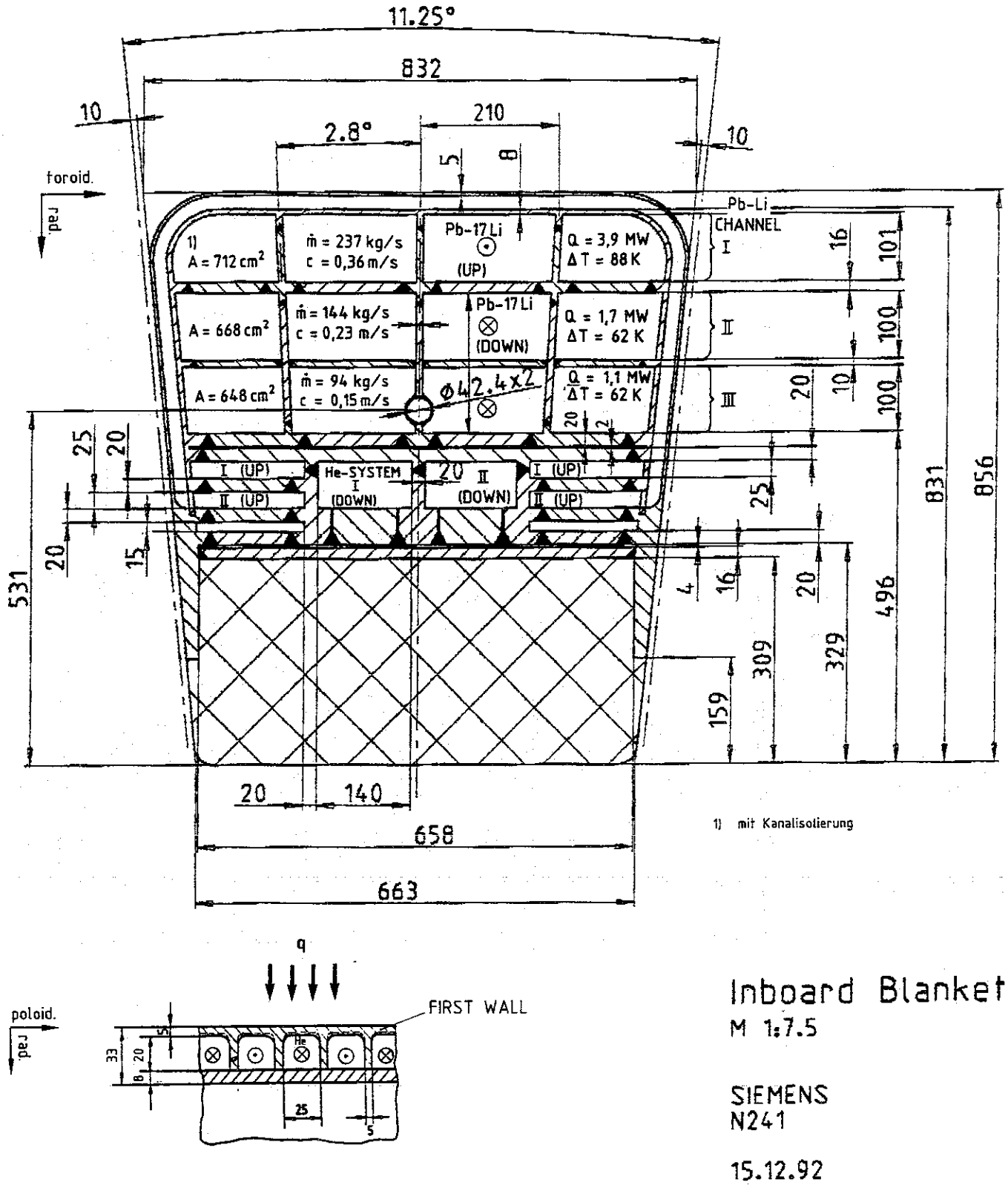

Fig. 5: Cross section of an inboard blanket segment.

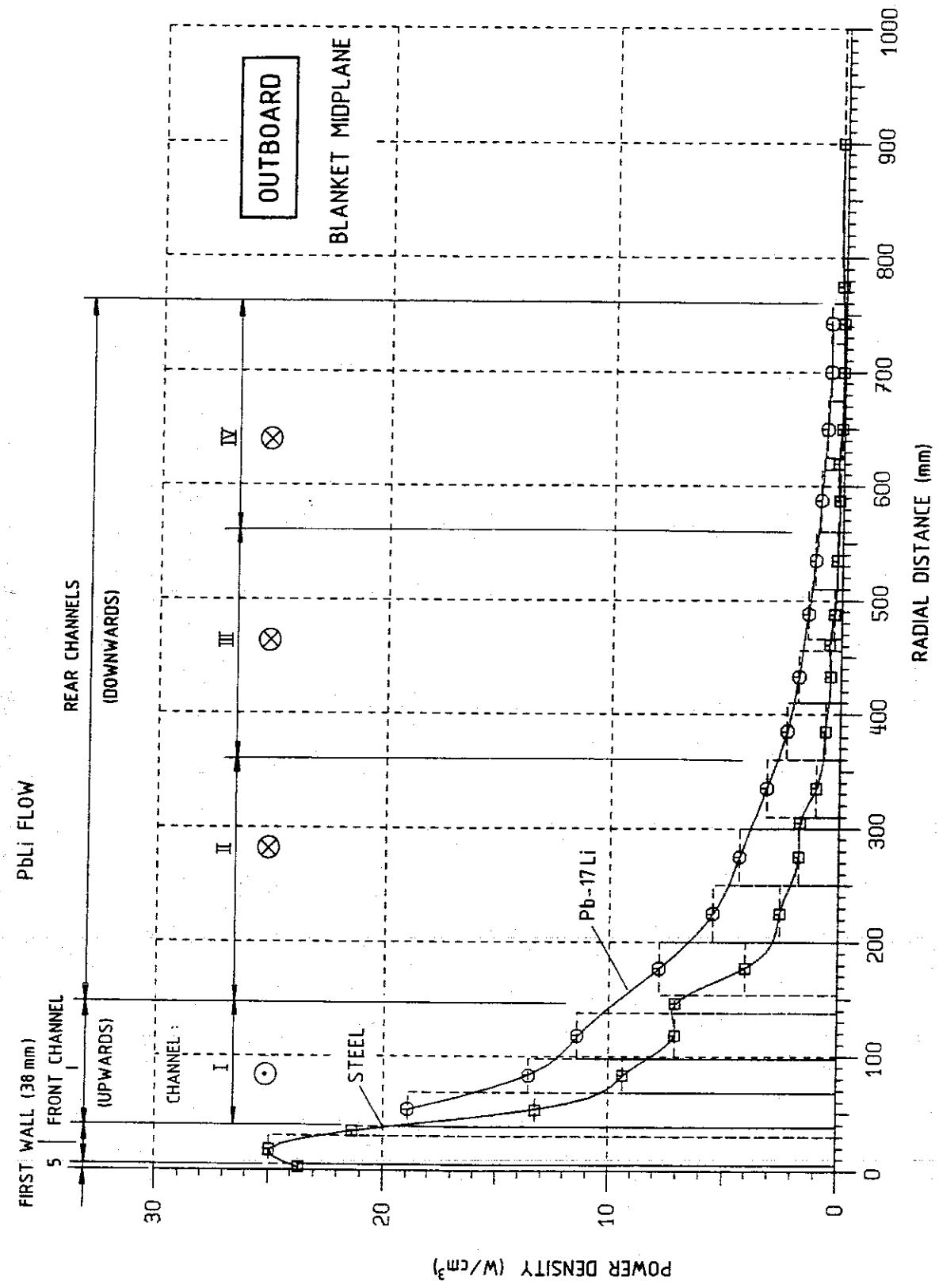

Fig. 6:: Radial power density distribution at the mid-plane of an outboard blanket.

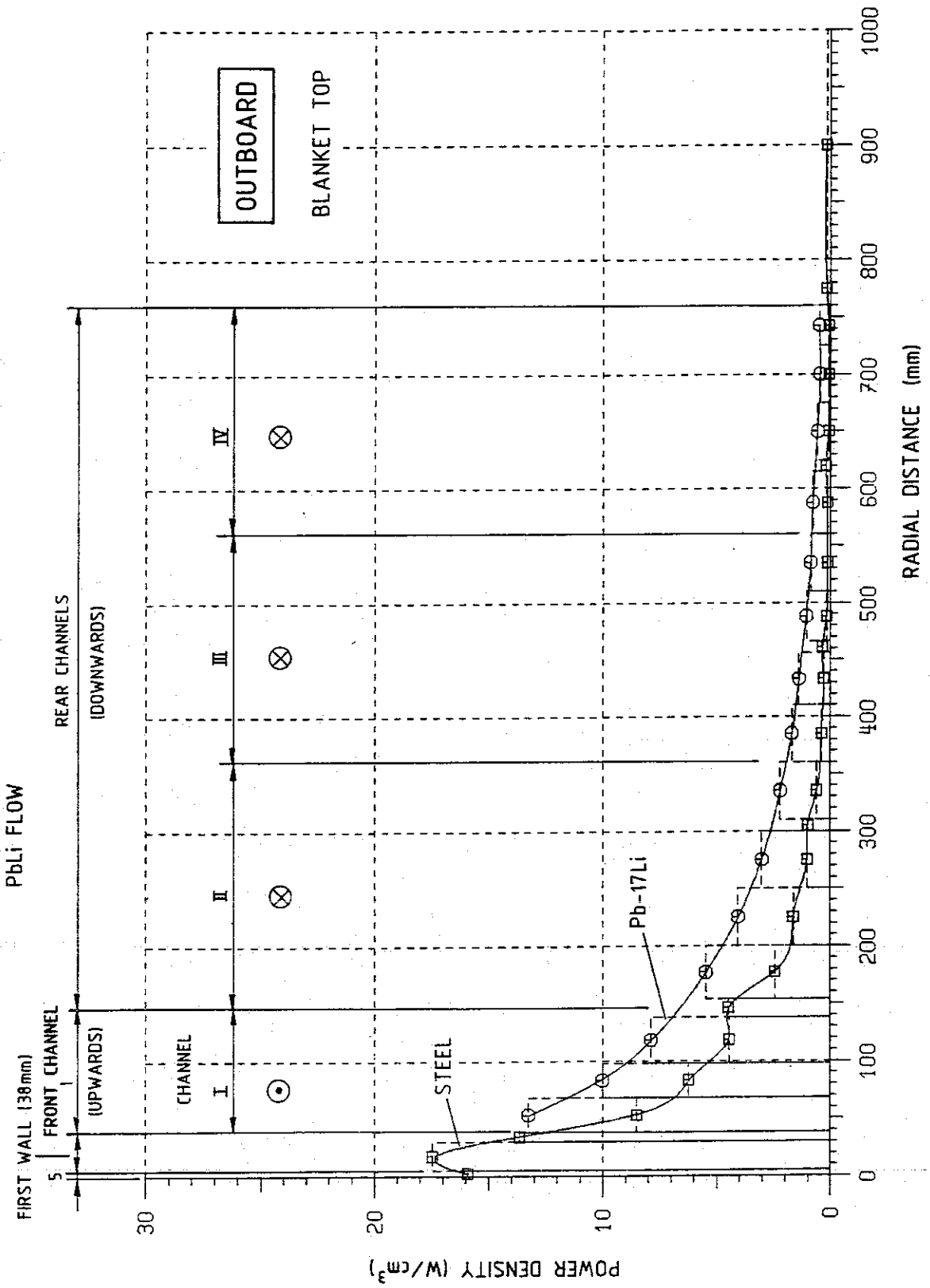

Fig. 7: Radial power density distribution at the top end of an outboard blanket.

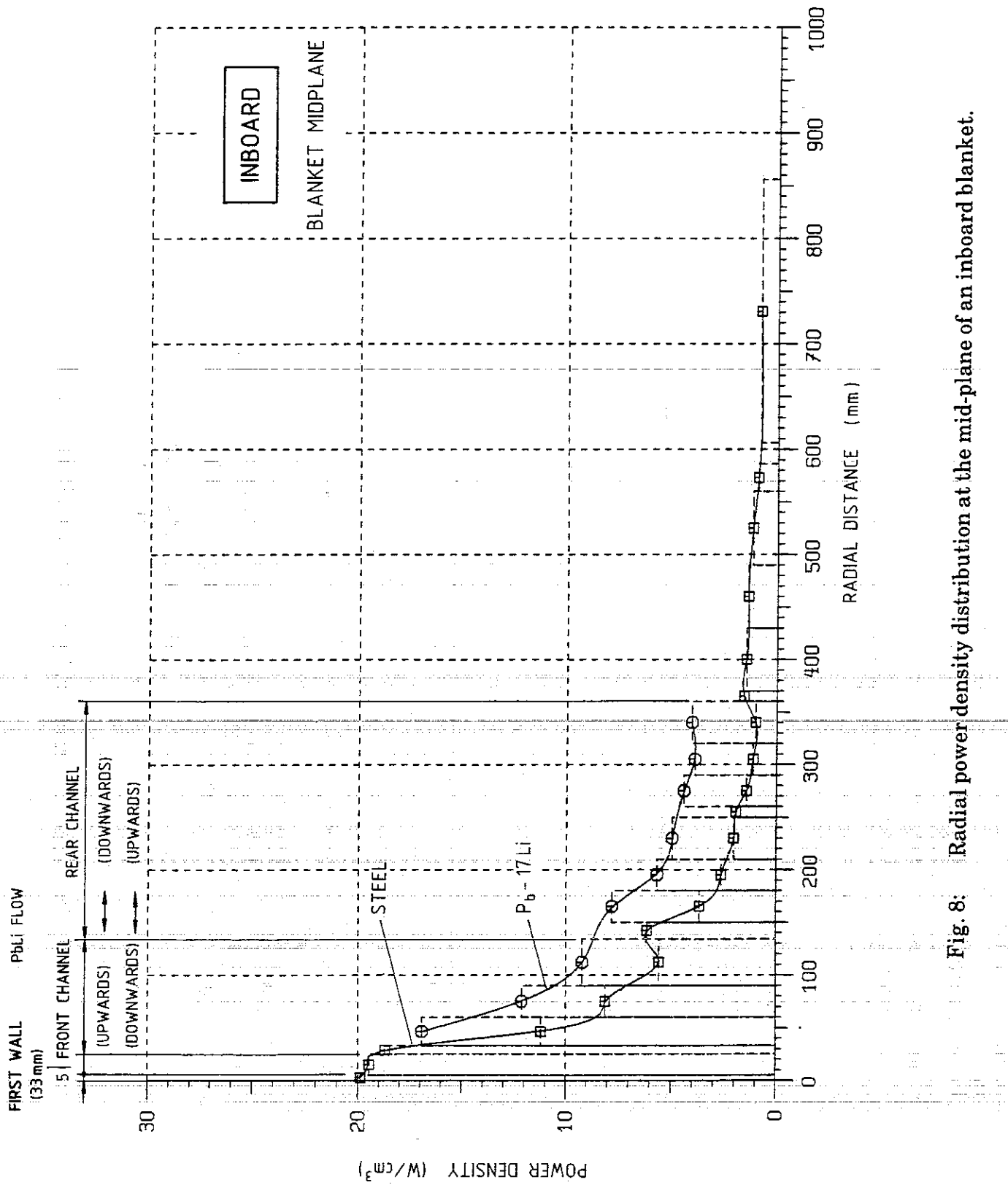

Fig. 8: Radial power density distribution at the mid-plane of an inboard blanket.

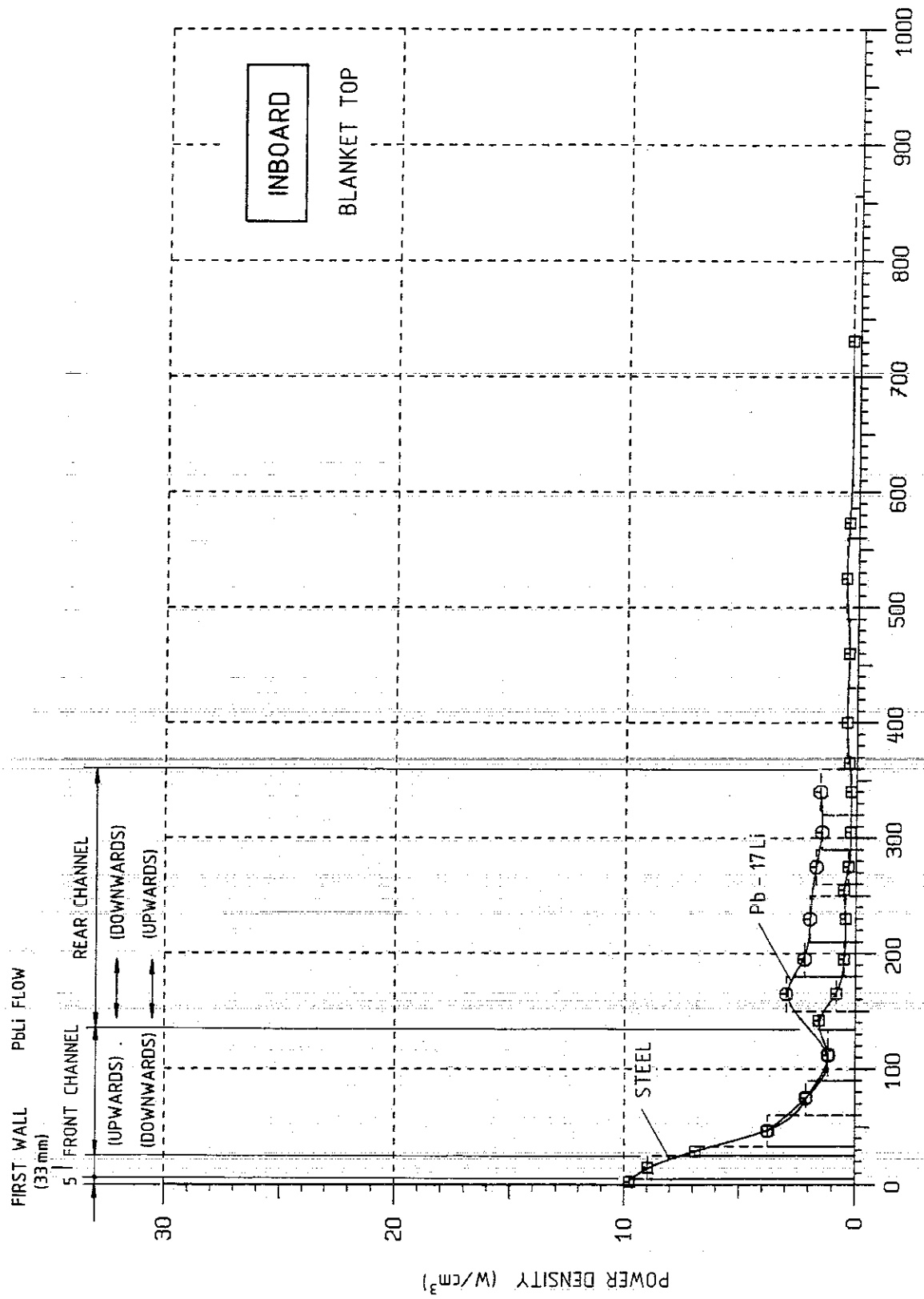

Fig. 9: Radial power density distribution at the top end of an inboard blanket.

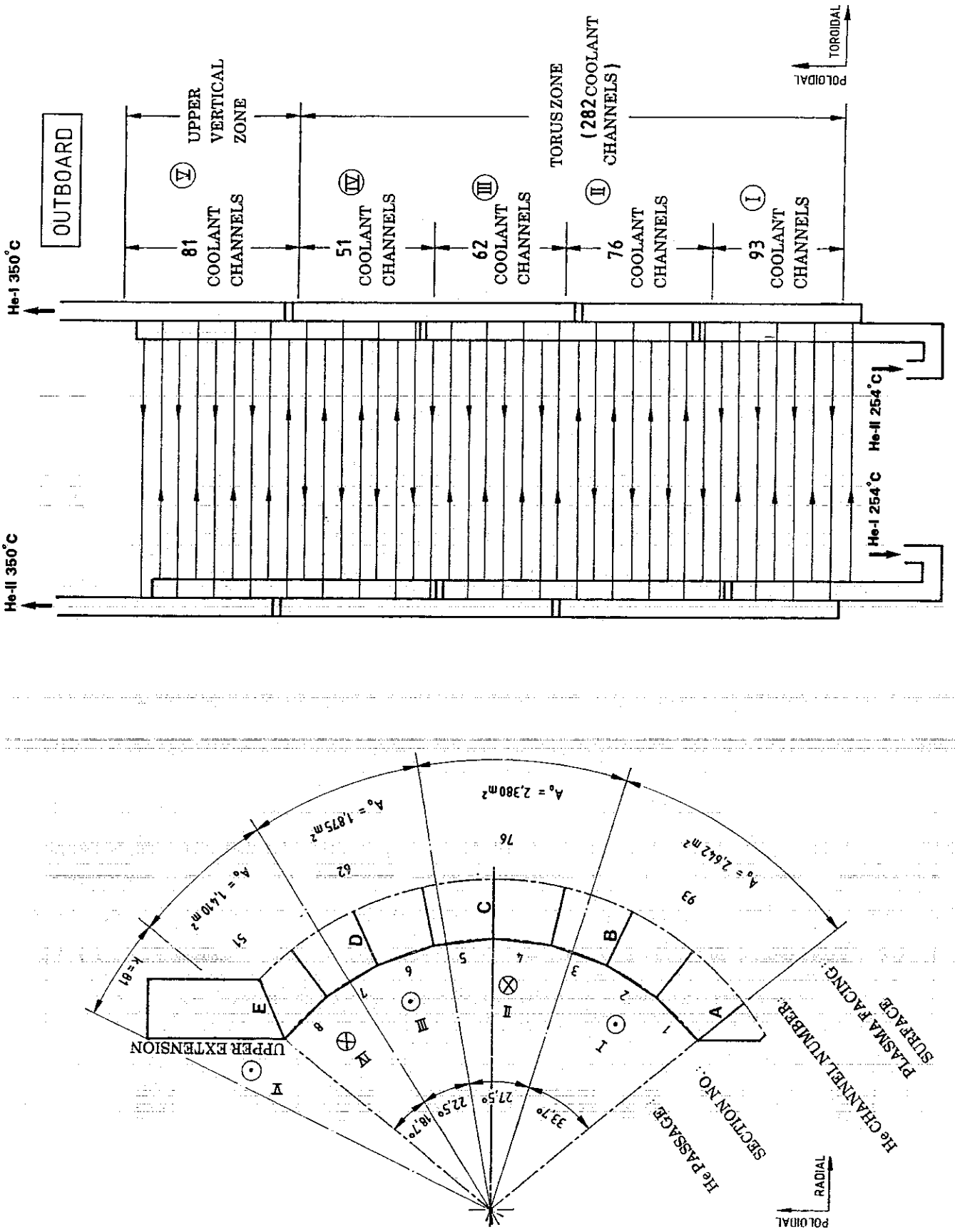

Fig. 10: Schematic of the He passages for First Wall cooling of an outboard blanket segment.

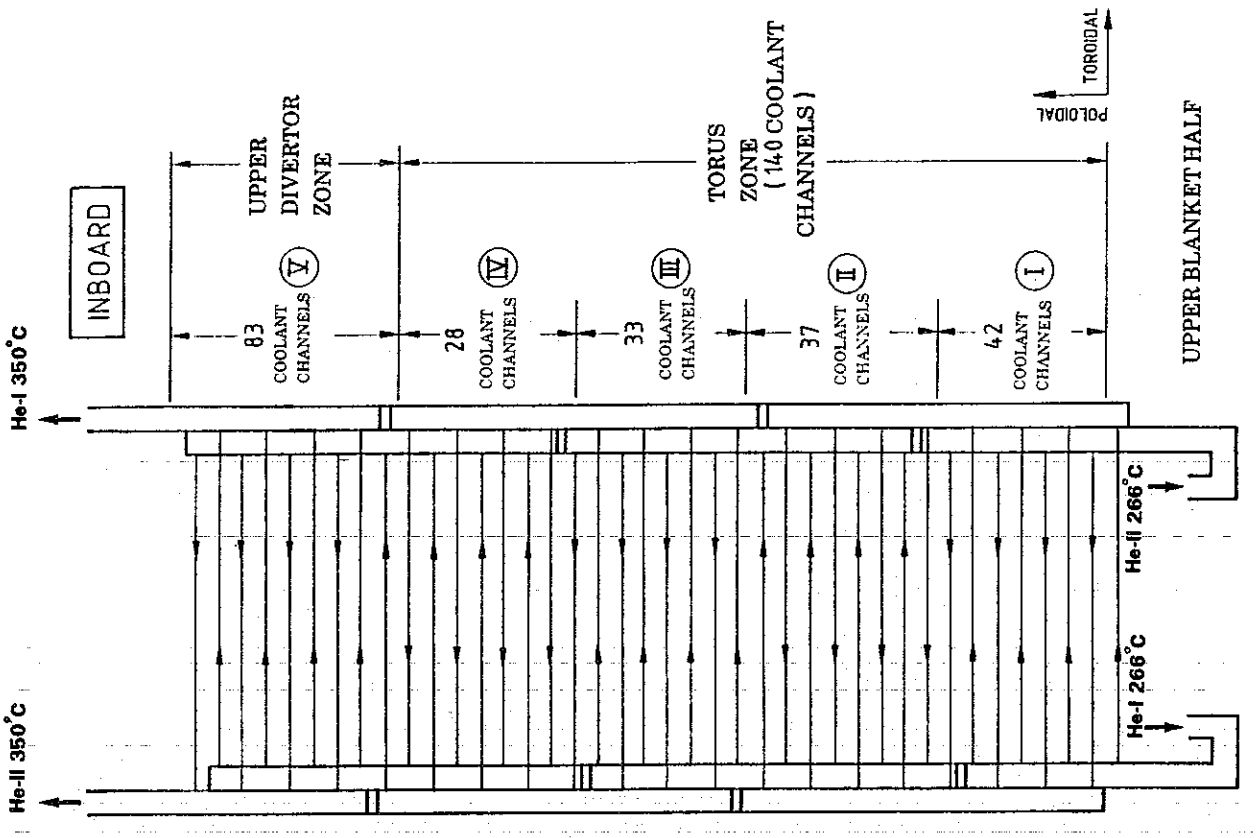

Fig. 11: Schematic of the He passages for First Wall cooling in the upper half of an inboard blanket.

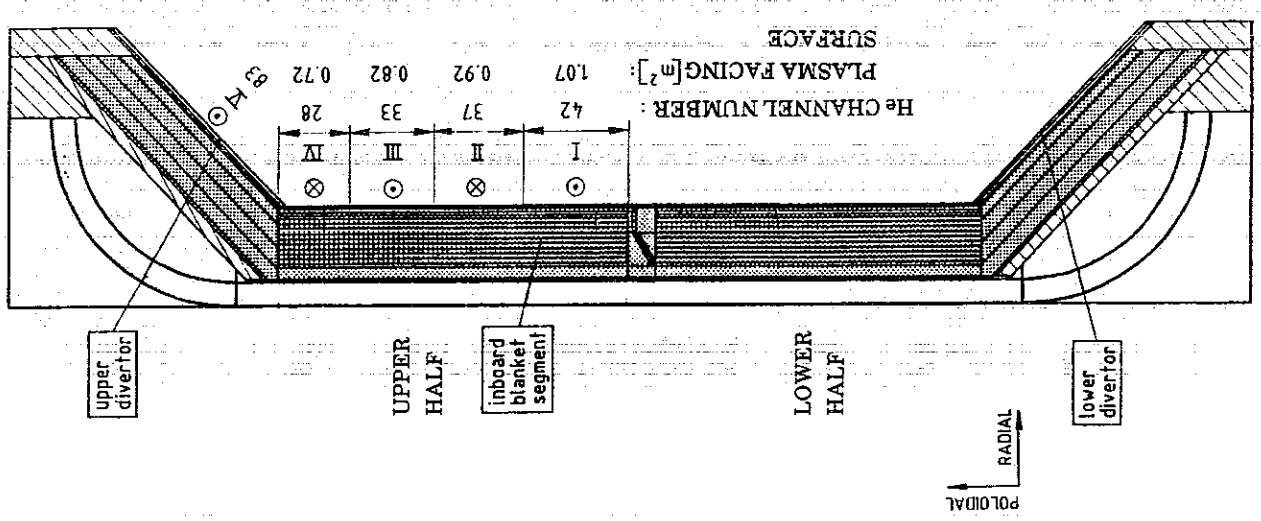

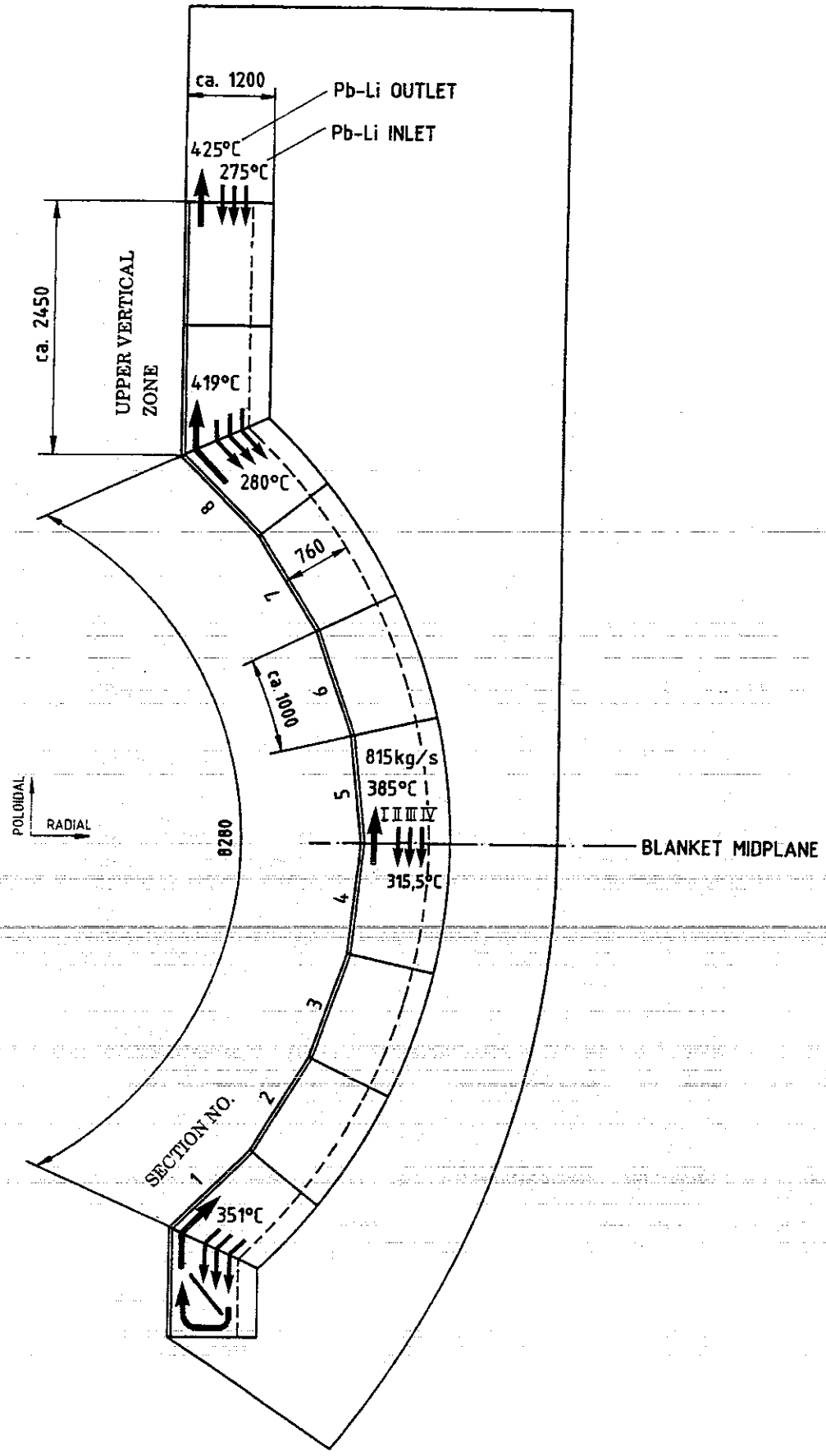

Fig. 12: Global liquid metal temperature distribution in the outboard blanket.

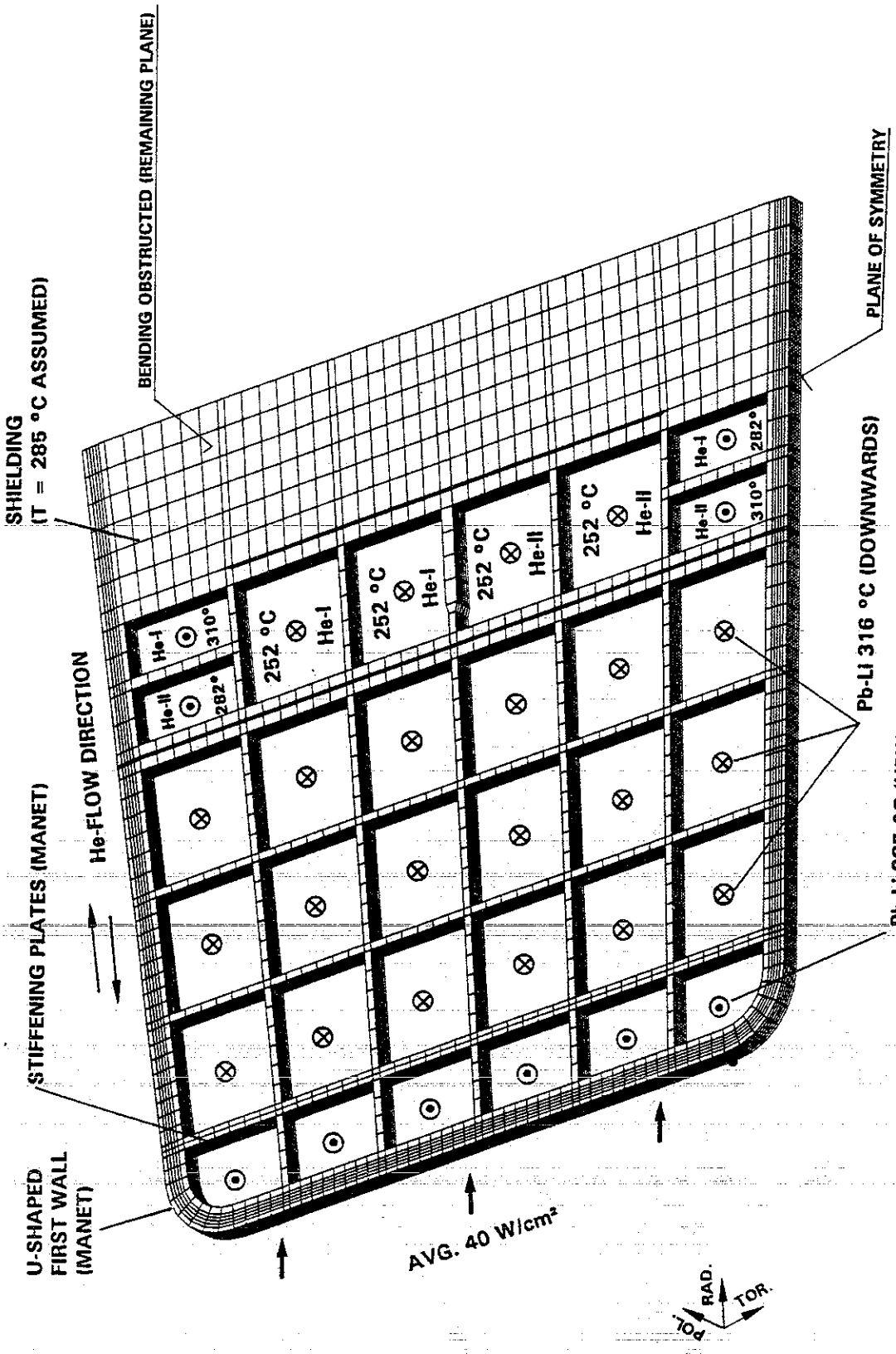

Figure 13: Finite Element model for stress computation.

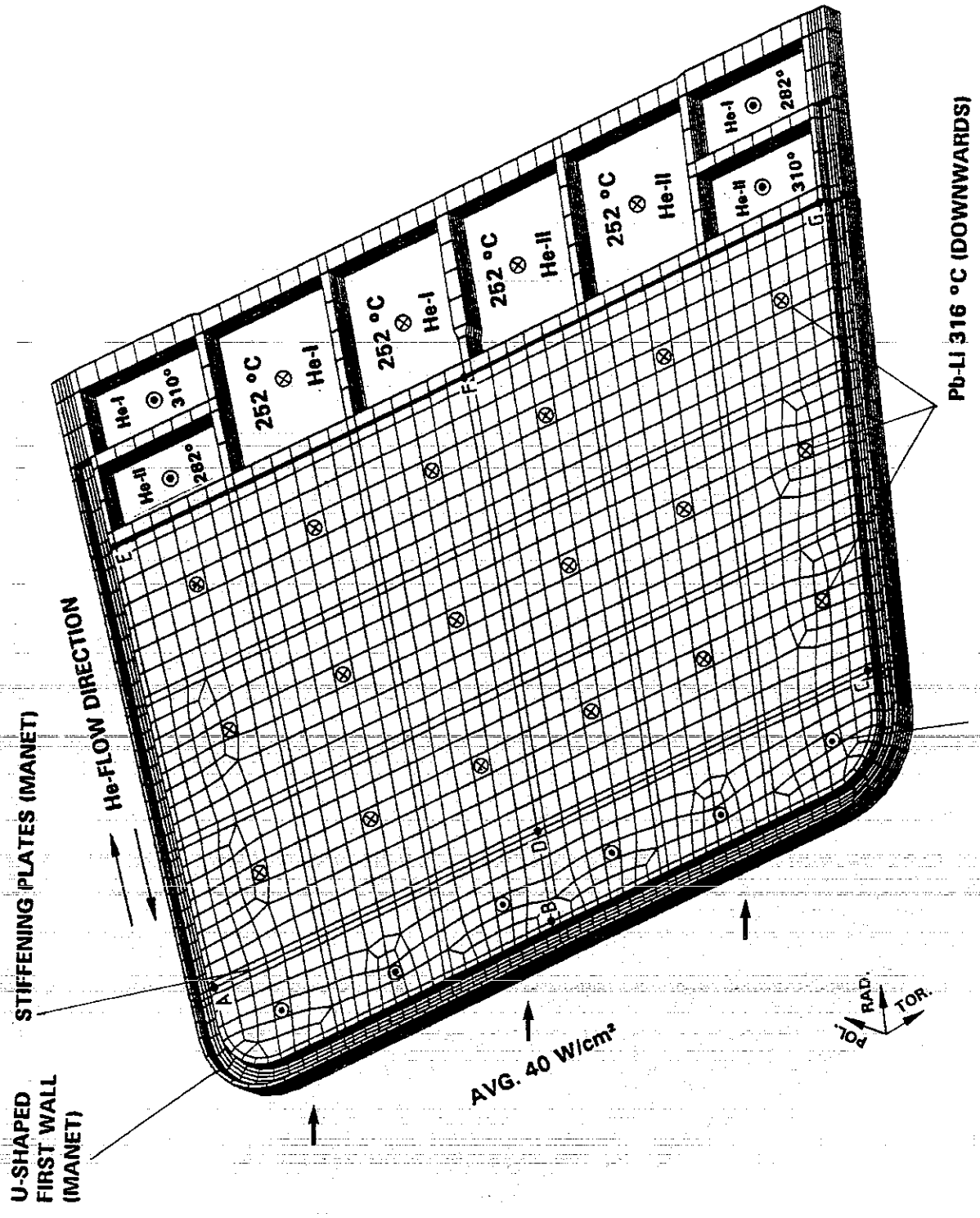

Figure 14: Finite Element model for temperature computation.

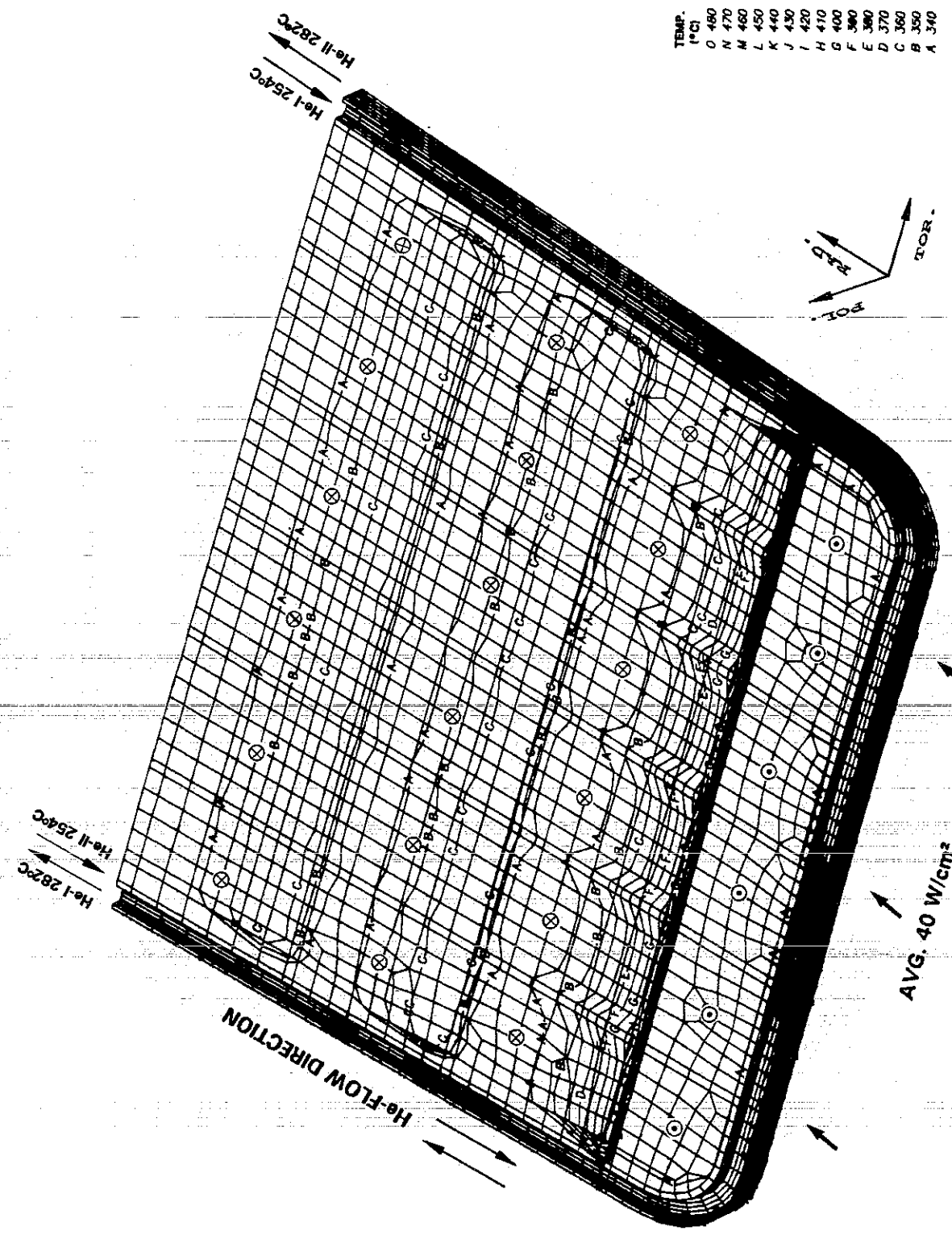

Figure 15: Temperature distribution in the blanket cross-section at the bottom end of the blanket.

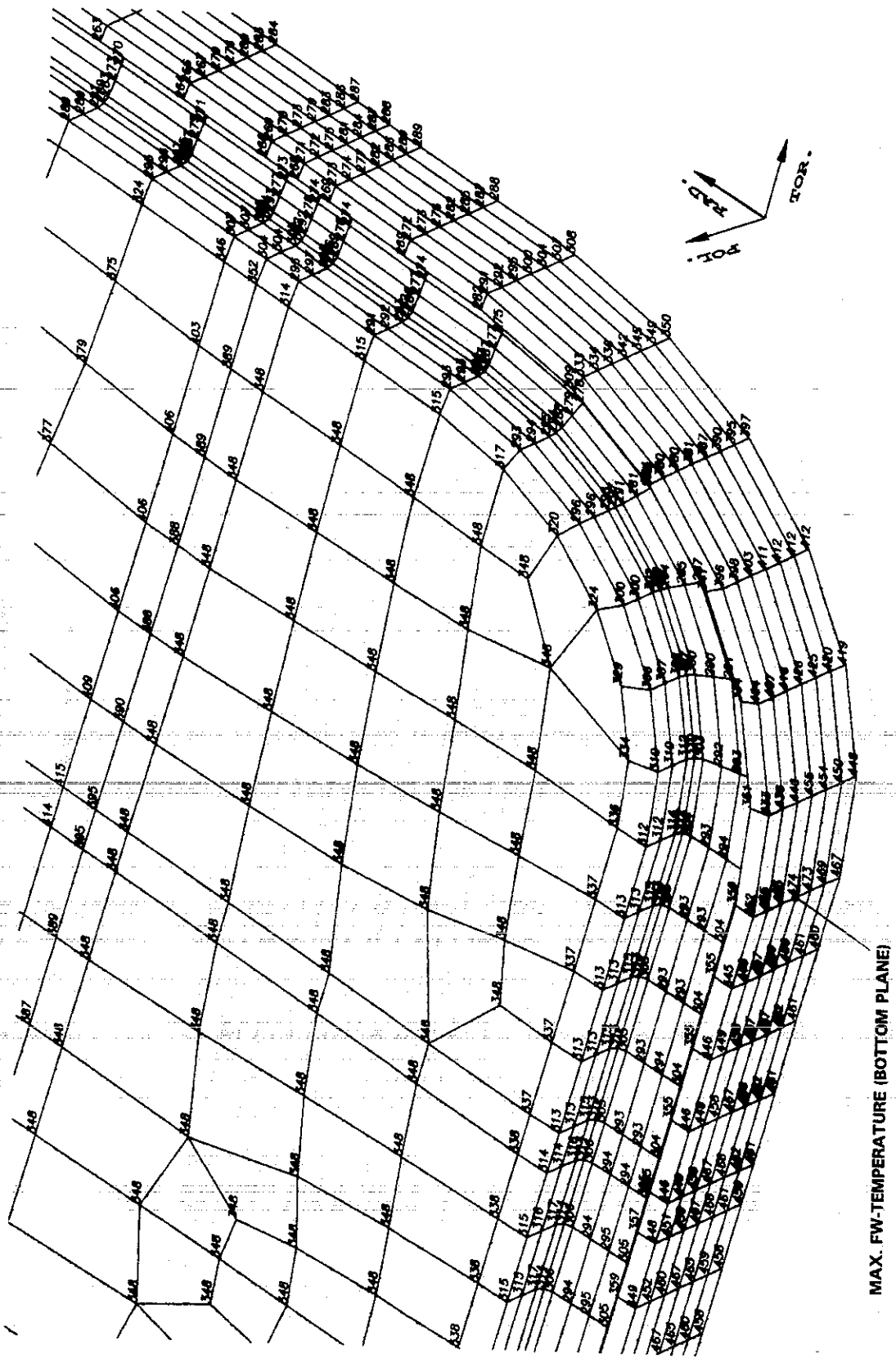

Figure 16: Detail of temperature distribution in a First Wall cutout from Fig. 15.

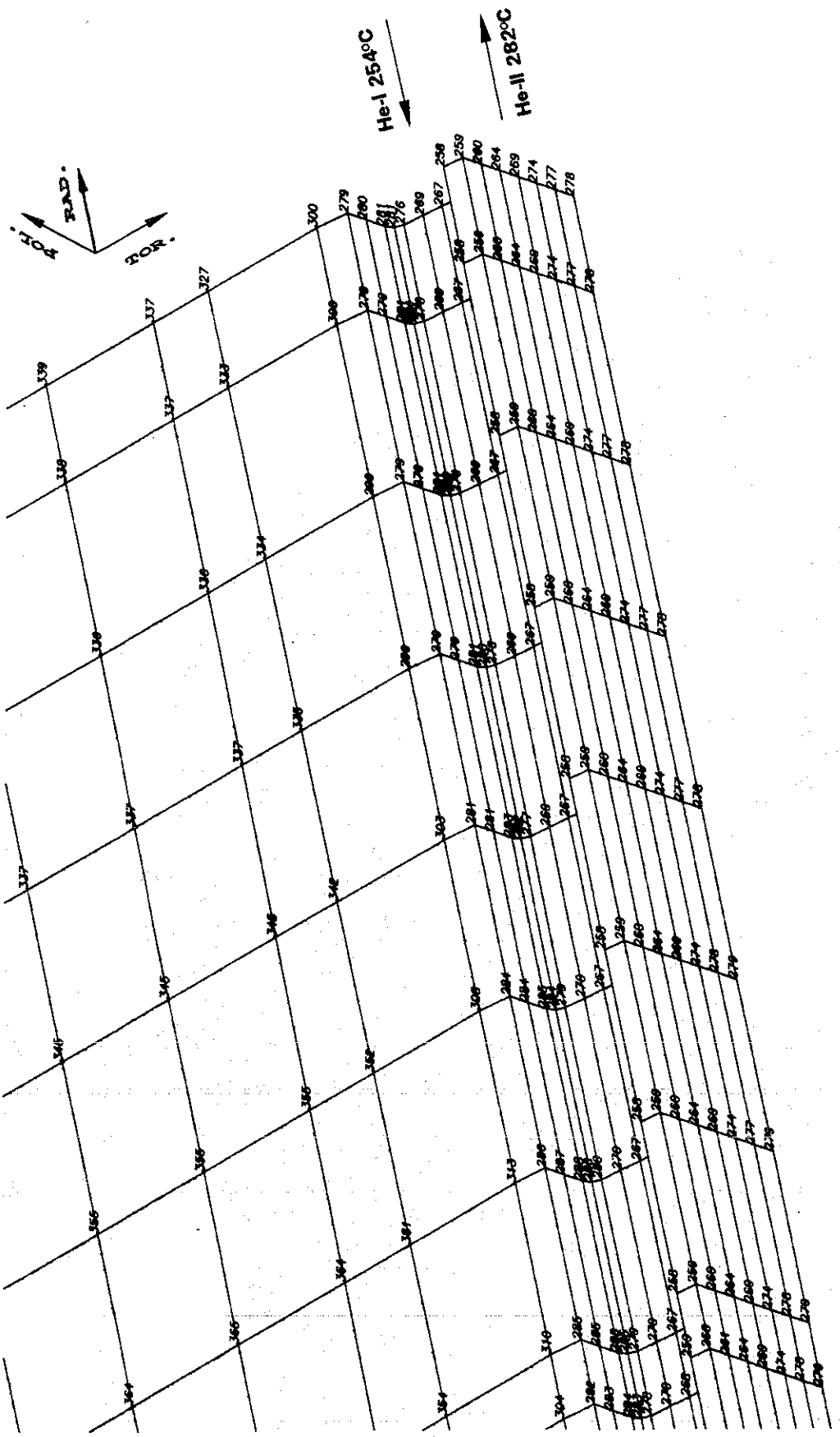

Figure 17: Detail of temperature distribution in a rear cutout from Fig. 15.

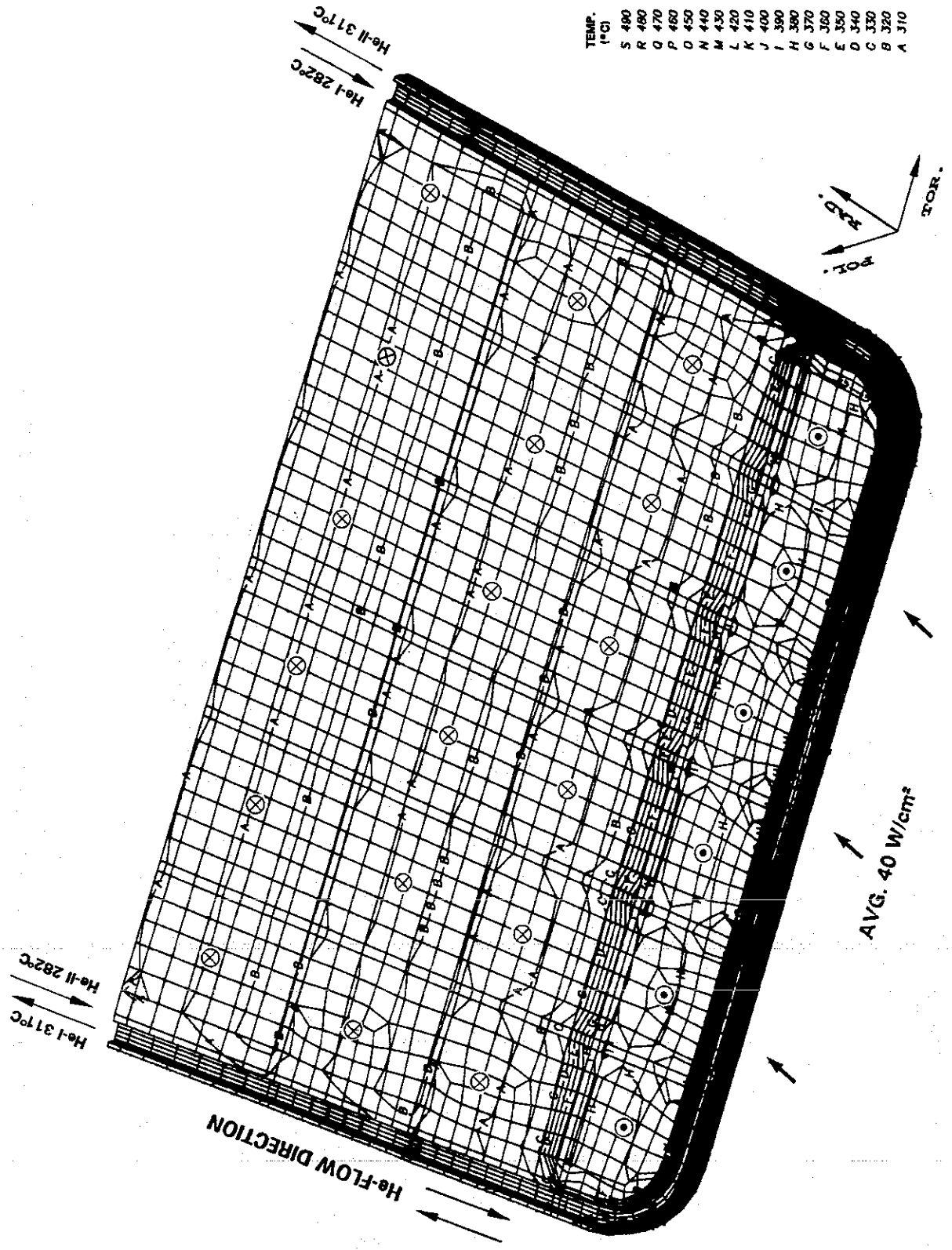

Figure 18: Temperature distribution in the equatorial blanket cross-section.

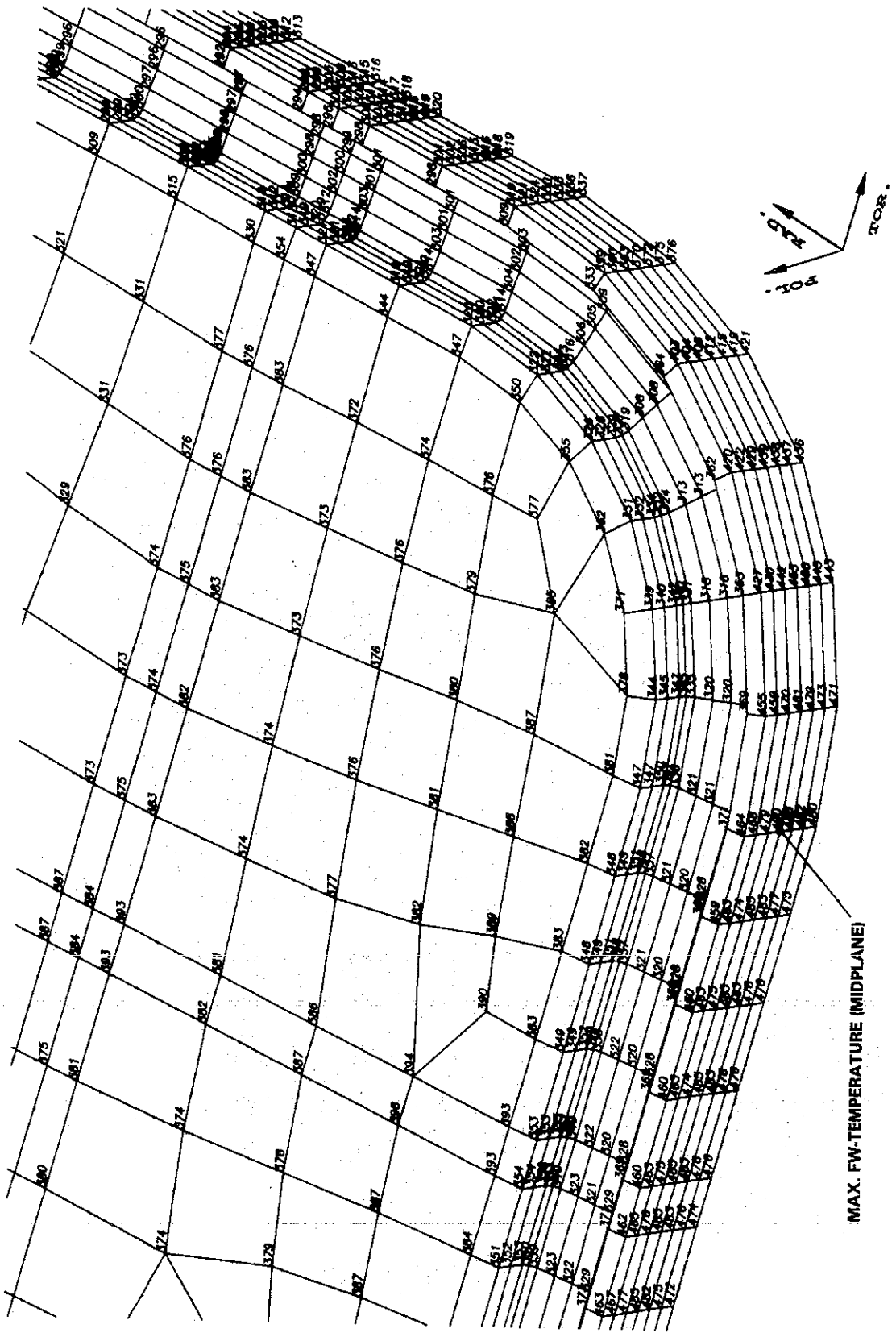

Figure 19: Detail of temperature distribution in a First Wall cutout from Fig. 18.

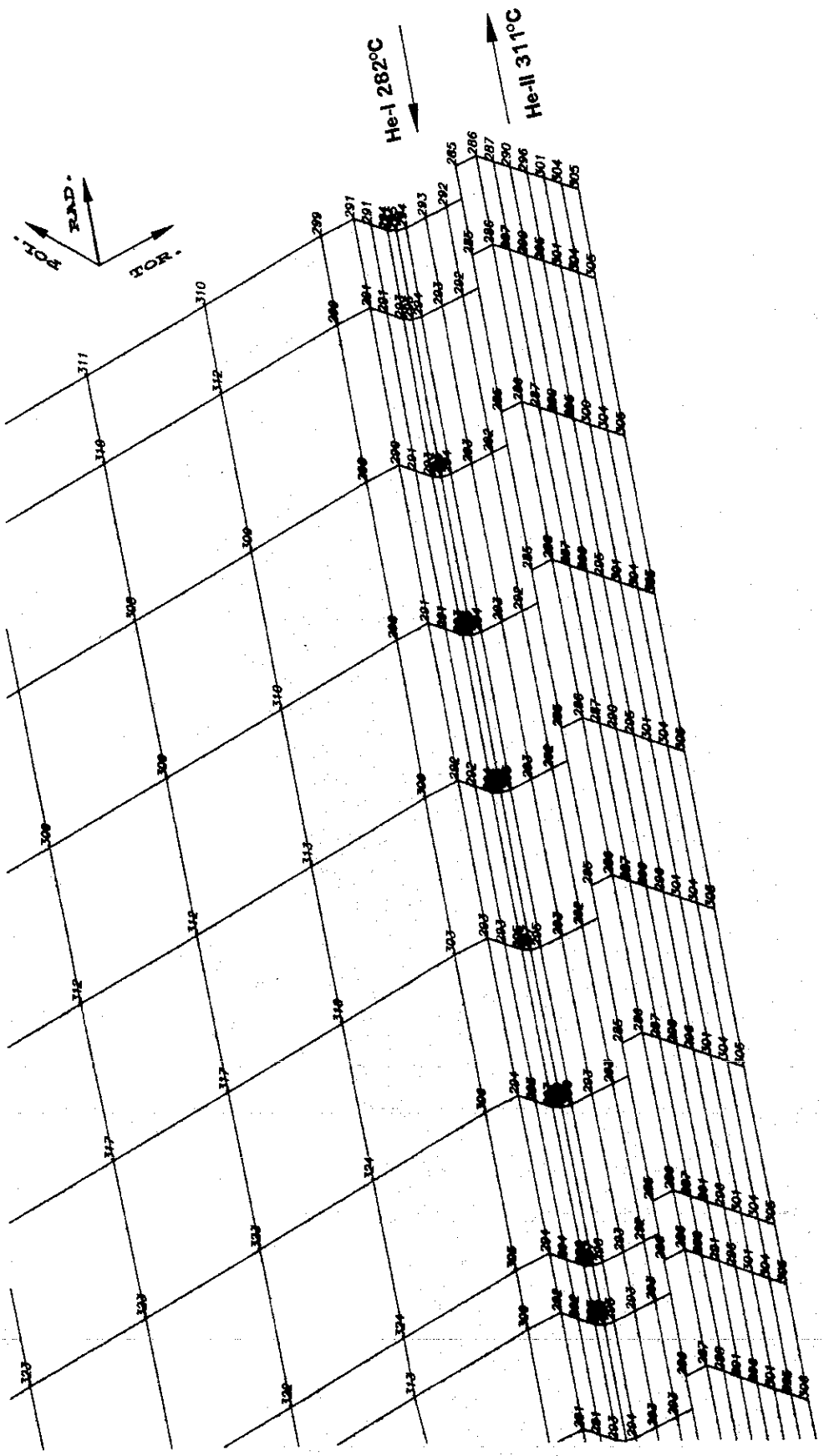

Figure 20: Temperature distribution in a rear cutout from Fig. 18.

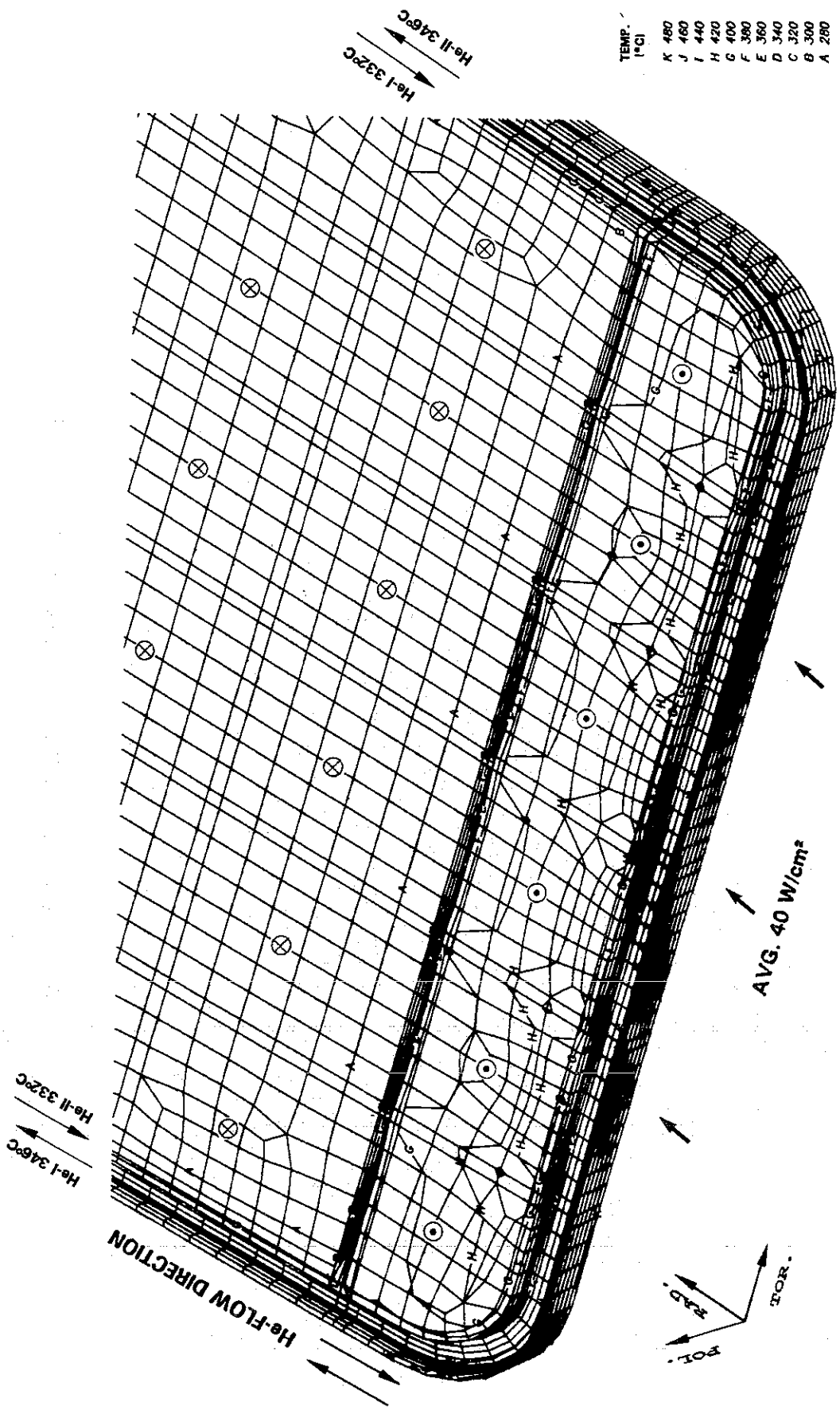

Figure 21: Temperature distribution in the blanket cross-section at the top blanket end.

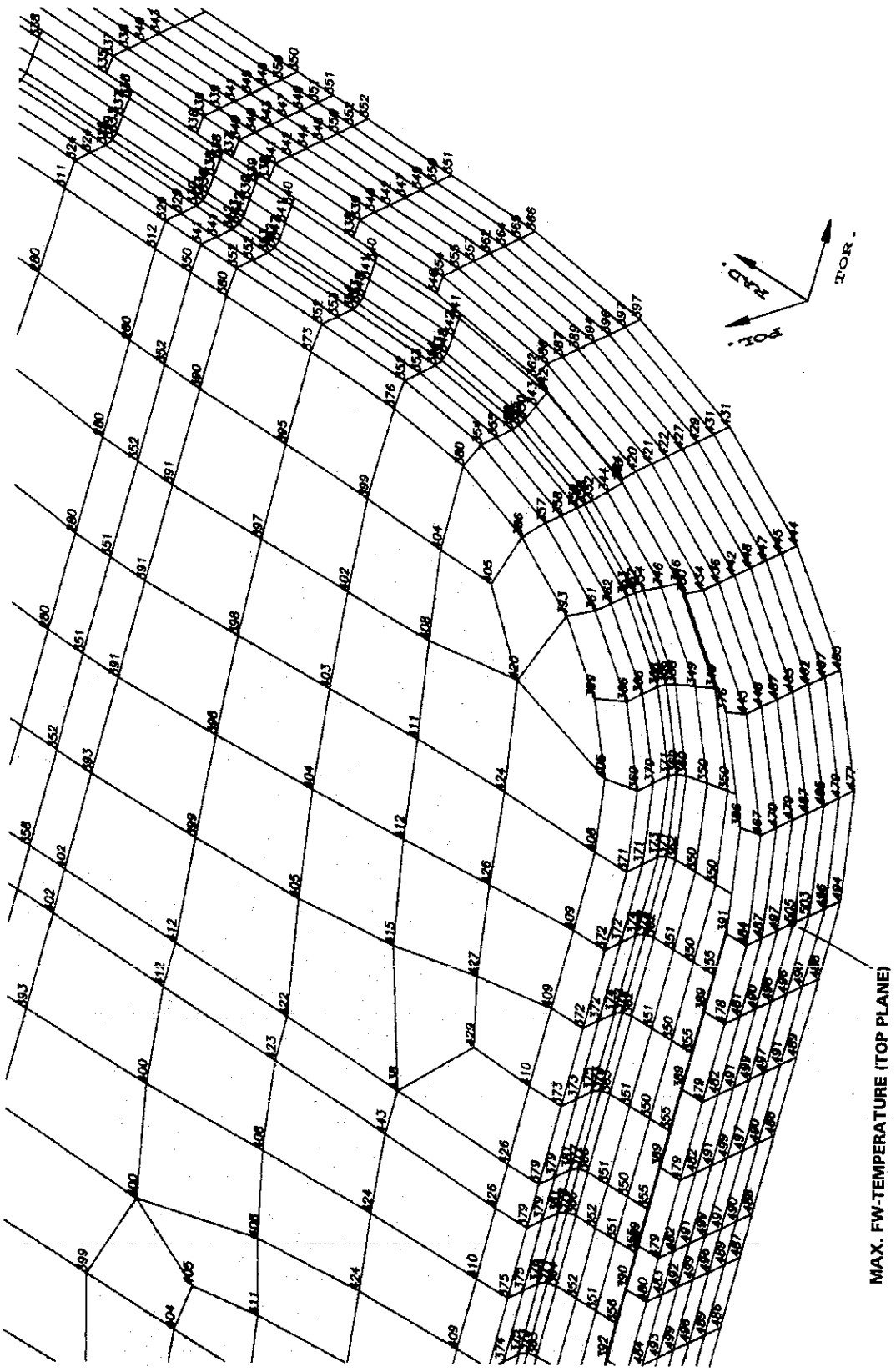

Figure 22: Temperature distribution in a First Wall cutout from Fig. 21.

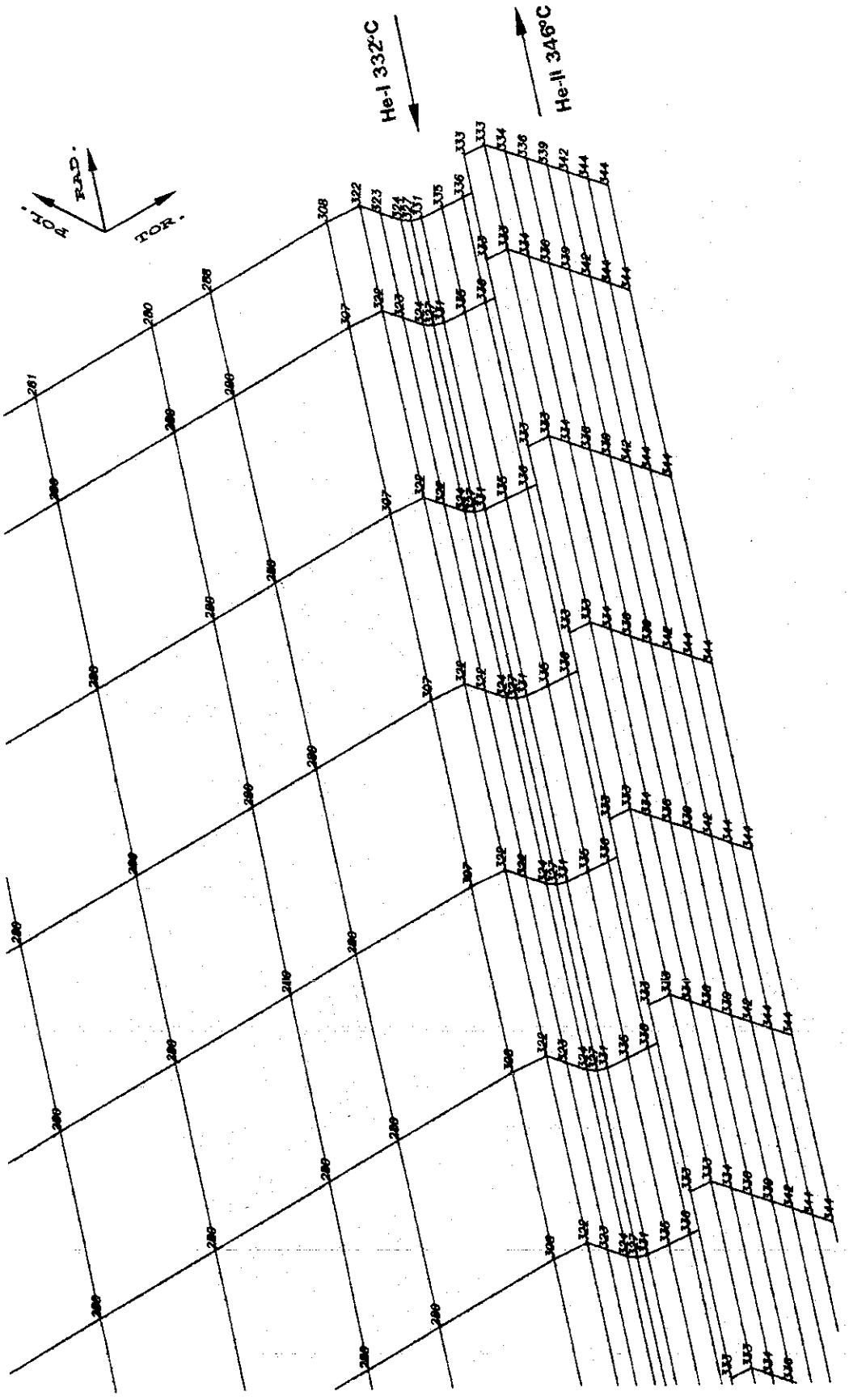

Figure 23: Temperature distribution in a rear cutout from Fig. 23.

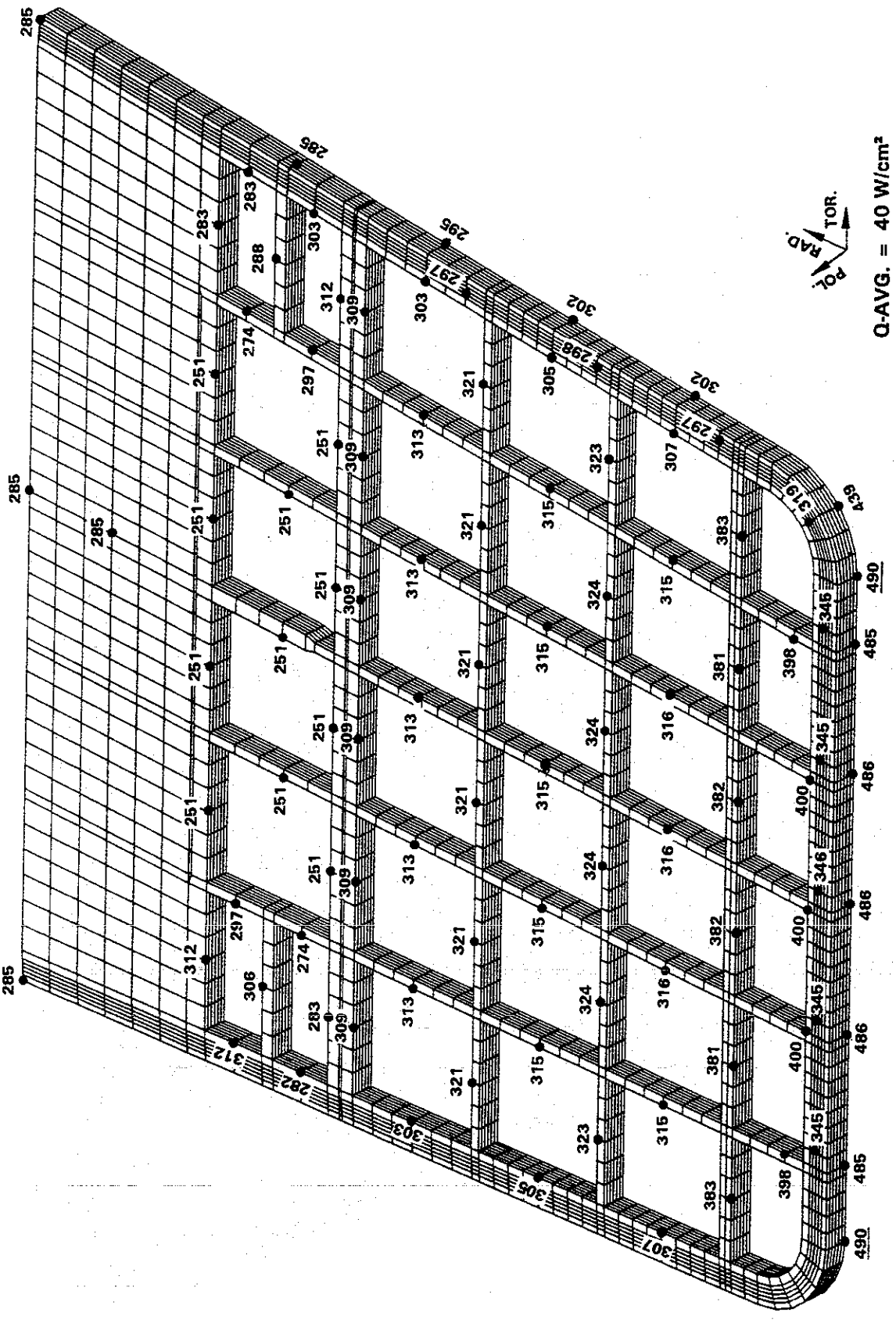

Figure 24: Temperature distribution in the center of the blanket for a mean thermal surface power of 40 W/cm².

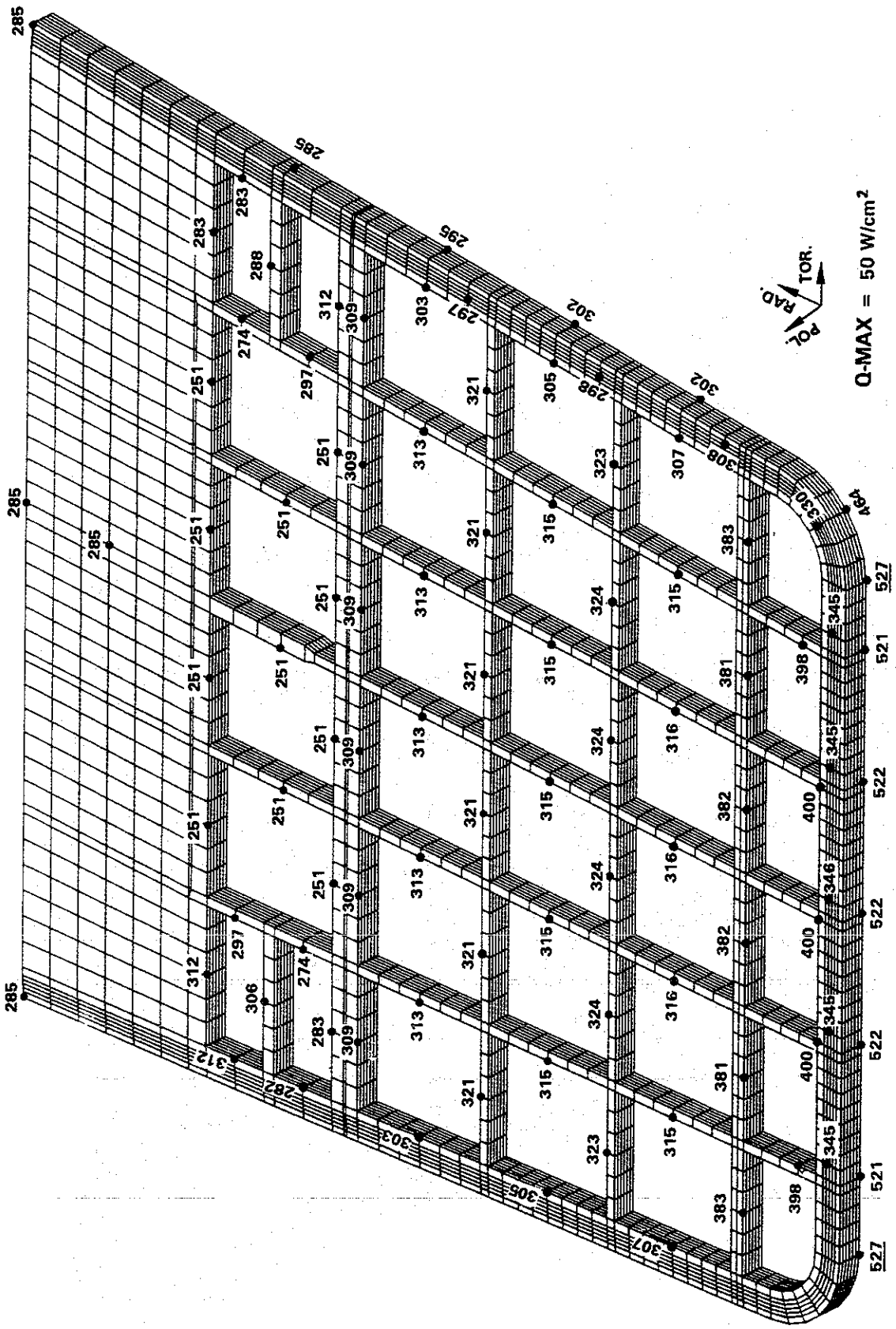

Figure 25: Temperature distribution in the center of the blanket for a maximum thermal surface power of 50 W/cm2 and unchanged helium flow.

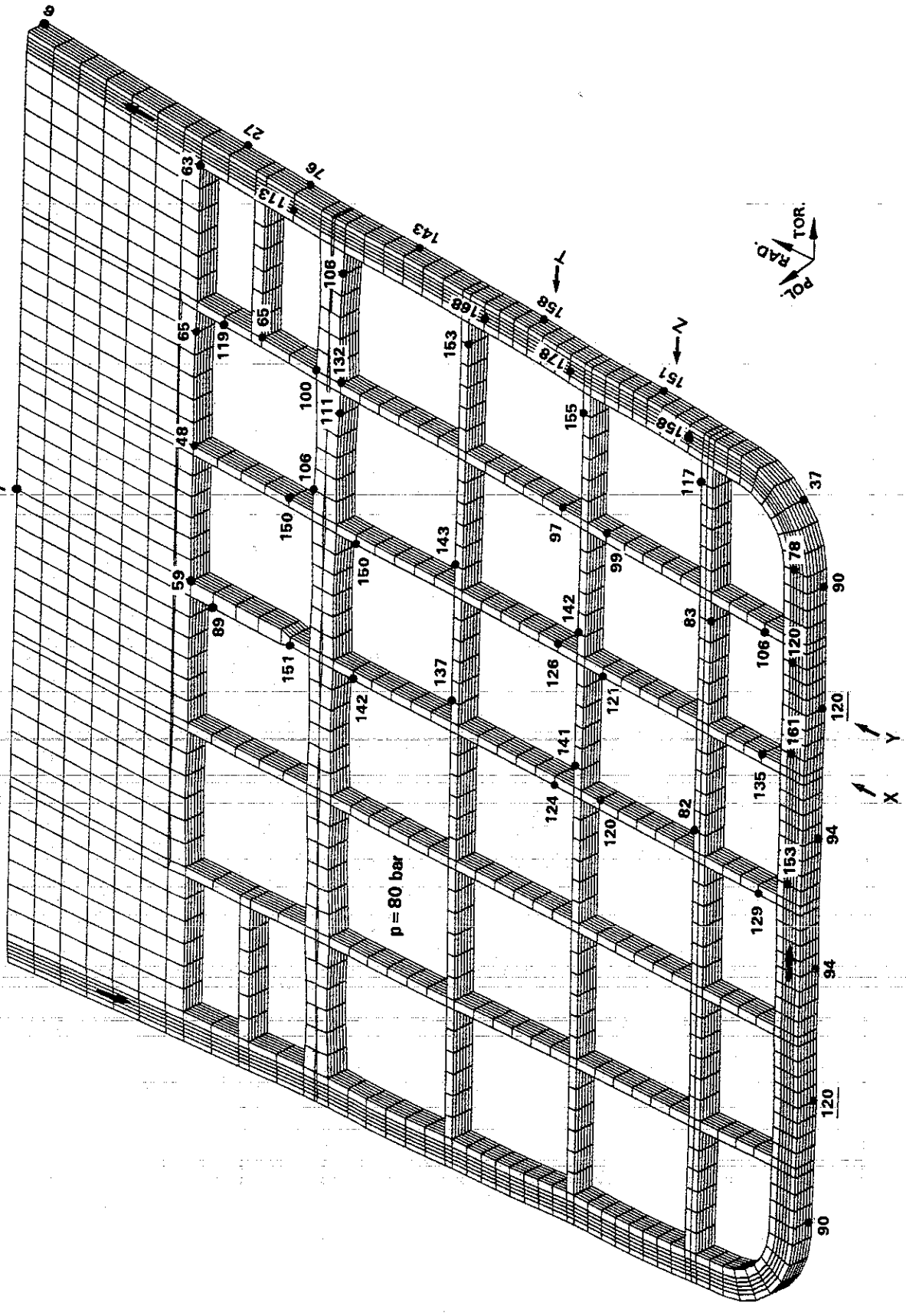

Figure 26: Von Mises primary stress in the center of the blanket.

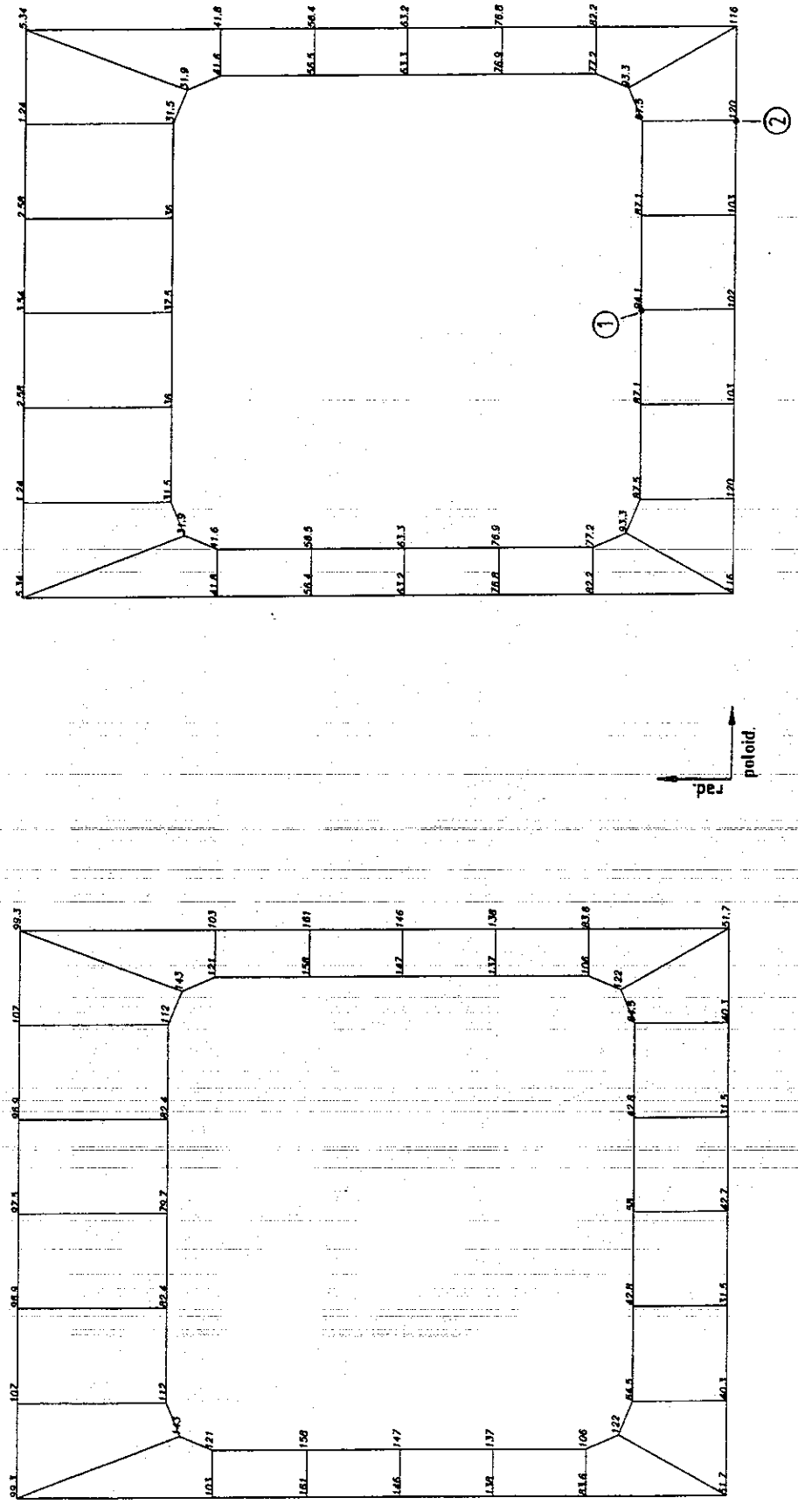

Figure 27: Von Mises primary stress in the First Wall cross-sections X and Y from Fig. 26.

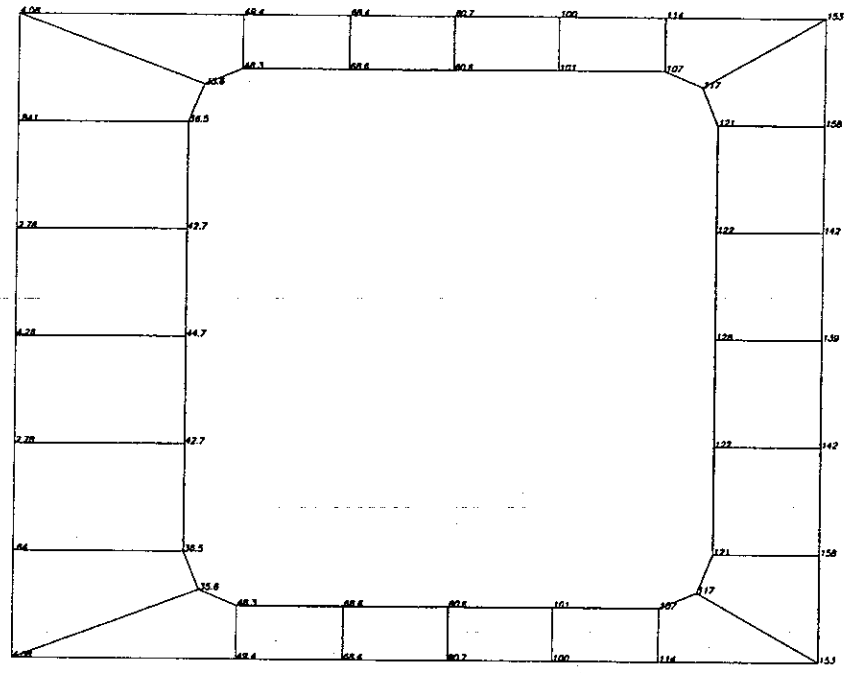

T

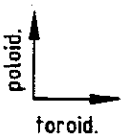

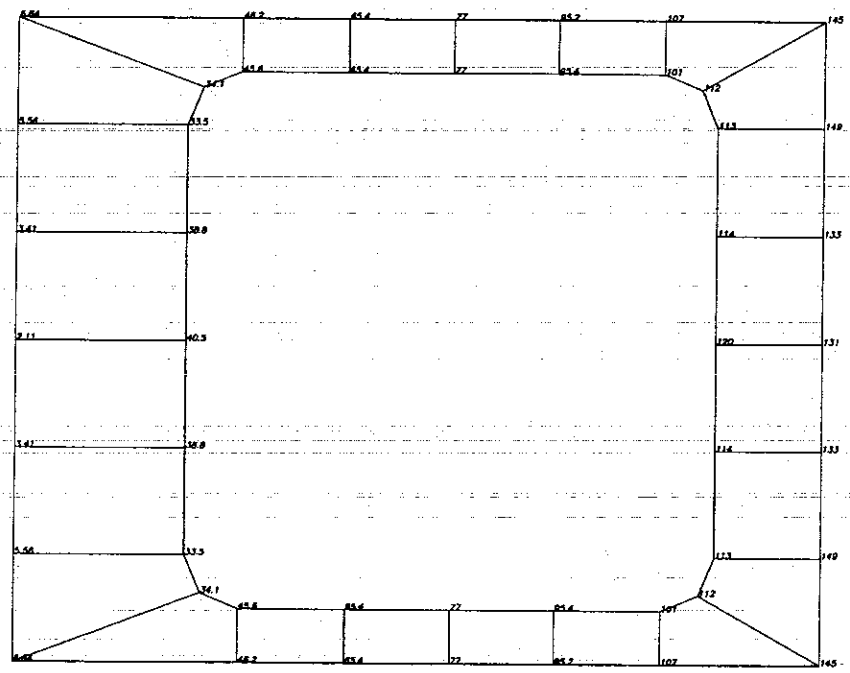

Z

Figure 28: Von Mises primary stress in the side wall cross-sections Z and T from Fig. 26.

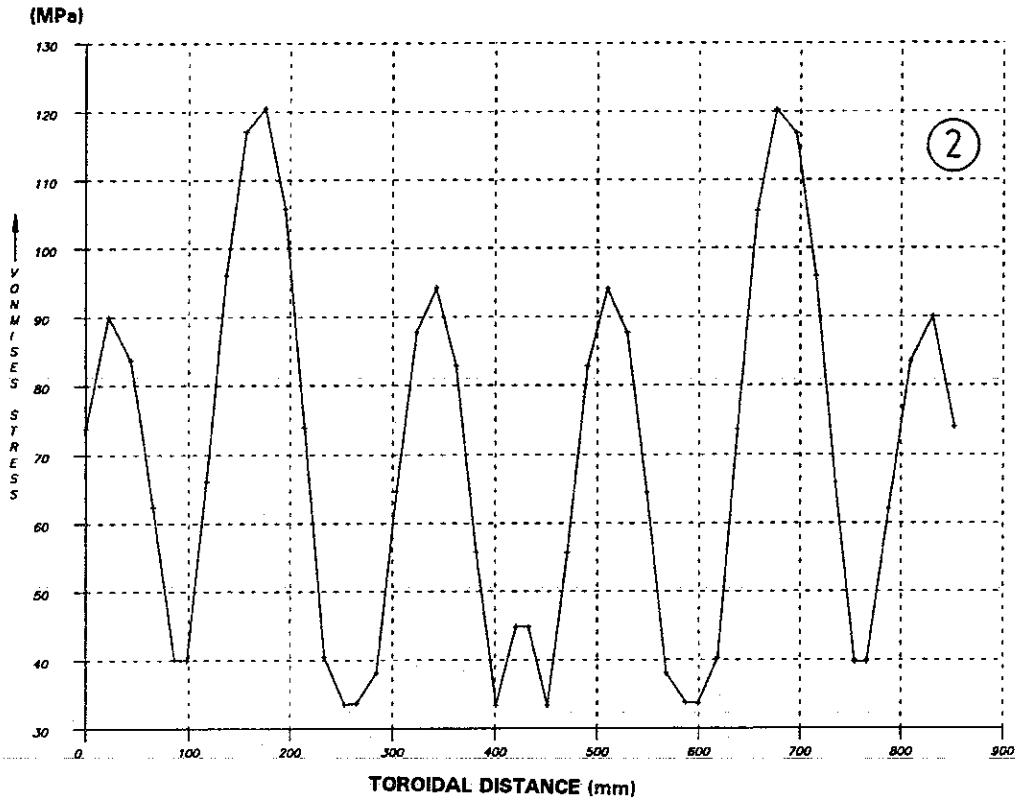

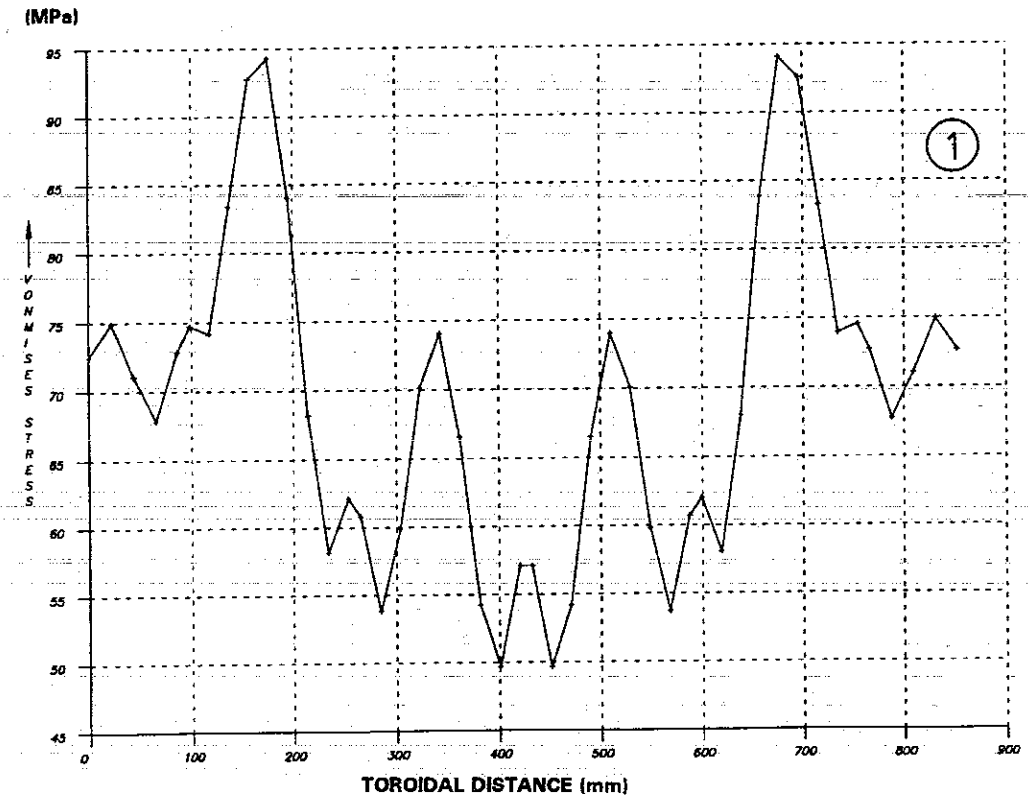

Figure 29: Toroidal development of primary stress on the inner channel wall (Point 1) and on the external wall (Point 2) from Fig. 27, respectively, in the straight part of the First Wall in direction of flow.

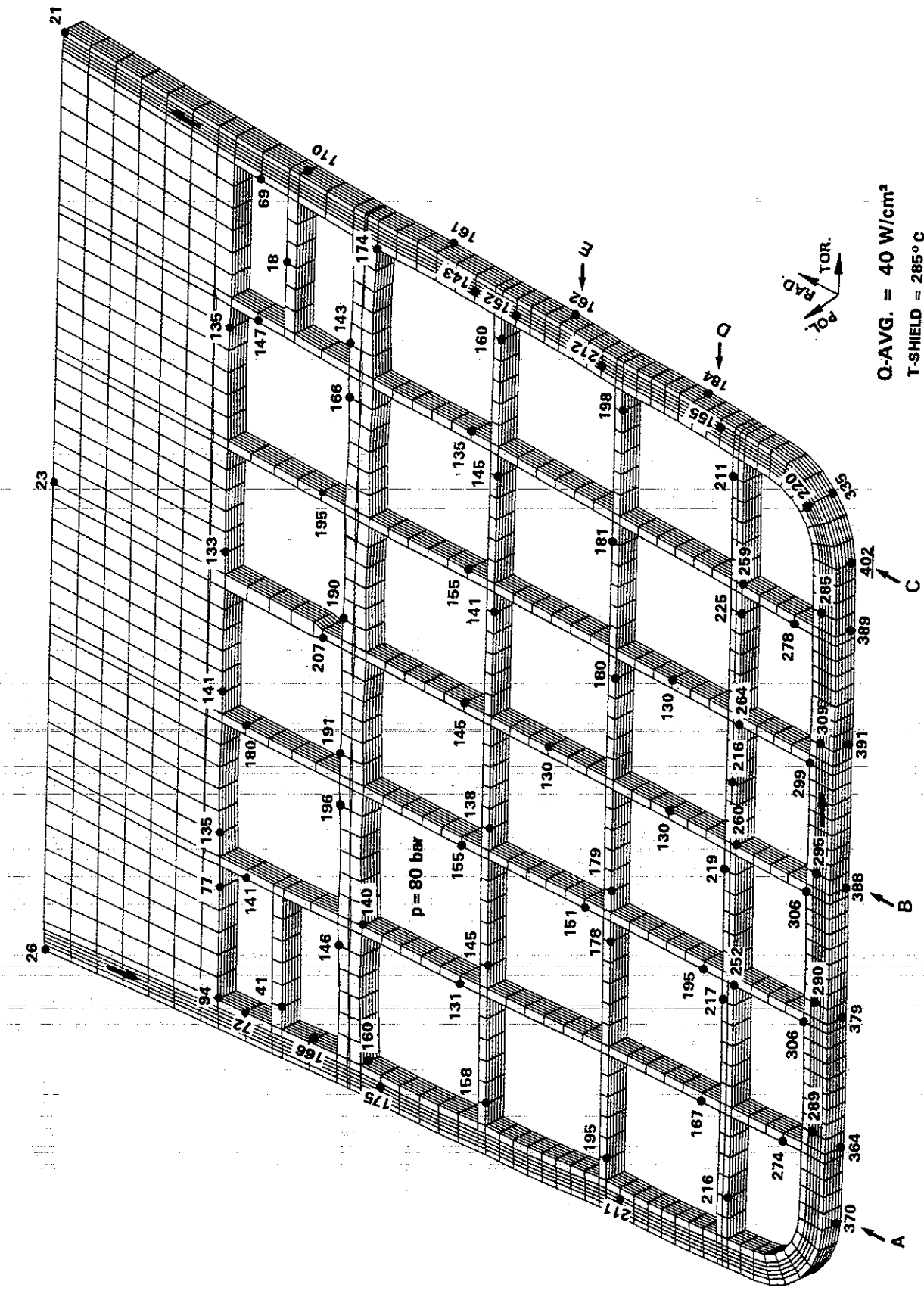

Figure 30: Von Mises primary plus secondary stresses in the center of the blanket for a mean thermal surface power of 40 W/cm².

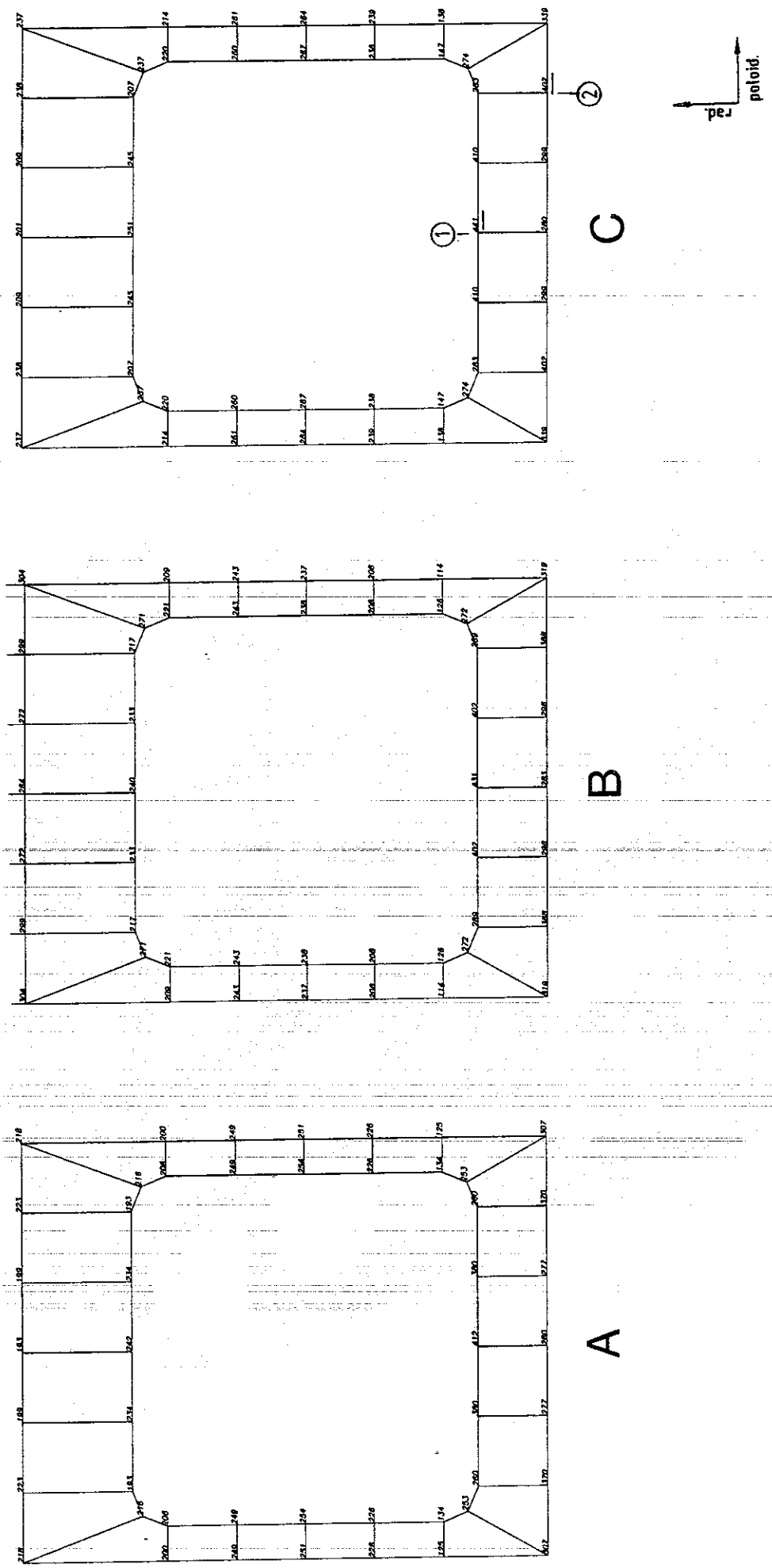

Figure 31: Von Mises primary plus secondary stresses in the First Wall cross-sections A, B and C from Fig. 30.

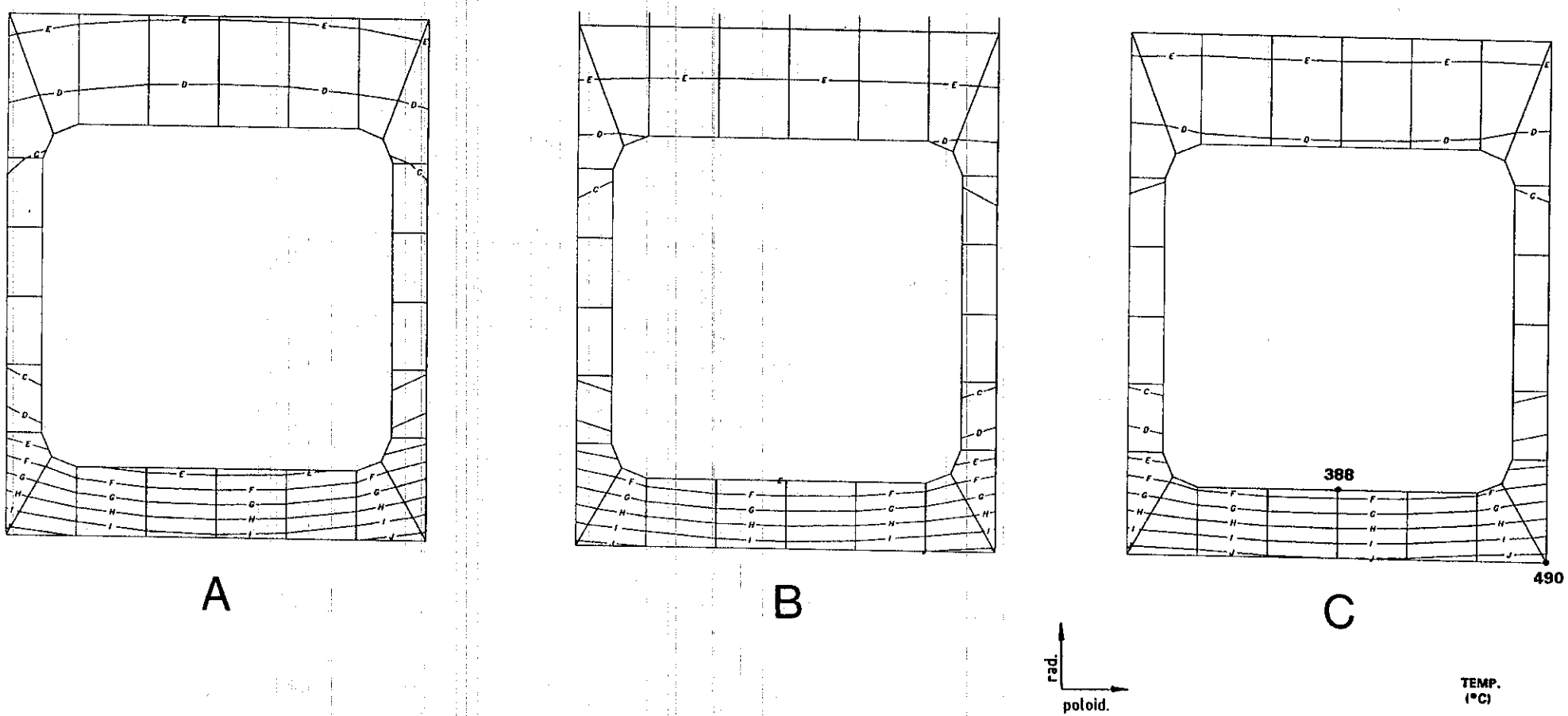

Figure 32: Temperature distribution in the First Wall cross-sections A, B and C for a mean thermal surface power of 40 W/cm^2.

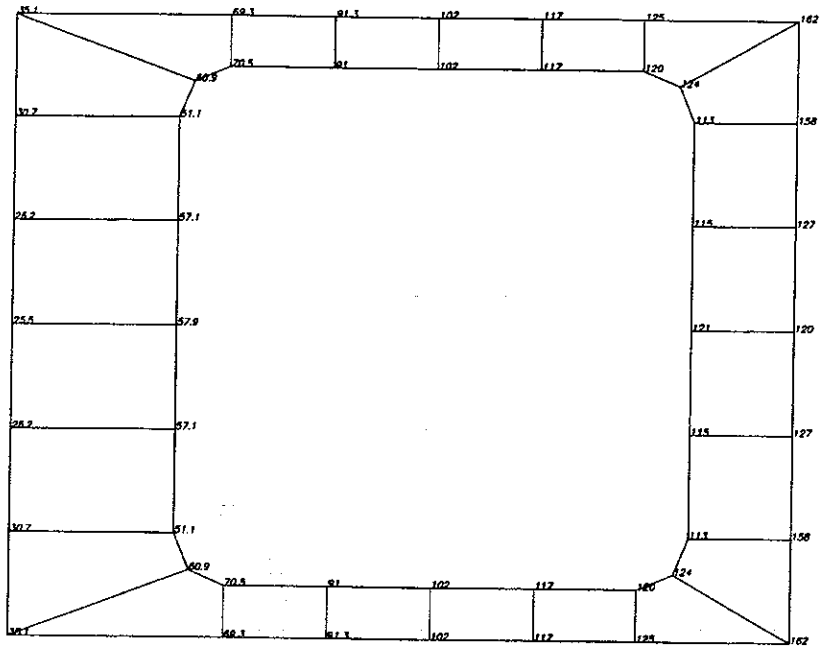

E

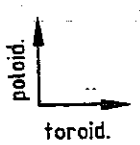

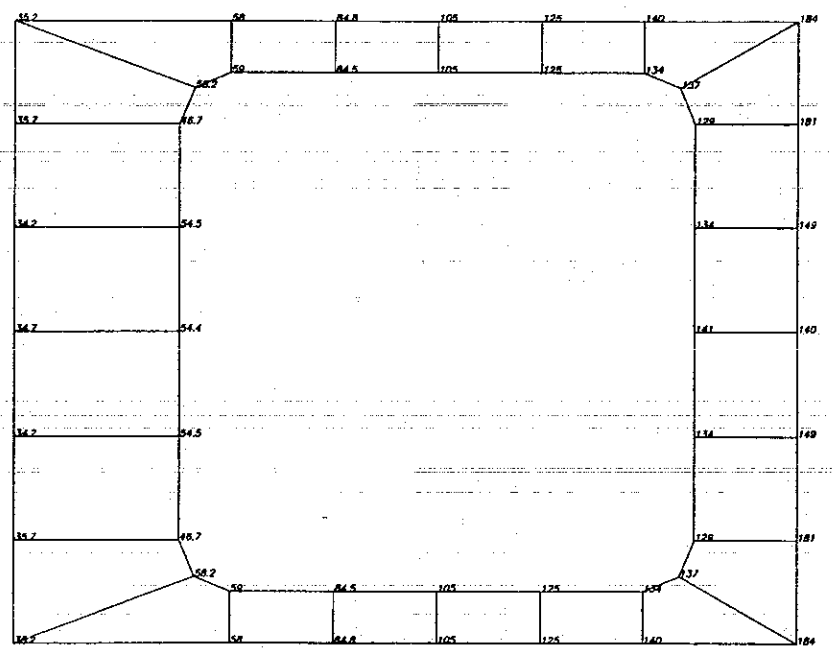

D

Figure 33: Von Mises primary plus secondary stresses in the side wall cross-sections D and E from Fig. 30.

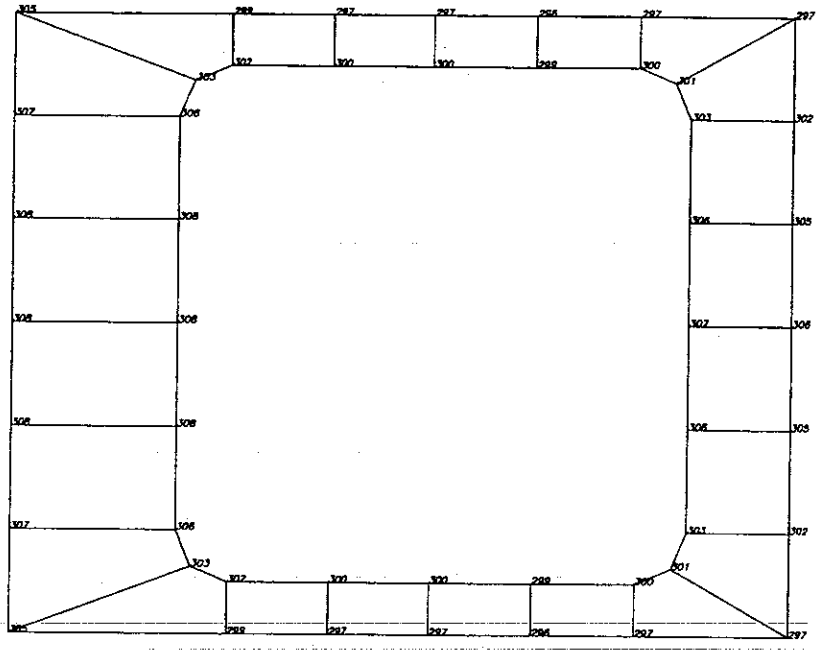

E

poloid.

toroid.

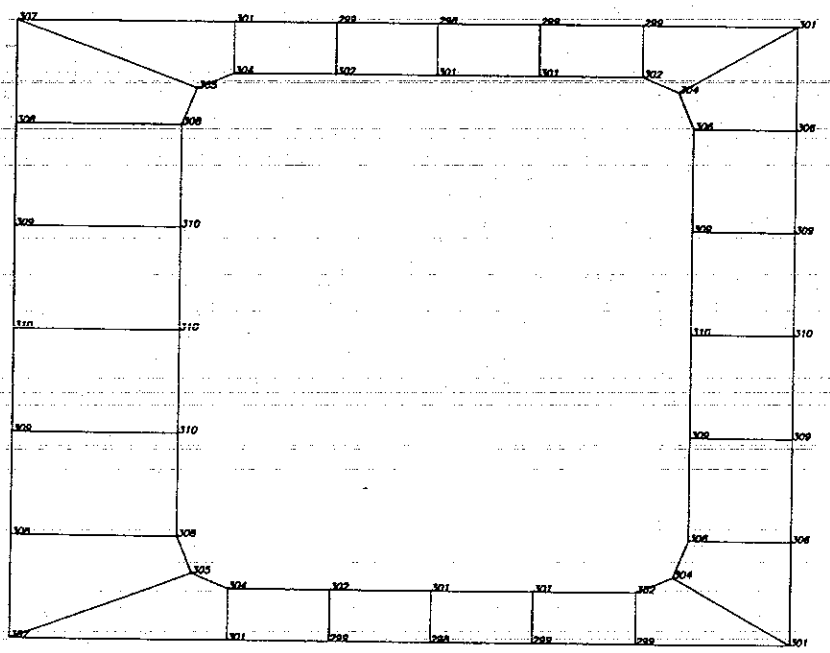

D

Figure 34: Temperature distribution in the side wall cross-sections D and E.

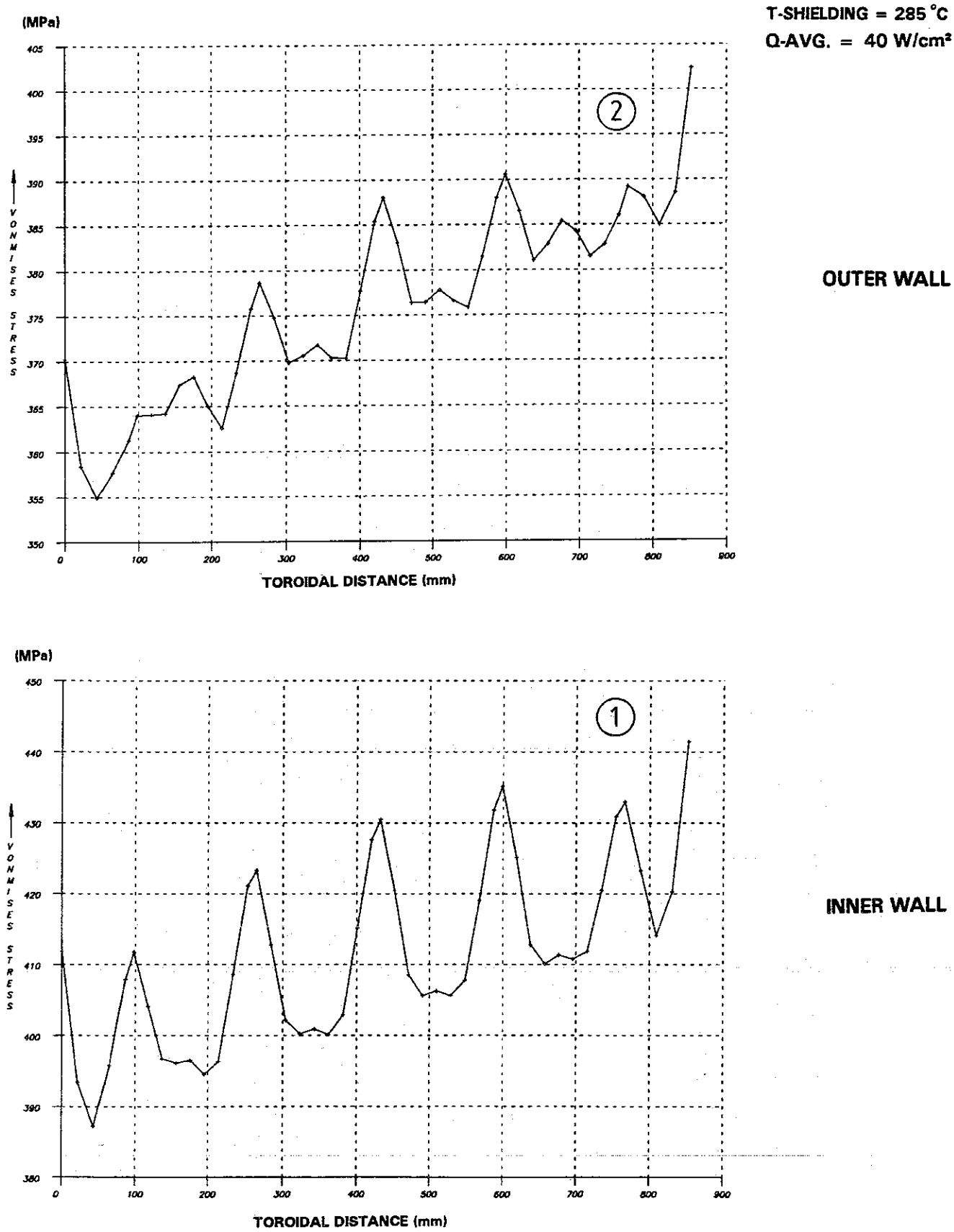

Figure 35: Toroidal development of the primary plus secondary stresses on the inner channel wall (Point 1) and on the external wall (Point 2) from Fig. 32, respectively, in the straight part of the First Wall in direction of flow.

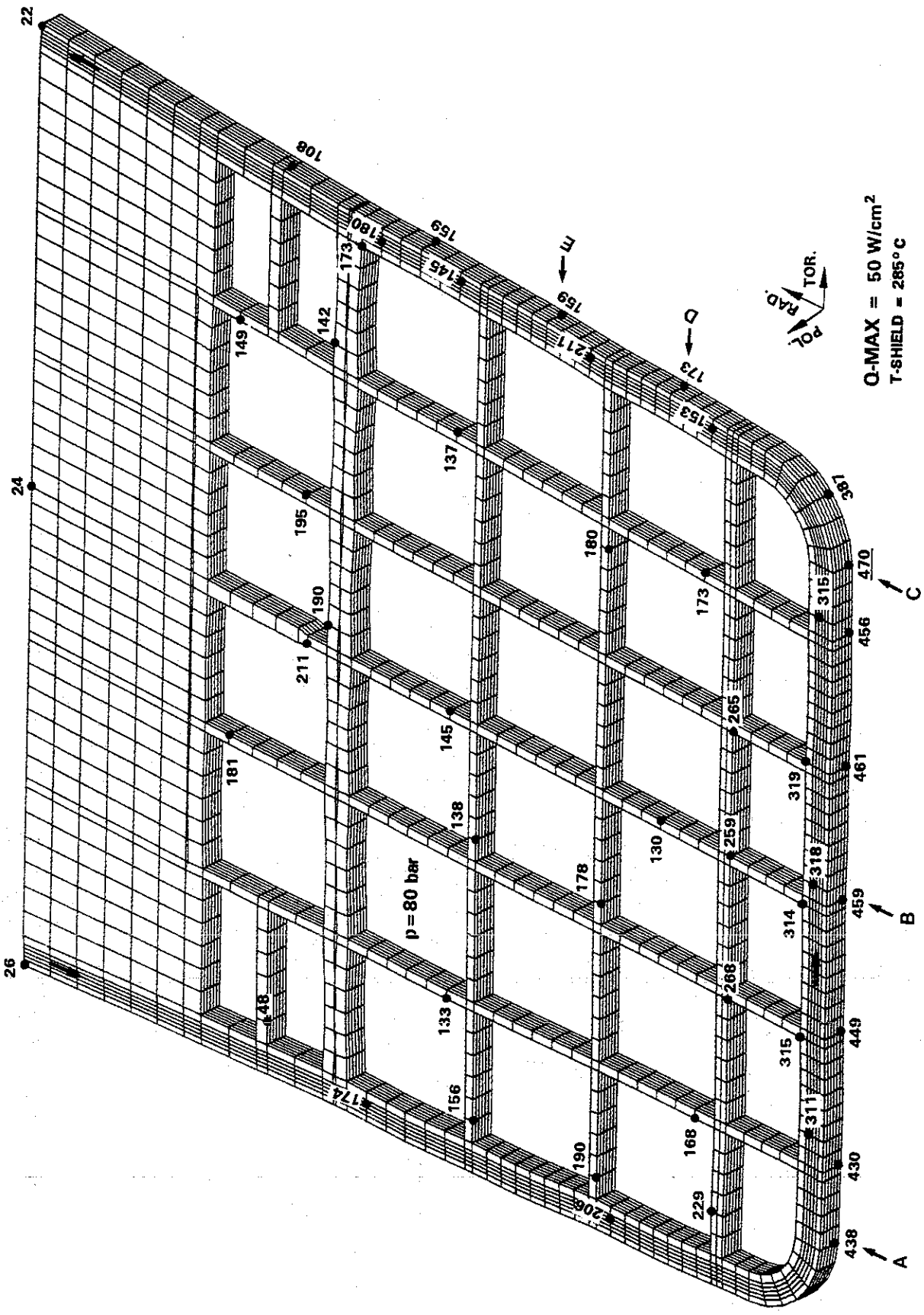

Figure 36: Von Mises primary plus secondary stresses in the blanket center for a maximum thermal surface power of 50 W/cm2.

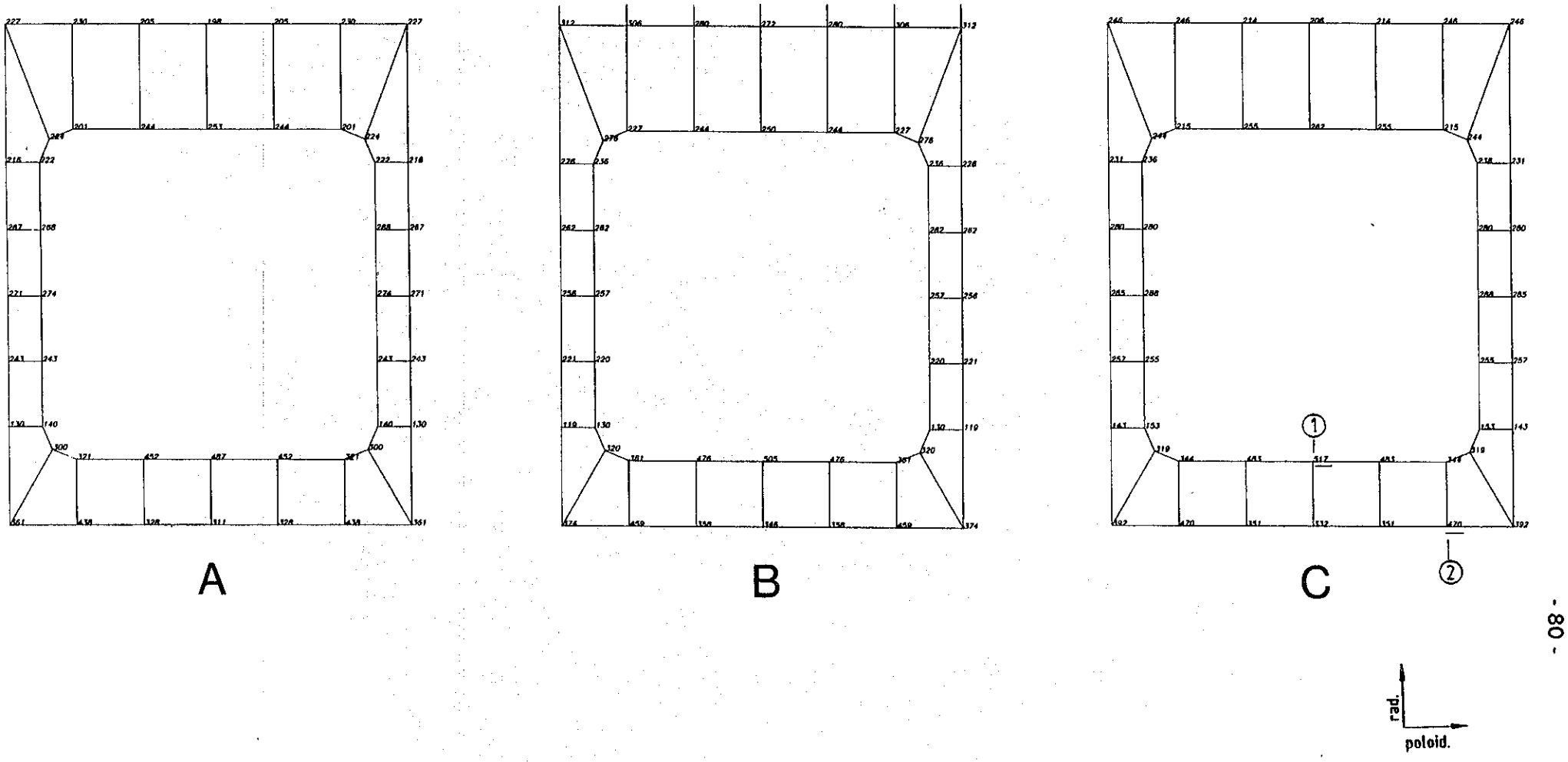

Figure 37: Von Mises primary plus secondary stresses in the First Wall cross-sections A, B and C from Fig. 36.

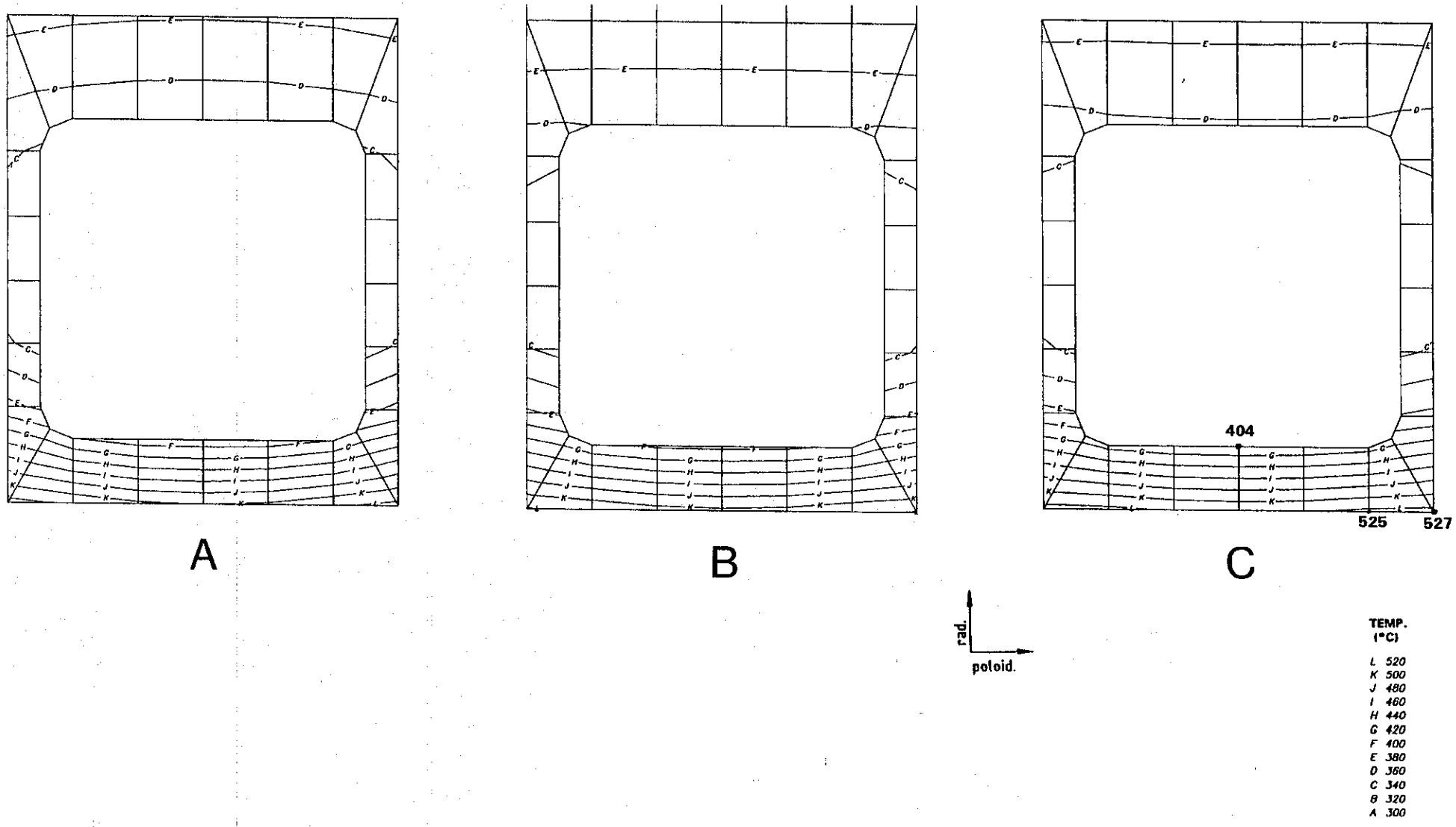

Figure 38: Temperature distribution in the First Wall cross-sections A, B and C for a maximum thermal surface power of 50 W/cm2.

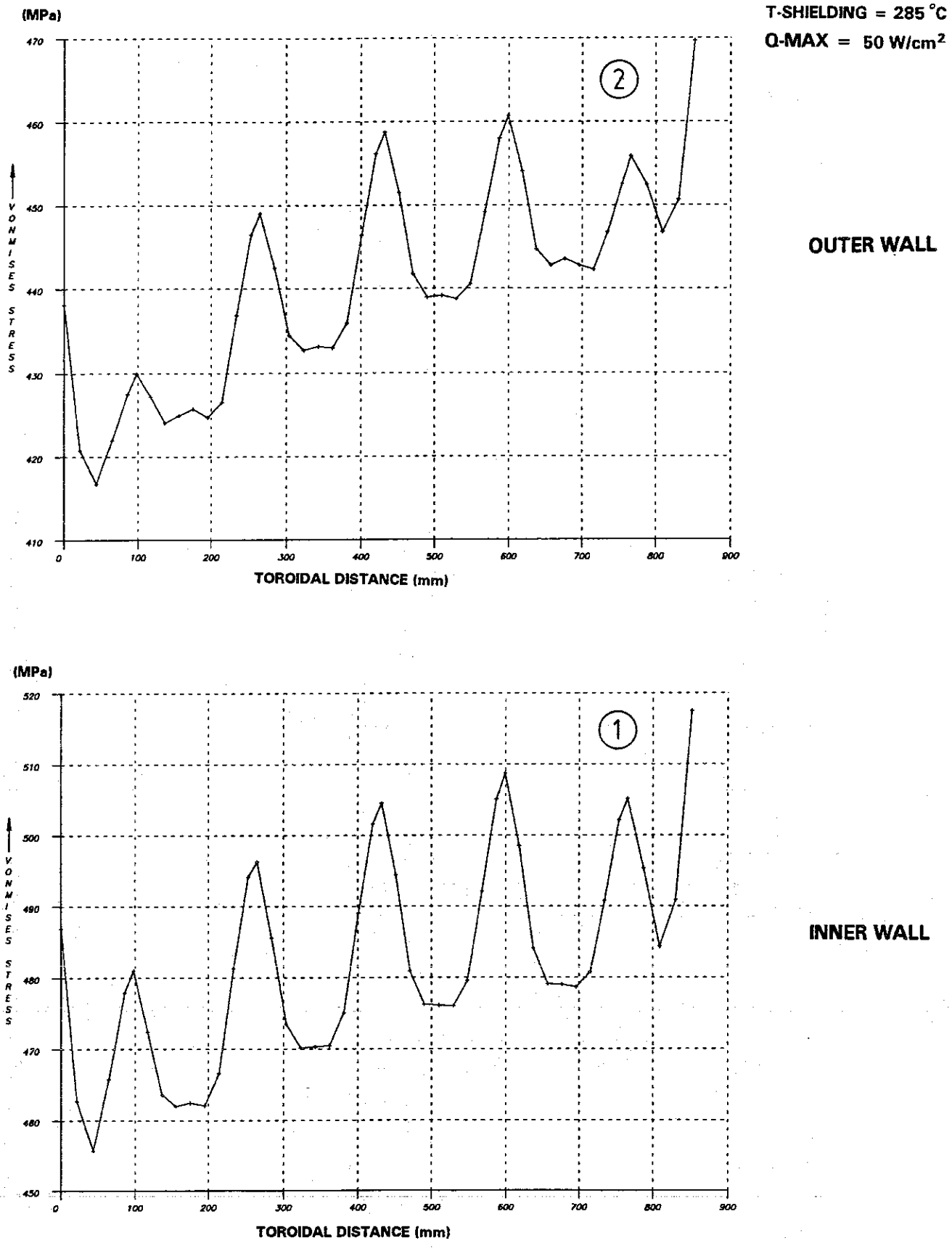

Figure 39: Toroidal development of the primary plus secondary stresses on the inner channel wall (Point 1) and on the external wall (Point 2) from Fig. 37, respectively, in the straight part of the First Wall in direction of flow, for an average temperature of shielding structure of 285 °C.

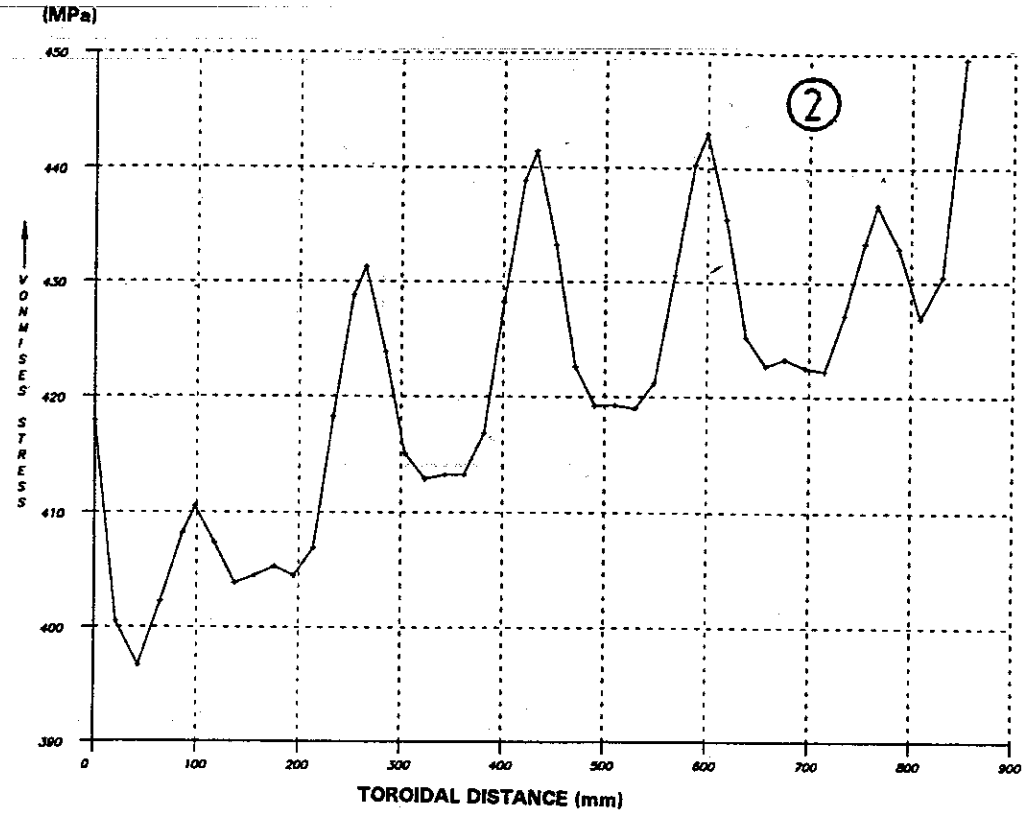

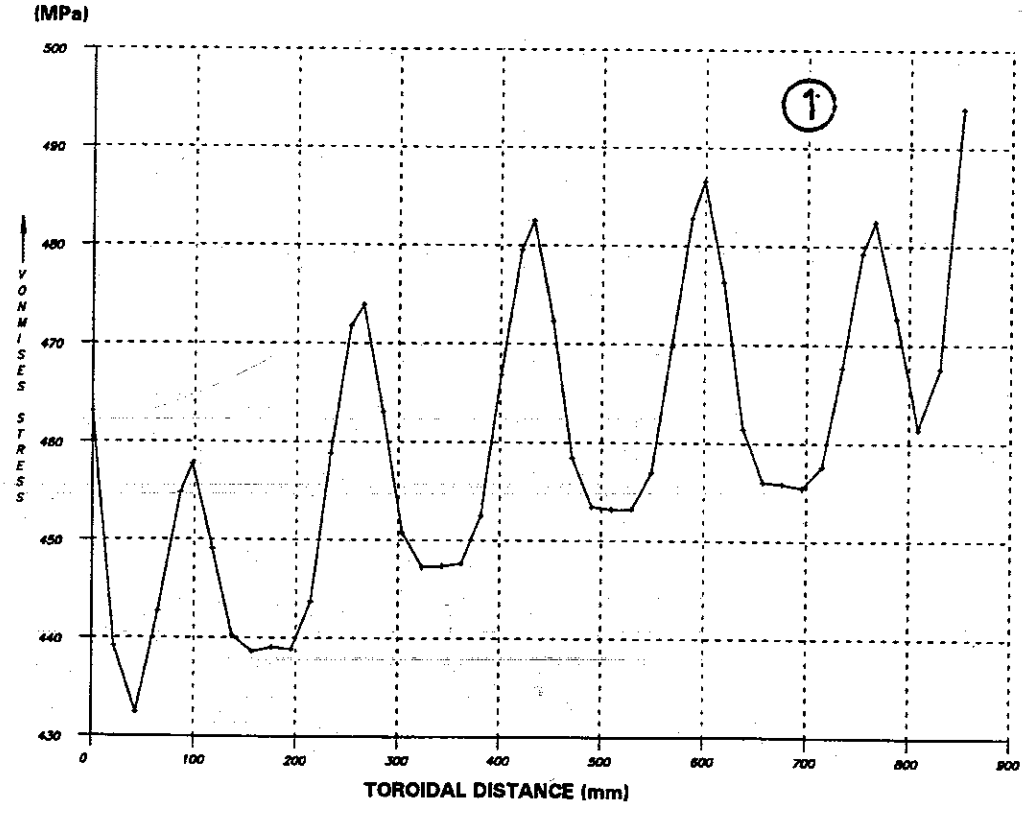

Figure 40: Toroidal development of the primary plus secondary stresses on the inner channel wall (Point 1) and on the external wall (Point 2) from Fig. 37, respectively, in the straight part of the First Wall in direction of flow, for an average temperature of shielding structure of 300 °C.